Title
Diels-Alder Reactivities of Cyclic Dienes and Dienophiles

Author
Levandowski, Brian

Publication Date
2018

Peer reviewed|Thesis/dissertation

UNIVERSITY OF CALIFORNIA

Los Angeles

Diels-Alder Reactivities of Cyclic Dienes and Dienophiles

A dissertation submitted in partial satisfaction

of the requirements for the degree Doctor of Philosophy in Chemistry

by

Brian James Levandowski

2018

ABSTRACT OF THE DISSERTATION

Diels-Alder Reactivities of Cyclic Dienes and Dienophiles

by

Brian James Levandowski

Doctor of Philosophy in Chemistry

University of California, Los Angeles, 2018

Professor Kendall N. Houk, Chair

Since the discovery of the Diels-Alder reaction in 1928, chemical theorists have pursued a deeper understanding of the factors controlling reactivity and stereoselectivity for this reaction. Cyclopentadiene and cyclopropene are unusual, in that they exhibit rapid Diels-Alder reactivity despite their lack of activating electron withdrawing or donating groups. The rapid reactivities of cyclopentadienes result from the minimal distortion required of cyclopentadiene to achieve the envelope-like geometry adopted in the transition state, while the rapid reactivities of cyclopropenes result from reactant distortion and the highly stabilizing orbital interactions present at the transition state.

Substituents at the 3-position of cyclopropenes and the 5-position of cyclopentadienes significantly influence the Diels-Alder reactivity through

hyperconjugative interactions of the substituent with the cyclic π-system. Hyperconjugative acceptors stabilize cyclopropenes and decrease the reactivity by invoking aromatic cyclic delocalization of the two π-electrons and the reactivity decreases. The effect is opposite for cyclopentadienes, where hyperconjugative acceptors induce antiaromatic cyclic delocalization of the four π-electrons, destabilizing the diene and promoting reactivity.

The *syn* and *anti* π-facial selectivity of 5-substituted cyclopentadienes is related to the electronic nature of the substituent. Experimentally, electron-withdrawing groups provide *syn* adducts, while electron-donating groups provide *anti* adducts. Structural analysis of the ground state geometries revealed that sigma-acceptors pre-distort the cyclopentadiene into an envelope-like geometry that minimizes the destabilizing effect of the negative hyperconjugation. This envelope geometry resembles the *syn* transition state geometry and promotes *syn* selectivity by minimizing the distortion energy required to achieve the *syn* transition state. Conversely, donors pre-distort in the opposite direction to maximize the stabilizing effect the hyperconjugative interaction towards an envelope geometry that favors the *anti* cycloaddition.

The computational insights into the reactivities of cyclopentadienes inspired us to develop cyclopentadiene as a bioorthogonal reagent. Bioorthogonal reactions take place rapidly and selectively in biological environments and enable the study of biomolecules in living systems. Highly accurate computational methods were used to screen potential bioorthogonal cyclopentadiene candidates. The screening revealed tetrachlorocyclopentadiene ketals as highly reactive and stable dienes with promising bioorthogonal potential. To verify our prediction, the Murphy group

bioconjugated a tetrachlorocyclopentadiene ketal it to a peptide and labeled the peptide with *trans*-cyclooctene dye. Some cyclopentadienes are now considered viable bio-orthogonal reagents.

The dissertation of Brian James Levandowski is approved.

Craig A. Merlic

Jorge R. Barrio

Kendall N. Houk, Committee Chair

University of California, Los Angeles

2018

Table of Contents

Figures

Schemes

Charts

Acknowledgements

I am grateful to my undergraduate organic chemistry Professors, Neal Yakelis and Craig Fryhle, for providing me with a strong foundation in organic chemistry through excellent teaching at Pacific Lutheran University.

I thank Professor Kendall Houk for allowing me to be a part of his distinguished research group. His enthusiasm for discovery and passion for cycloadditions resonates throughout the scientific community. He and fellow "Houkies" have been instrumental in my growth as a scientist.

Curriculum Vitae

Education

Pacific Lutheran University, Tacoma, WA (2009-2013)

B.S. Chemistry, Departmental Honors (3.49 GPA)

Thesis: Synthesis and Thermal Decomposition of 3,6-dihydro-1,2-oxazines.

Publications (UCLA)

1) Levandowski, B. J.; Gamache, R. F.; Murphy, J. M.; Houk, K. N. "Readily Accessible Ambiphilic Cyclopentadienes for Bioorthogonal Labeling." *J. Am. Chem.* **2018**, 140, 6426−6431. *J. Am. Chem. Soc.*, **2018**, *140*, 6727–6728. *JACS* Spotlight *J. Am. Chem. Soc.* 1*40*, 6727-6728

2) Levandowski, B. J.; Hamlin, T. A.; Helgeson, R. C.; Bickelhaupt, F. M.; Houk, K. N. **"**Origins of the *Endo* and *Exo* Selectivities in Cyclopropenone, Iminocyclopropene, and Triafulvene Diels–Alder Cycloadditions." *J. Org. Chem.* **2017**, *82*, 8668−8675.

3) Levandowski, B. J.; Herath, D.; Gallup, N. M.; Houk, K. N. "Origin of π-Facial Stereoselectivity in Thiophene 1-oxide Cycloadditions." *J. Org. Chem.* **2018**, *83*, 2611-2616.

4) Kerisit N.; Gawel, P.; Levandowski, B.; Yang, Y.; Garcia-Lopez, V.; Trapp, N.; Ruhlmann, L. Boudon, C.; Houk, K. N.; Diederich, F. "A Four-Step Synthesis of Substituted 5,11-Dicyano-6,12-diaryltetracenes with Enhanced Stability and High Fluorescence Emission." *Chem. Eur. J.*, **2018**, 24, 159-168.

5) Levandowski, B. J.; Hamlin, T. A.; Bickelhaupt, F. M.; Houk, K. N. "Role of Orbital Interactions and Activation Strain (Distortion Energies) on Reactivities in the Normal and Inverse Electron-Demand Cycloadditions of Strained and Unstrained Cycloalkenes." *J. Org. Chem.* **2017**, *82*, 8668−8675.

6) Levandowski, B. J. and Houk, K. N. "Hyperconjugative, Secondary Orbital, Electrostatic, and Steric Effects on the Reactivities and *Endo* and *Exo* Stereoselectivities of Cyclopropene Diels-Alder Reactions." *J. Am. Chem. Soc.* **2016**, *138*, 16731-16736.

7) Levandowski, B. J.; Zou L.; Houk, K. N. "Schleyer Hyperconjugative Aromaticity and Diels-Alder Reactivity of 5-substituted Cyclopentadienes." *J.Comp. Chem.*, **2016**, *37*, 117-123.

8) Levandowski, B. J. and Houk, K. N. "Theoretical Analysis of Reactivity Patterns in Diels–Alder Reactions of Cyclopentadiene, Cyclohexadiene, and Cycloheptadiene with Symmetrical and Unsymmetrical Dienophiles." *J. Org. Chem.*, **2015**, *80*, 3530-3537.

Manuscripts in Preparation

9) Hamlin, T. A.; Levandowski, B. J.; Narsaria, A. K.; Houk, K. N.; Bickelhaupt, F. M. "Rates of 1,3-Dipolar Cycloadditions of Strained and Unstrained Alkynes are Influenced by Distortion and Orbital Interactions" Submitted

10) Levandowski, B. J.; Zou L.; Houk, K. N. "Hyperconjugative Aromaticity and Antiaromaticity Control the Reactivity and π-Facial Stereoselectivity of 5-Substituted Cyclopentadiene Cycloadditions." Submitted

11) Levandowski, B. J.; Hamlin, T. A.; Bickelhaupt, F. M.; Houk, K. N. "Diels-Alder Reactivities of Cycloalkenediones with Tetrazine." Submitted

Patents (UCLA)

1) Cyclopentadiene Compounds for use in Bioorthogonal Coupling Reactions Levandowski, B. J.; Gamache, R. F.; Murphy, J. M.; Houk, K. N.

Awards

Saul and Sylvia Winstein Award (UCLA 2018)

Christopher S. Foote Fellowship (UCLA 2015)

ACS Division of Organic Chemistry Undergraduate award in (PLU 2013)

American Institute of Chemists Student Award (PLU 2013)

Teaching Experience (UCLA)

30A Organic Chemistry I: Structure and Reactivity (2 quarters)
14BL General and Organic Chemistry Laboratory I (2quarters)
30CL Organic Chemistry Laboratory II (1 quarter)
14CL General and Organic Chemistry Laboratory I (1 quarter)

Chapter 1. Diels-Alder Reactivity Trends of Cyclic Dienes

1.1 Introduction to Diels-Alder Reactions of Cyclic Dienes

The high reactivities of cyclopentadienes in the Diels−Alder reaction have led to applications including organic synthesis,[1] biomolecule immobilization,[2] thermally sensitive polymers,[3] and the functionalization[4] of materials. Cyclohexadiene and cycloheptadiene are less reactive and less useful in such applications. A SciFinder[5] search for Diels−Alder reactions of cyclopentadiene, cyclohexadiene, and cycloheptadiene gave □5000 reactions involving cyclopentadiene, □1500 with cyclohexadiene, and only □70 with cycloheptadiene.

The poor reactivity of cyclohexadiene and Cycloheptadiene relative to that of cyclopentadiene with cyclobutenone was recently reported by Danishefsky and computationally investigated by our lab (Scheme 1).[6] The experimentally determined HOMO energies of the cyclic dienes range only from −8.6 to −8.3 eV.[7,8] If the frontier molecular orbitals governed the reactivity, then similar reactivities would be expected for all three cyclic dienes. The computed transition state barriers, however, show that, with cyclobutenone, cyclopentadiene is about 100 times more reactive than cyclohexadiene and about 15,000 times more reactive than cycloheptadiene, at 298 K.[6] We have shown that the reactivity is controlled by distortion energies: cyclopentadiene requires only 15.0 kcal/mol to distort into the transition state geometry, which is 4.2 kcal/mol less than that for cyclohexadiene and 7.1 kcal/mol less than that for cycloheptadiene.

Scheme 1.1 Diels–Alder reactions of cyclobutenone with the three cyclic dienes[6]

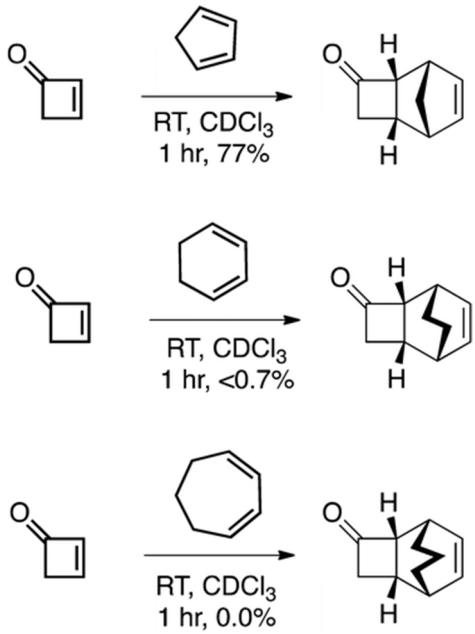

The hetero-Diels−Alder reactions of both N-phenyl-1,2,4-triazolin-3,5-dione (PTAD) and nitrosobenzene with all three cyclic dienes, however, occur readily under mild conditions, as shown in Scheme 2.[9–13] The Diels−Alder reactions of cyclopentadiene with PTAD and nitrosobenzene occur at 0 °C (Scheme 2a,d). Cyclohexadiene reacts with nitrosobenzene (Scheme 2e) and a cyclohexadiene derivative reacts with PTAD (Scheme 2b) at 0 °C with comparable yields to the corresponding reactions with cyclopentadiene. At room temperature, a Cycloheptadiene derivative is reactive with both PTAD and nitrosobenzene (Scheme 2c,f). Unlike the reactions with cyclobutenone, the reactions of the cyclic dienes with PTAD and nitrosobenzene occur under similar conditions, with a cycloheptadiene derivative being only modestly less reactive.

Scheme 1.2 Diels–Alder reactions of PTAD and nitrosobenzene with the three cyclic dienes

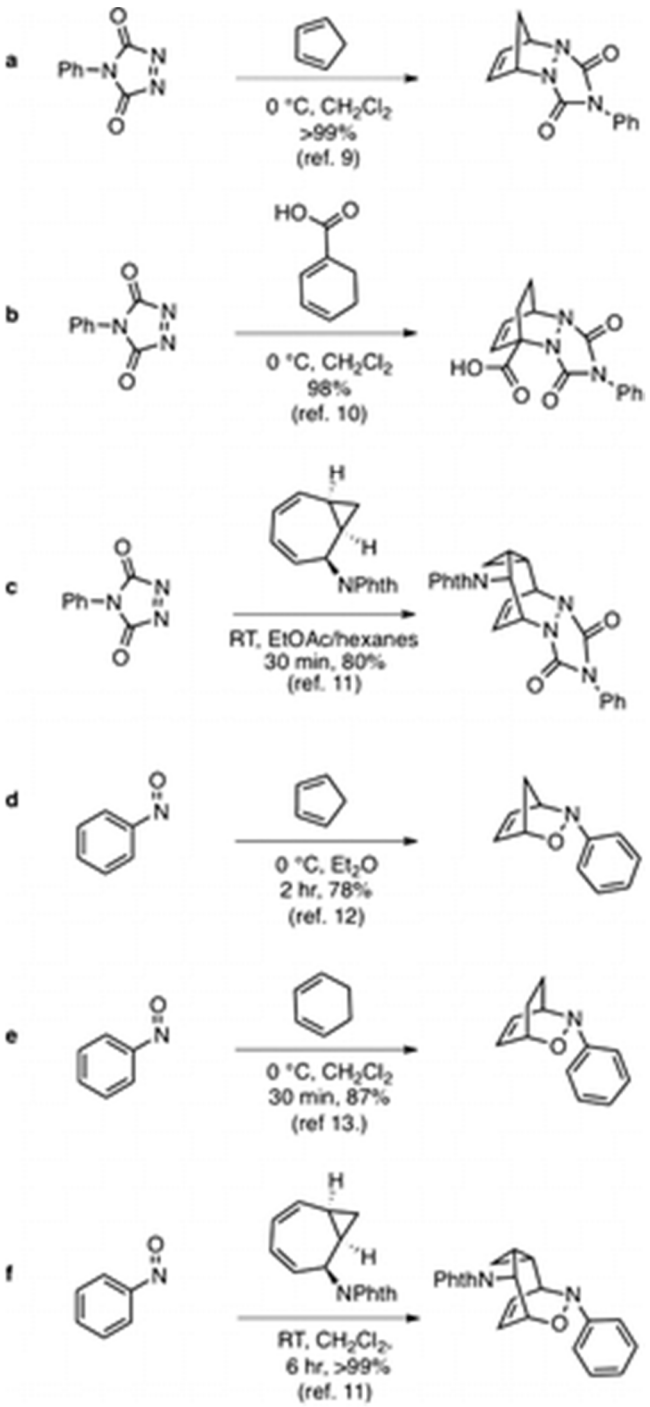

1.2 Previous Explanations of Reactivity Differences in Cyclic Dienes

Cyclic dienes are more reactive than acyclic dienes in Diels− Alder reactions, in part because they are locked into the s-cis conformation required of concerted Diels−Alder transition states.[14] To rationalize the poor reactivities of cyclohexadiene and cycloheptadiene relative to that of cyclopentadiene in the Diels−Alder reaction, it has been proposed that the steric interactions between the bridges of cyclohexadiene and cycloheptadiene result in repulsive steric interactions with the dienophile and inhibit the double bonds from adopting the necessary planar geometry in the transition state.[15] Correlations between the diene 1,4-distance and the reactivity of dienes identify an additional factor controlling the high reactivity of cyclopentadiene and poor reactivity of cycloheptadiene with dienophiles.[16] That is, the termini of cyclopentadiene are closer together than termini of acyclic dienes, whereas in cycloheptadiene the termini are fixed further apart. These models explain why dienophiles such as maleic anhydride readily react with anthracene and show no reactivity with 1,3-cyclooctadiene.[17] Nitrosobenzene, however, reacts with 1,3-cyclooctadiene and fails to react with anthracene even after prolonged reflux in chloroform.[17]

Scheme 1.3 Dienes 1–3 and Dienophiles A–J

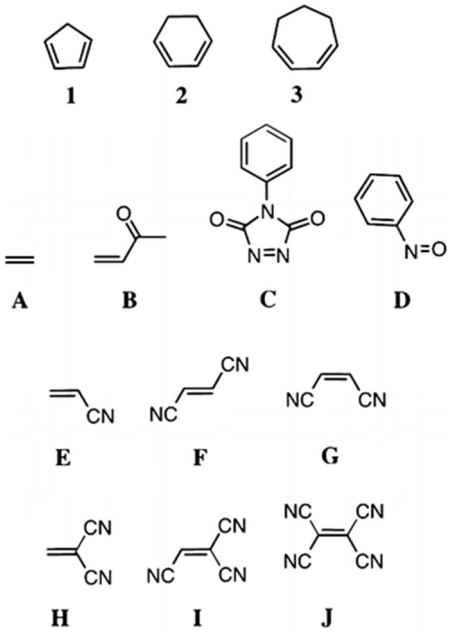

1.3 Computational Methods

Computations were carried out with Gaussian 09, Revision D.01.[21] Geometry optimizations and frequency calculations were performed using the M06-2X[22] density functional with the 6-31+G(d) basis set. The M06-2X functional is known to reproduce the free energies of cycloadditions better than other functionals.[23] Single-point energies were evaluated using the 6-311++G(d,p) basis set. Solvation effects of dichloromethane (DCM) for the reactions of A−D and 1,4-dioxane for the reactions of E−J with cyclic dienes 1−3 were included in the optimizations and single-point energies by the self-consistent reaction field (SCRF) using the CPCM model.[24,25] Normal mode analysis of each structure verified that each stationary point is either a first-order saddle point or a minimum. The thermal corrections were computed from unscaled M06-2X/6-31+G(d) frequencies for a standard state of 1 M and 298.15 K.

1.4 Influence of Distortion on the Reactivity Cyclic Dienes

The transition structures of the cycloadditions involving dienes 1−3 and dienophiles A−D are shown in Figure 1. In the reactions of ethylene, MVK, and PTAD with the three cyclic dienes, the activation free energies increase from cyclopentadiene to cycloheptadiene. The activation free energies for the reactions of cyclopentadiene with ethylene and MVK are 29.1 and 22.4 kcal/mol, respectively. The barriers increase to 32.9 and 26.5 kcal/mol with cyclohexadiene and to 37.9 and 31.8 kcal/mol with cycloheptadiene. With PTAD, the reactivity differences are smaller. The activation free energy of cyclopentadiene with PTAD is 9.6 kcal/mol. With cyclohexadiene and cycloheptadiene, the barriers with PTAD are 10.9 and 13.7 kcal/mol, respectively. The activation free energies for the reactions of nitrosobenzene with the three cyclic dienes are comparable, ranging from 22.1 to 23.5 kcal/ mol. The computed rate constants for the reactions of the three cyclic dienes span 6 orders of magnitude with ethylene and MVK, 3 orders of magnitude with PTAD, and 1 order of magnitude with nitrosobenzene.

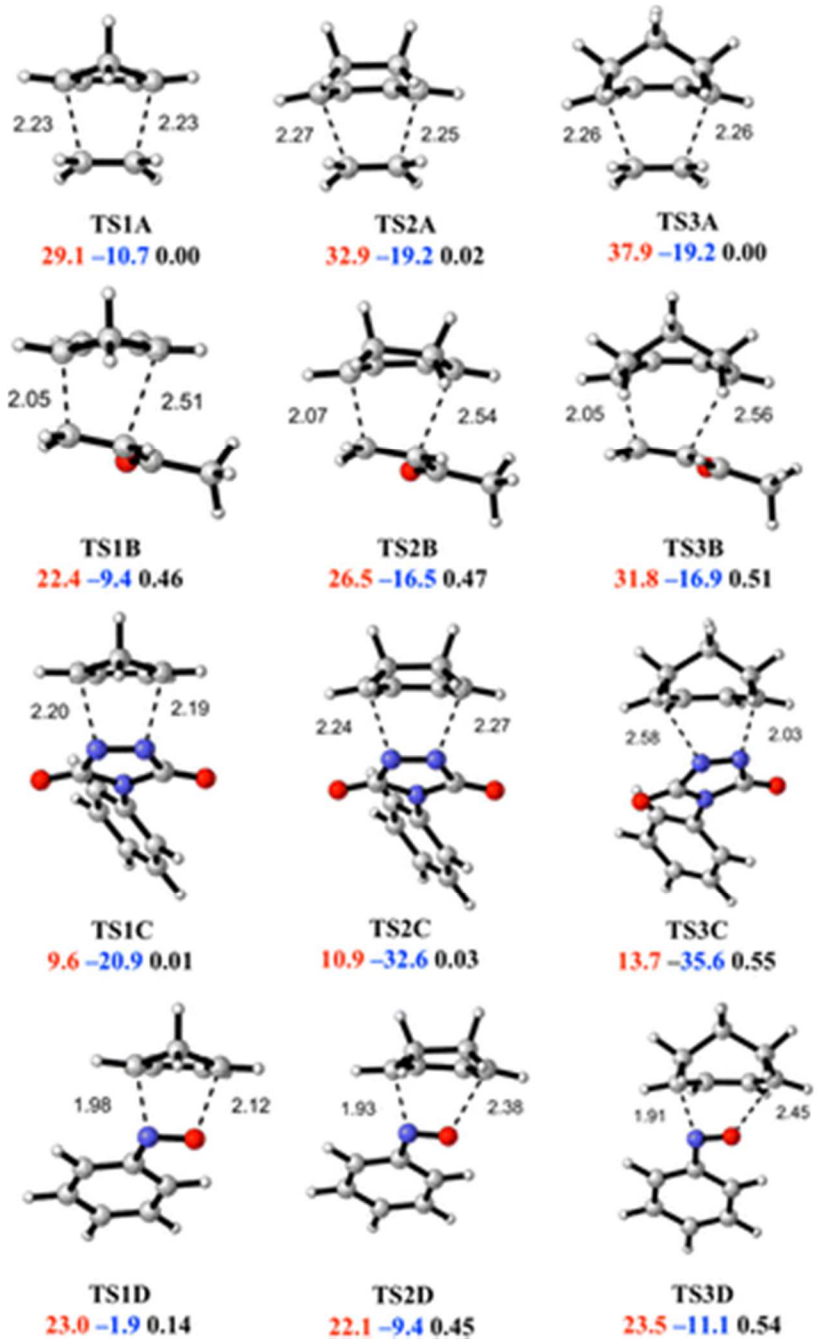

Figure 1.1 M06-2X/6-31+G(d) transition structures for the reactions of dienes 1–3 with dienophiles A–D. The forming bond lengths are reported in angstroms (red, activation free energy ($\Delta G^{\ddagger}$, kcal/mol); blue, reaction free energy (ΔG, kcal/mol); black, asynchronicity ($\Delta r^{\ddagger}$, angstroms)).

The transition states are all concerted but with varying degrees of asynchronicity. The transition states involving ethylene TS(1−3)A are all nearly synchronous, with $\Delta r^{\ddagger}$ = 0.02 Å at most. The reactions of PTAD with cyclopentadiene TS1C and cyclohexadiene TS2C proceed through approximately synchronous transition structures, whereas the reaction with cycloheptadiene TS3C occurs through a highly asynchronous transition structure. The transition structures for the reactions of the cyclic dienes with unsymmetrical dienophiles, MVK TS(1−3)B and nitrosobenzene TS(1−3)D, are all asynchronous. The asynchronicity of the transition structures increases from cyclopentadiene to cycloheptadiene for the reactions of MVK ($\Delta r^{\ddagger}$ = 0.46−0.51 Å), PTAD ($\Delta r^{\ddagger}$ = 0.01− 0.55 Å), and nitrosobenzene ($\Delta r^{\ddagger}$ = 0.14−0.54 Å). The reactions of cyclohexadiene and cycloheptadiene are 7−15 kcal/mol more exothermic than the reactions of cyclopentadiene. Consistent with the Hammond postulate, the transition structures of cyclohexadiene and cycloheptadiene are earlier than with cyclopentadiene.

The distortion/interaction (or activation strain) model was applied in order to determine the origins of these differences in reactivity.[26] When applied to the intermolecular Diels−Alder reactions studied here, this model dissects the activation energy into the energies required to distort the diene ($\Delta E^{\ddagger}_{d-diene}$) and the dienophile ($\Delta E^{\ddagger}_{d-dienophile}$) into the transition state geometry without allowing them to interact and the interaction energy ($\Delta E^{\ddagger}_{i}$), which is the difference between the total distortion energy ($\Delta E^{\ddagger}_{d} = \Delta E^{\ddagger}_{d-diene} + \Delta E^{\ddagger}_{d-dienophile}$) and the activation energy ($\Delta E^{\ddagger}$).

Trends in activation enthalpies ($\Delta H^{\ddagger}$) are often described in terms of the relative heat of reactions (ΔHrxn). Such correlations are known as BEMA HAPOTHLE relationships developed from insight by Bell, Marcus, Hammond, Polanyi, Thornton, and

Leffler to explain and rationalize linear free energy relationships.[27] As shown in Figure 2, the activation enthalpies for the cycloadditions involving cyclic dienes do not correlate with the reaction enthalpies, whereas there is a better, if still rough, correlation between the activation energies and distortion energies. This modest correlation is a result of a wide range of interaction energies, from −5.5 to −20.9 kcal/mol, associated with the very different electronic properties of the dienophiles studied.

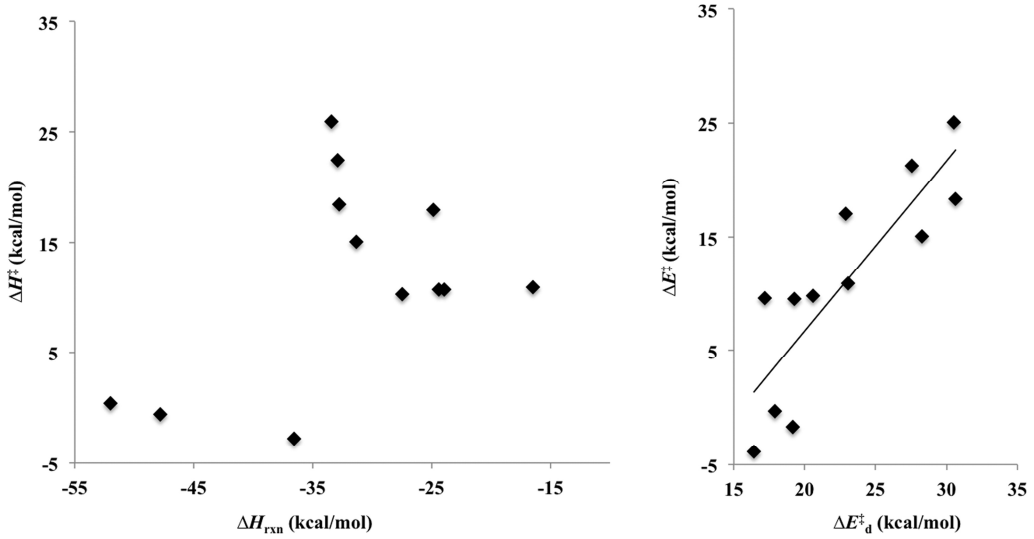

Figure 1.2 Plots of activation enthalpy (ΔH□) versus enthalpy of reaction (ΔH_{rxn}) (left, r^2 = 0.21, $\Delta H^{\square}$ = 0.42 ΔH_{rxn} + 25.0) and the activation energy (ΔE□) versus distortion energy (ΔE_d) (right, r^2 = 0.73, $\Delta E^{\square}$ = 1.50 ΔE_d – 23.2) for the reactions of cyclic dienes 1–3 with dienophiles A–D.

Figure 3 shows the distortion/interaction analysis for the Diels−Alder reactions of the cyclic dienes 1−3 with dienophiles A−D. For a given dienophile, the distortion energies of the dienophile are nearly constant to within 1−2 kcal/mol. The distortion energies of the dienes increase from 15.9 to 22.6 kcal/mol as the diene changes from cyclopentadiene to cycloheptadiene with ethylene TS(1−3)A and from 13.5 to 19.5 kcal/mol with MVK TS(1−3)B. The increases in the diene distortion energies parallel the increases in the activation energies among the cyclic dienes with ethylene and MVK.

MVK is a more reactive dienophile than ethylene because it has stronger interaction energies and smaller diene distortion energies, the latter being a result of the asynchronous transition structures that we will discuss later.

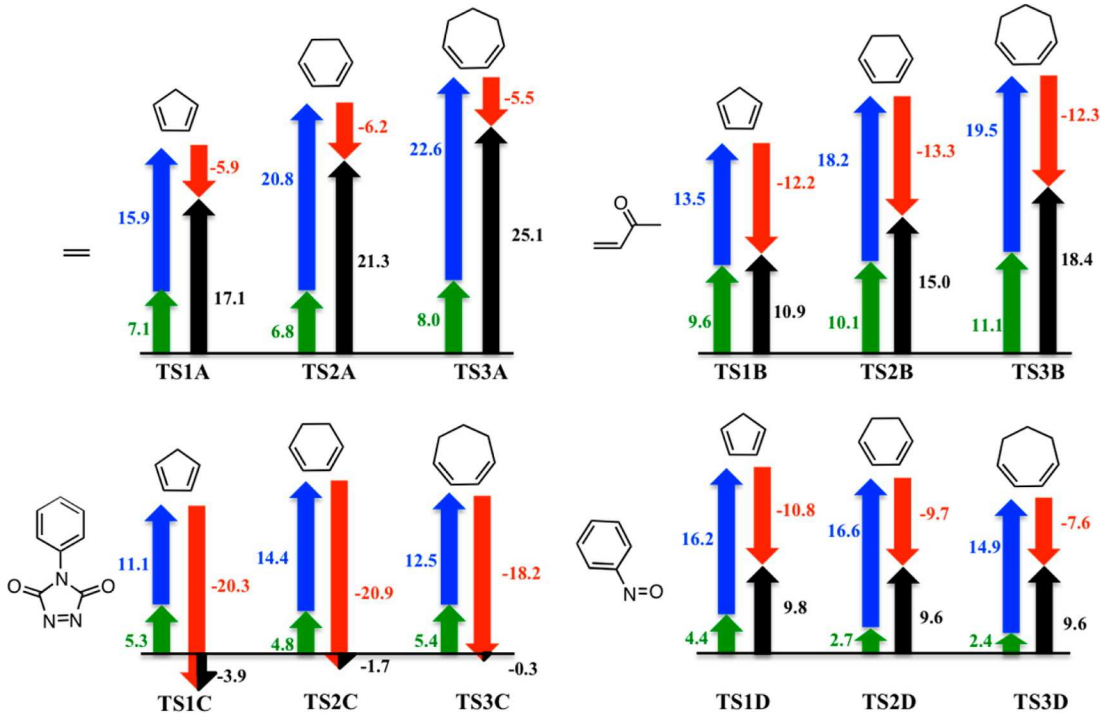

Figure 1.3 Plots of the distortion, interaction, and activation energies for the transition states involving dienophiles A–D and cyclic dienes 1–3 (green, distortion energy of dienophile; blue, distortion energy of diene; red, interaction energy; black, activation energy; in kcal/mol).

PTAD and nitrosobenzene show similar reactivities toward the three cyclic dienes because the differences in diene distortion are small. In the highly asynchronous transition state TS3C (0.54 Å), the diene distortion energy of cycloheptadiene is 12.5 kcal/mol, only 1.4 kcal/mol higher than that for cyclopentadiene TS1C and 1.9 kcal/mol lower than that for cyclohexadiene TS2C. For nitrosobenzene, the distortion energy of cycloheptadiene TS3D is 14.9 kcal/mol, 1.3 kcal/mol lower than that for cyclopentadiene TS1D and 1.7 kcal/mol lower than that for cyclohexadiene TS2D.

The interaction energies are nearly constant in reactions of the cyclic dienes with ethylene and MVK. However, the interaction energies decrease in the reactions involving PTAD and nitrosobenzene as the asynchronicity of the reaction increases. The interaction energy for the asynchronous transition structure of TS3C is lower than that of the synchronous transition states TS1C and TS2C by 2.1 and 2.7 kcal/mol, respectively. For the nitrosobenzene series, the interaction energies decreases from −10.8 kcal/mol with cyclopentadiene to −9.7 and −7.6 kcal/mol with cyclohexadiene and cycloheptadiene, respectively. This trend corresponds with the increase in asynchronicity, which results in similar diene distortion energies and decreasing interaction energies.

The distortion of each diene is associated with the pyramidalization of the diene termini required in order to form both new bonds simultaneously. Pyramidalization enables overlap of the hybrid orbitals at the diene termini with the π orbitals at the termini of the dienophile. As the dienophile approaches, the diene distorts from planarity at the termini of the C_1C_2 and C_3C_4 double bonds of the diene. This distortion unfavorably reduces the C_1C_2 and C_3C_4 π overlap. The dihedral angles θ_1 and θ_2, across the C_1C_2 and C_3C_4diene double bonds, measure the out-of-plane distortion of the carbon atoms in the diene bridge directly attached to the double bond. Figure 4 shows θ_1 in the transition structures for the reactions of ethylene with the cyclic dienes. The increase in diene distortion energy from cyclopentadiene to cycloheptadiene in the nearly synchronous transition structures, TS1A to TS3A, results from the increase in the out-of-plane distortion across the C_1C_2 and C_3C_4 double bonds in the transition structures. The difference in the transition state structures is reflected in the geometry of the Diels−Alder

adducts (Figure 5). With a longer diene bridge, θ_1 and θ_2 increase to minimize ring strain in the tether connecting C_1 to C_4.

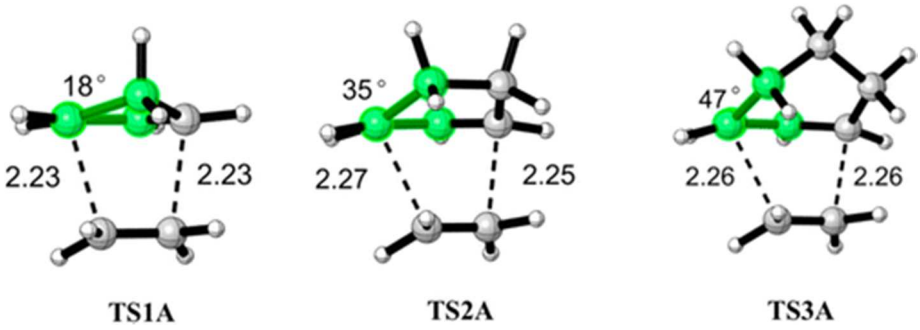

Figure 1.4 Nearly synchronous Diels–Alder transition structures of cyclic dienes, 1–3, with ethylene, showing dihedral angle θ_1 that measures the out-of-plane distortion along the C_1C_2 double bond of the diene. The highlighted atoms define θ_1.

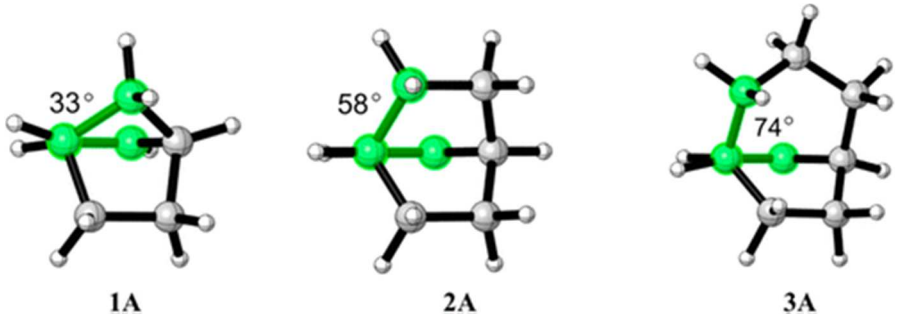

Figure 1.5 Diels–Alder adducts from the reactions of ethylene with cyclic dienes, 1–3, showing dihedral angle θ_1.

Figure 6 shows for the nearly synchronous transition structures with ethylene TS(1−3)A that the out-of-plane distortion is the same on each side of the diene such that $\theta_1 = \theta_2$. For asynchronous transition structures TS(1−3)D, the dihedral angle associated with the lesser-formed C−O bond is less distorted from the plane of the diene than the dihedral angle associated with the forming C−N bond. The sum of θ1 and θ2 ($\sum(\theta_1 + \theta_2)$) and the diene distortion energies for the synchronous reaction TS1A and the asynchronous reaction TS1D are nearly identical at 36° and 15.9 kcal/mol and 35° and

16.2 kcal/mol, respectively. For the reactions with cyclohexadiene, the $\sum(\theta_1 + \theta_2)$ is 70° for TS2A and the diene distortion energy is 20.8 kcal/mol compared to that of TS2D, where the $\sum(\theta_1 + \theta_2)$ is only 58° and the diene distortion energy is only 16.6 kcal/mol. For the reactions with cycloheptadiene, the $\sum(\theta_1 + \theta_2)$ is 94° and the diene distortion energy is 22.6 kcal/mol in the synchronous reaction TS3A compared to that for the highly asynchronous TS3D, where the $\sum(\theta_1 + \theta_2)$ is only 74° and the diene distortion energy is only 14.9 kcal/mol.

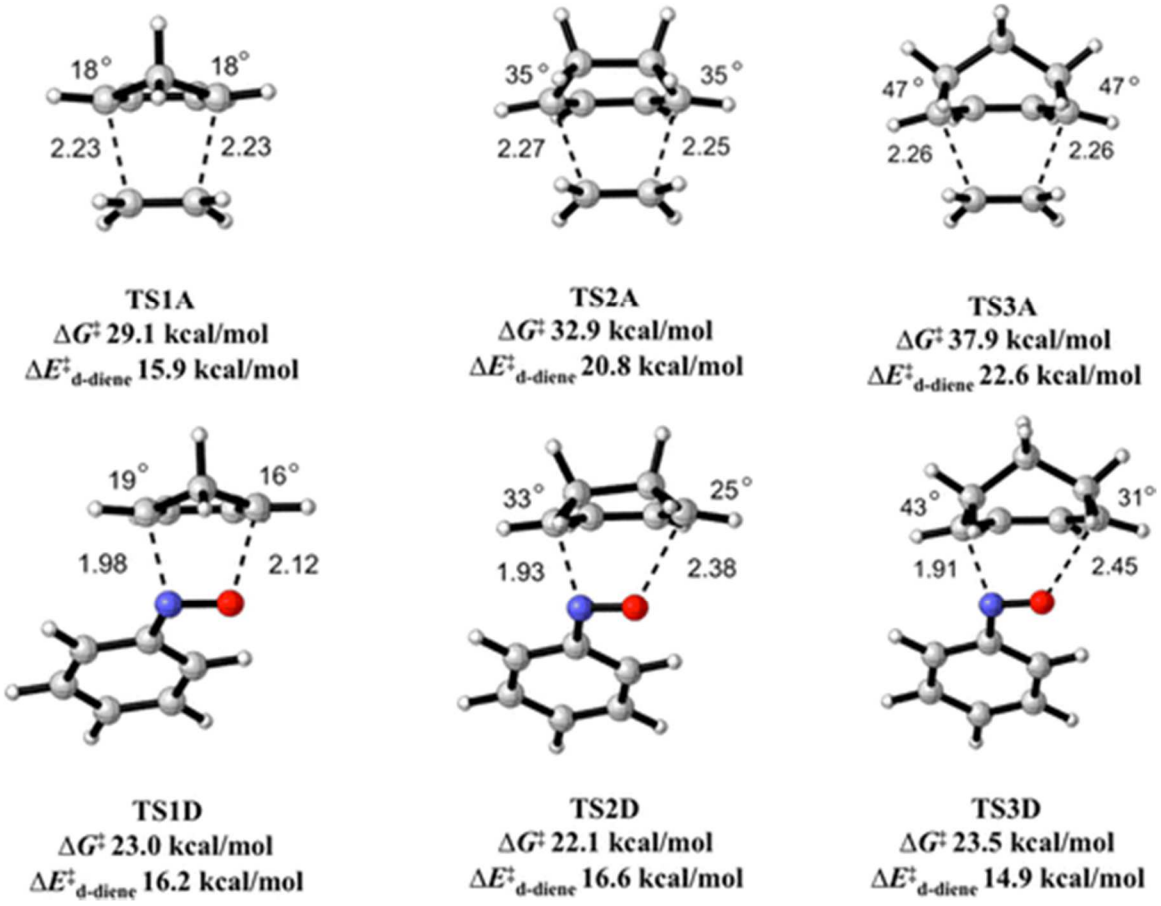

Figure 1.6 Transition structures for the reactions of dienes 1–3 with dienophiles A and D showing dihedral angle θ_1 across the C_1C_2 diene double bond and dihedral angle θ_2 across the C_3C_4 diene double bond.

Figure 7 shows the energetic cost for the out-of-plane distortion about the double bond of dienes 1−3, 1,3-butadiene, and 1,3-cyclooctadiene. The shorter rigid bridges of

cyclopentadiene and cyclohexadiene restrict the out-of-plane motion, resulting in a substantial increase in the force constants associated with the out-of-plane distortion. The 3- and 4-atom bridges of cycloheptadiene and cyclooctadiene are flexible enough that the force constants for the out-of-plane motion are similar to the model acyclic diene, 1,3-butadiene

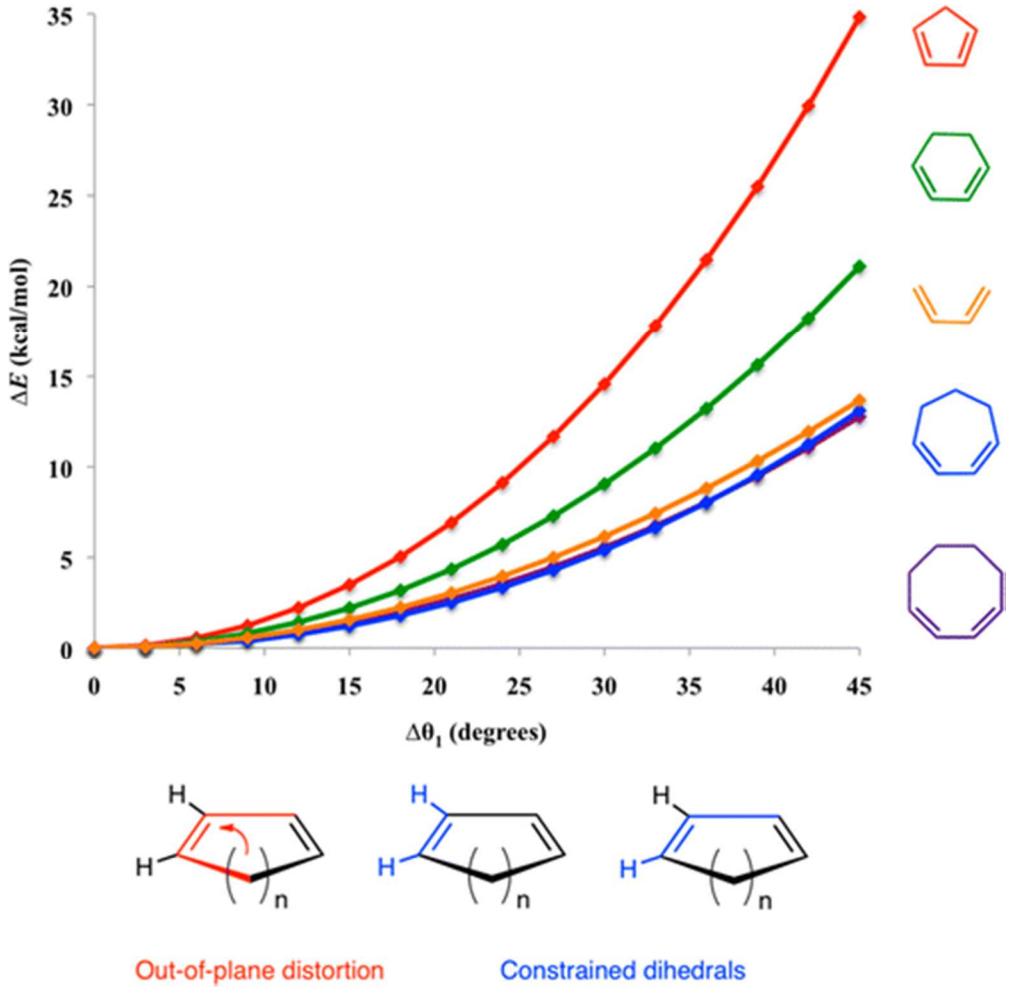

Figure 1.7 M06-2X/6-31+G(d)/CPCM(DCM) deformation energy (relative to fully optimized cyclic diene) for the out-of-plane motion ($\Delta\theta_1$) across the C_1C_2 double bond of dienes 1–3, 1,3-butadiene, and 1,3-cyclooctadiene from 0° to 45° in 5° increments.

1.5 Diels-Alder Reactivity of Cyanoethylenes with Cyclopentadiene

Having established the role of asynchronicity in the reactivity of cyclic dienes, we revisited the classic Sauer18 rate constants for the reactivities of cyclopentadiene with cyanoethylenes E−J. The nature of the transition states of these and other Diels− Alder reactions have been explored in many prominent studies,[19] most recently by Politzer, Murray, and co-workers.[20] They analyzed the asynchronicity of transition states of unsymmetrically substituted dienophiles, using the force constants along the reaction pathway, and found that highly asynchronous processes have two minima of the second derivative in the transition region, indicative of a stepwise formation of bonds even in the absence of an energetic intermediate.[20a] They also analyzed these reactions in terms of an electron density analysis[20b] and electrostatic potentials.[20c]

The experimental rate constants for the reactions of cyclopentadiene with the cyanoethylenes are summarized in Table 1 along with the computed activation free energies. Figure 8 shows a comparison of the M06-2X computed activation free energies ($\Delta G^{\ddagger}_{calc}$) and the log of the experimental rate constants. Previous studies have shown that the B3LYP functional poorly predicts the substituent effects for the reactions of tricyanoethylene and tetracyanoethylene with cyclopentadiene.[19k–l] The M06-2X functional predicts the correct reactivity pattern for the differently substituted cyanoethylenes. Both the experimental rates and computed activation barriers show that the reactivity increases with the number of electron withdrawing cyano substituents. The reason why 1,1-dicyanoethylene is 500 times more reactive than the cis- and trans-1,2-dicyanoethylene, as well as a theoretical explanation of all of these data, has been the focus of numerous computational studies.[19]

Table 1.1 Experimental Rate Constants and Calculated Activation Energies for the Reactions of Cyclopentadiene with Ethylene and Cyanoethylenes E–J.

dienophile	log k_{exp} [M^{-1} s^{-1}]	$\Delta G^{\ddagger}_{calc}$ (kcal/mol, 298 K)
ethylene (**TS1A**)	1.9[a]	29.1
acrylonitrile (**TS1E-*endo***)	5.0[b]	21.8
fumaronitrile (**TS1F**)	5.9[b]	16.8
maleonitrile (**TS1G-*endo***)	6.0[b]	16.2
vinylidene cyanide (**TS1H**)	9.7[b]	12.5
tricyanoethylene (**TS1I-*endo***)	10.7[b]	9.6
tetracyanoethylene (**TS1J**)	12.6[b]	5.9

[a]Adjusted to 293 K from ref 28. [b]Dioxane, 293 K; see ref 18.

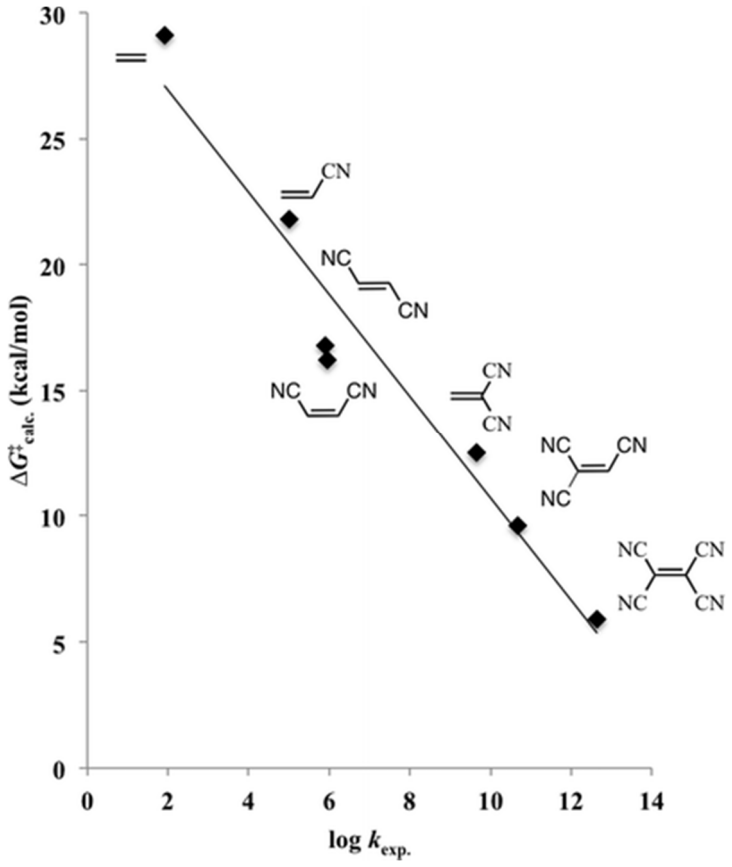

Figure 1.8 Plot of computed activation free energies (298 K) vs log k_{exp} (r^2 = 0.95, $\Delta G^{\ddagger}_{calc} = -2.0 \log k_{exp} + 31.0$).

Figure 9 shows the distortion/interaction analysis of these reactions. The difference in the reactivity between the unsymmetrically and symmetrically substituted dienophiles is related to both the energy required to distort cyclopentadiene and the interaction energy that has been discussed previously in terms of FMO interactions between the reactants. For the reactions of cyclopentadiene with ethylene A and cyanoethylenes E−J, the activation free energies range from 29.1 to 5.9 kcal/mol. The different reactivities along the series of dienophiles with cyclopentadiene results from increases in interaction energies as the number of cyano substituents on the dienophile increases. Figure 10 shows an excellent linear correlation of the transition state interaction energies with the number of cyano substituents. The interaction energies range from −5.9 to −30.0 kcal/mol and become 1−11 kcal/mol stronger with each additional cyano substituent.

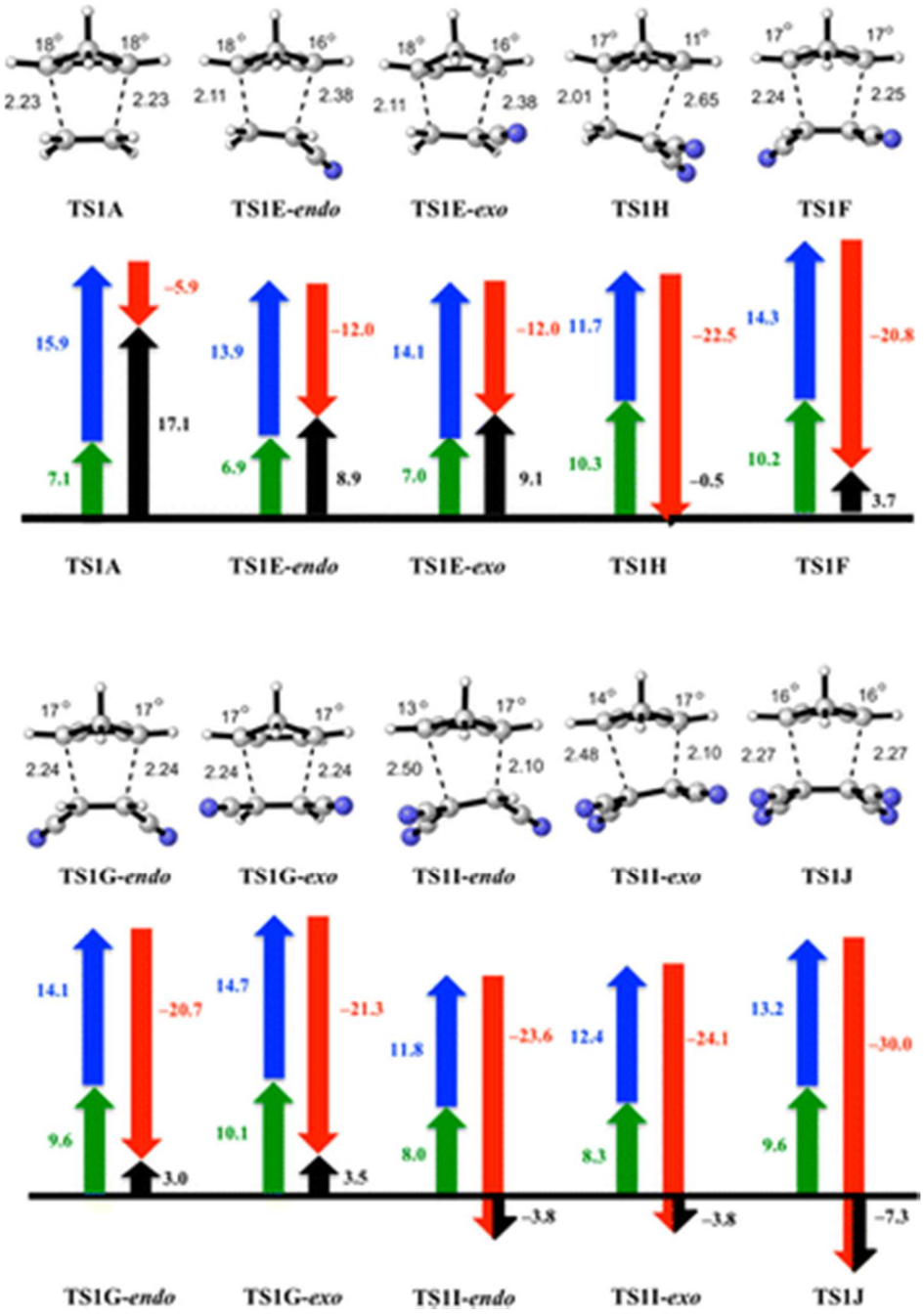

Figure 1.9 Optimized transition structures for reactions of cyclopentadiene with dienophiles A and E−J. The forming bond lengths are reported in angstroms, and dihedral angles for θ_1 and θ_2 are reported in degrees. Distortion, interaction, and activation energies for the transition structures are shown below each structure (green, distortion energy of dienophile; blue, distortion energy of diene; red, interaction energy; black, activation energy; in kcal/mol).

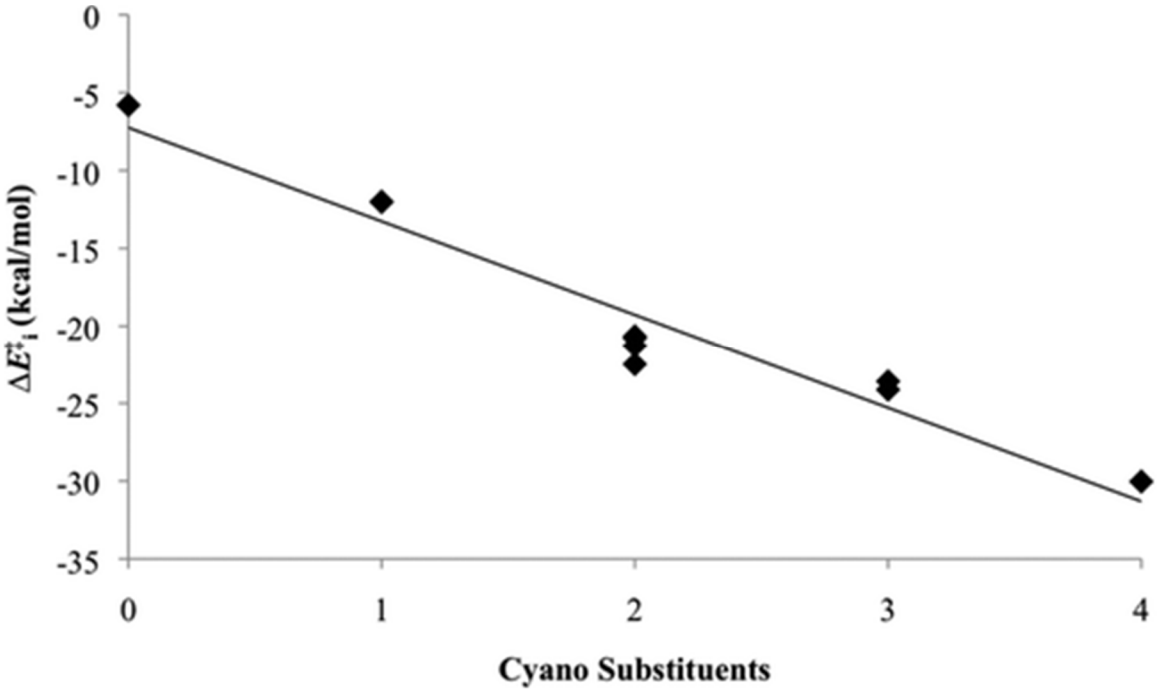

Figure 110 Plot of the interaction energy for the reactions of cyclopentadiene with dienophiles A and E–J vs the number of cyano substituents ($r^2 = 0.94$, $\Delta E^{\ddagger}_{i} = 6.0x - 7.3$).

The diene distortion energy for the reactions of cyclopentadiene with A and cyanoethylenes E−J ranges from 11.7 to 15.9 kcal/mol. Figure 11 shows an excellent linear relation between the diene distortion energy and the $\sum(\theta_1 + \theta_2)$, discussed earlier. The diene distortion energies increase as the out-of-plane distortion from the C_1C_2 and C_3C_4 double bonds increases. The range, however, is small in the context of the interaction energies, with only a 4.2 kcal/mol difference at most. The high reactivity of dicyanoethylenes is mainly due to the interaction energies, but the 500-fold increase in reactivity of 1,1-dicyanoethylene relative to that of the cis- and trans-1,2-dicyanoethylenes is a result of the asynchronous transition state with the former. The 2.4−3.0 kcal/mol lower cyclopentadiene distortion energy of the transition state with 1,1-dicyanoethylene is because only one terminus of the diene is distorted appreciably. This

is a result of a less fully formed C−C bond (2.65 Å) in TS1H and less distortion about the double bonds than that in the synchronous transitions states TS1F and TS1G.

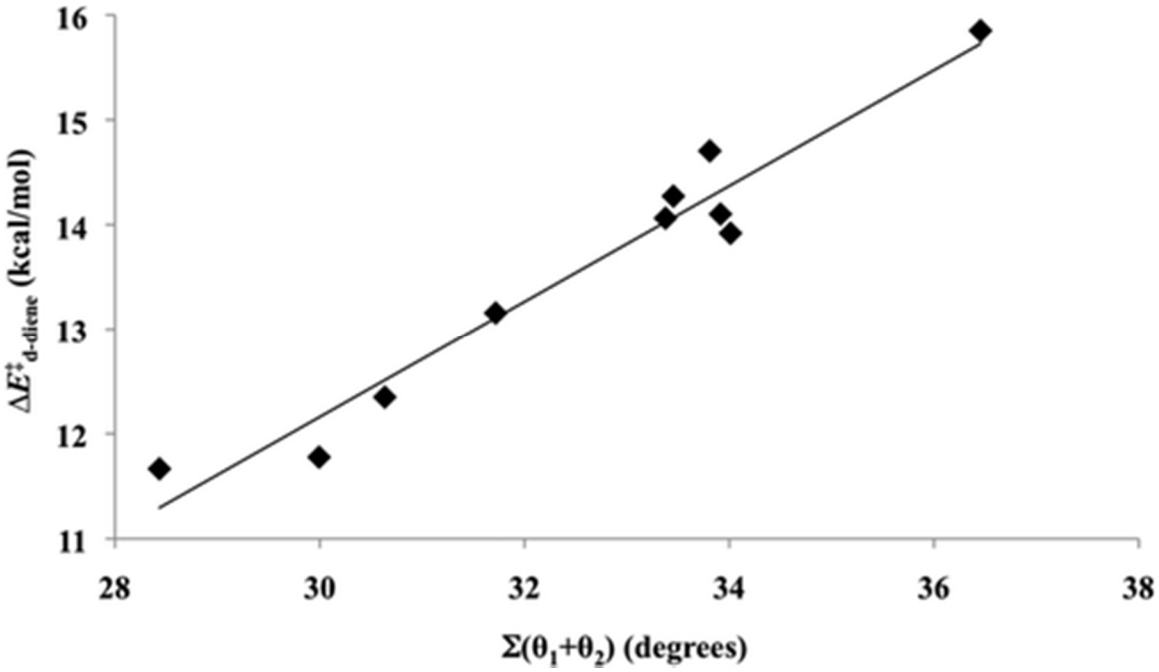

Figure 1.11. Plot of the diene distortion energy for the reactions of cyclopentadiene with dienophiles A and E–J against $\sum(\theta_1 + \theta_2)$ ($r^2 = 0.95$, $\Delta E^{\ddagger}_{d\text{–}diene} = 0.55 \sum(\theta_1 + \theta_2) – 4.4$).

1.6 Conclusions

The out-of-plane distortion across the C1C2 and C3C4 diene double bonds has a significant impact on the Diels−Alder reactivities of cyclic dienes. Cyclopentadiene is highly reactive in Diels−Alder reactions because only minimal out-of-plane distortion is required to achieve the transition state geometry compared with that of other cyclic and acyclic dienes. Asynchronous transition states have significant out-of-plane distortion about only one double bond. With heterodienophiles, such as nitrosobenzene and PTAD, the asynchronicity of the transition states results in similar reactivities for all three cyclic dienes.

1.7 References

(1) (a) Wyvratt, M. J.; Paquette, L. A. *J. Am. Chem. Soc.* **1974**, *96*, 4671. (b) Kentgen, G.; Balogh, W. D.; Ternansky, R. J.; Paquette, L. A. *J. Am. Chem. Soc*. **1983**, *105*, 5446. (c) Shi, Y.; Wilmot, J. T.; Nordstrøm, L. U.; Tan, D. S.; Gin, D. Y. *J. Am. Chem. Soc*. **2013**, *135*, 14313.

(2) Kron, J. S.; Huh, J. H.; Mrksich, M.; Houseman, B. T. *Nat. Biotechnol*. **2002**, *20*, 270.

(3) Samoshin, A. V.; Hawker, C. J.; de Alaniz, J. R. *ACS Macro. Lett*. **2014**, *3*, 753.

(4) Bian, S.; Scott, A. M.; Cao, Y.; Liang, Y.; Osuna, S.; Houk, K. N.; Braunschweig, A. B. *J. Am. Chem. Soc*. **2013**, *135*, 9240.

(5) SciFinder. https://scifinder.cas.org.

(6) Paton, R. S.; Kim, S. K.; Ross, A. G.; Danishefsky, S. J.; Houk, K. N. *Angew. Chem., Int. Ed*. **2011**, *50*, 10366.

(7) Worley, S. D.; Dewar, M. J. S. *J. Chem. Phys*. **1968**, *49*, 2454.

(8) Bischof, P.; Heilbronner, E. *Helv. Chim. Acta* **1970**, *53*, 1677.

(9) Perez Luna, A.; Ceschi, M. A.; Bonin, M.; Micouin, L.; Husson, H. P. *J. Org. Chem*. **2002**, *67*, 3522.

(10) Hennig, A.; Schwarlose, T.; Nau, W. N. *ARKIVOC* **2007**, *8*, 341.

(11) Templin, S. S.; Wallock, N. J.; Bennett, D. W.; Siddiquee, T.; Haworth, D. T.; Donaldson, W. A. J. *Heterocycl. Chem*. **2007**, *44*, 719.

(12) Kresze, G.; Schulz, G. *Tetrahedron* **1961**, *12*, 7.

(13) Yang, B.; Miller, M. J. *Org. Lett*. **2010**, *12*, 392.

(14) Alder, K.; Stein, G. *Angew. Chem*. **193**7, *50*, 510.

(15) (a) Martin, J. G.; Hill, R. K. *Chem. Rev*. **1961**, *61*, 542. (b) Craig, D.; Shipman, J. J.; Fowler, R. B. *J. Am. Chem. Soc*. **1961**, *83*, 2885.

(16) (a) Sustmann, R.; Bö hm, M.; Sauer, *J. Chem. Ber*. **1979**, *112*, 883. (b) Pfeffer, H. U.; Klessinger, M. *Chem. Ber*. **1979**, *112*, 890.

(17) (a) Andrews, L. J.; Keefer, L. M. *J. Am. Chem. Soc*. **199**5, *77*, 6284. (b) Holliday, R. E.; Hamer, J. *J. Org. Chem*. **1963**, *28*, 3034.

(18) Sauer, J.; Wiest, H.; Mielert, A. *Chem. Ber*. **1964**, *97*, 3183.

(19) (a) Munchausen, L. L.; Houk, K. N. *J. Am. Chem. Soc*. **1976**, *4*, 937. (b) Houk, K. N.; Loncharich, R. J.; Blake, J. F.; Jorgensen, W. L. *J. Am. Chem. Soc*. **1989**, *111*, 9172. (c) Karcher, T.; Sicking, W.; Sauer, J.; Sustmann, R. *Tetrahedron Lett*. **1992**, *33*, 8027. (d) Jorgensen, W. L.; Lim, D.; Blake, J. F. *J. Am. Chem. Soc*. **1993**, *115*, 2936. (e) Jursic, B. S. *J. Mol. Struct.: THEOCHEM* **1995**, 358, 139. (f) Branchadell, V. *Int. J. Quantum Chem.* **199**7, *61*, 381. (g) Froese, R. D.; Humbel, S.; Svensson, M.; Morokuma, K. *J. Phys. Chem. A* **1997**, *101*, 227. (h) Froese, R. D.; Coxon, J. M.; Wesr, S. C.; Morokuma, K. *J. Org. Chem*. **1997**, *62*, 6991. (i) Coxon, J. M.; Froese, R. D.; Ganguly, B.; Marchand, A. P.; Morokuma, K. *Syn. Lett*. **1999**, *11*, 1681. (j) Hehre, J. W. A Guide to Molecular Mechanics and Quantum Chemical Calculations; Wavefunction, Inc.: Irvine, CA, 2003; p 304. (k) Domingo, L. R.; Aurell, M. J.; Perez, P.; Contreras, R. *J. Org. Chem*. **2003**, *68*, 3884. (m) Jones, G. O.; Guner, V. A.; Houk, K. N. J. Phys. *Chem. A* **2006**, *110*, 1216.

(20) (a) Yepes, D.; Donoso-Tauda, O.; Murray, J. S.; Politzer, P.; Jaque, P. *Phys. Chem. Chem. Phys.* **2013**, *15*, 7311. (b) Yepes, D.; Murray, J. S.; Domingo, L. R.; Politzer, P.; Jaque, P. *Phys. Chem. Chem. Phys*. **2014**, *16*, 6726. (c) Murray, J. S.; Yepes, D.; Jaque, P.; Politzer, P. *Comput. Theor. Chem*. **2015**, *1052*, 270−280.

(21) Frisch, M. J.; Trucks, G. W.; Schlegel, H. B.; Scuseria, G. E.; Robb, M. A.; Cheeseman, J. R.; Scalmani, G.; Barone, V.; Mennucci, B.; Petersson, G. A.; Nakatsuji, H.; Caricato, M.; Li, X.; Hratchian, H. P.; Izmaylov, A. F.; Bloino, J.; Zheng, G.; Sonnenberg, J. L.; Hada, M.; Ehara, M.; Toyota, K.; Fukuda, R.; Hasegawa, J.; Ishida, M.; Nakajima, T.; Honda, Y.; Kitao, O.; Nakai, H.; Vreven, T.; Montgomery, J. A., Jr.; Peralta, J. E.; Ogliaro, F.; Bearpark, M.; Heyd, J. J.; Brothers, E.; Kudin, K. N.; Staroverov, V. N.; Kobayashi, R.; Normand, J.; Raghavachari, K.; Rendell, A.; Burant, J. C.; Iyengar, S. S.; Tomasi, J.; Cossi, M.; Rega, N.; Millam, M. J.; Klene, M.; Knox, J. E.; Cross, J. B.; Bakken, V.; Adamo, C.; Jaramillo, J.; Gomperts, R.; Stratmann, R. E.; Yazyev, O.; Austin, A. J.; Cammi, R.; Pomelli, C.; Ochterski, J. W.; Martin, R. L.; Morokuma, K.; Zakrzewski, V. G.; Voth, G. A.; Salvador, P.; Dannenberg, J. J.; Dapprich, S.; Daniels, A. D.; Farkas, Ö.; Foresman, J. B.; Ortiz, J. V.; Cioslowski, J.; Fox, D. J. Gaussian 09, Revision D.01; Gaussian, Inc.: Wallingford CT, 2009.

(22) Zhao, Y.; Truhlar, D. G. *Theor. Chem. Acc.* **2008**, *120*, 215.

(23) (a) Pieniazek, S.; Houk, K. N. *Angew. Chem.* **2006**, *118*, 1470. (b) Pieniazek, S.; Clemente, F. R.; Houk, K. N. *Angew. Chem., Int. Ed*. **2008**, *47*, 7746.

(24) Barone, V.; Cossi, M. *J. Phys. Chem. A* **1998**, *102*, 1995.

(25) Cossi, M.; Rega, N.; Scalmani, G.; Barone, V. *J. Comput. Chem*. **2003**, *24*, 669.

(26) (a) Ess, D. H.; Houk, K. N. *J. Am. Chem. Soc*. **2007**, *129*, 10646. (b) Ess, D. H.; Houk, K. N. *J. Am. Chem. Soc*. **2008**, *130*, 10187. (c) Hayden, A. E.; Houk, K. N. *J. Am.*

Chem. Soc. **2009**, *131*, 4084. (d) van Zeist, W. J.; Bickelhaupt, F. M. *Org. Biomol. Chem*. **2010**, *8*, 3118. (e) Liu, F.; Paton, R. S.; Kim, S.; Liang, Y.; Houk, K. N. *J. Am. Chem. Soc*. **2013**, *135*, 15642. (f) Fernandez, I.´ *Phys. Chem. Chem. Phys*. **2014**, 16, 7662. (g) Fernandez, I.; Bickelhaupt, F. M.´ *Chem. Soc. Rev*. **2014**, *43*, 4953.

(27) Jencks, W. P. *Chem. Rev*. **1985**, *85*, 511.

(28) Walsh, R.; Wells, J. M. *J. Chem. Soc., Perkin Trans*. **1972**, *2*, 52.

(29) Legault, C. Y. CYLview, 1.0b; Université de Sherbrooke: Sherbrooke, QC, Canada, 2009; http://www.cylview.org.

Chapter 2. Diels-Alder Reactivity of 5-substituted Cyclopentadienes

2.1 Introduction to 5-subbstituted Diels-Alder reactions

Aromaticity has long been a topic of great interest and increasing influence.[1] The effect of aromaticity on reactivity is well established and one of the defining characteristics of aromaticity. Nyuászi and Schleyer showed that the aromatic character of cyclopentadiene is tunable through substituents at the 5-position.[2] They demonstrated that the aromaticity of 5,5-disilylcyclopentadiene is comparable to that of furan, and that 5,5-difluorocyclopentadiene is antiaromatic. The aromatic or antiaromatic character of 5-substituted cyclopentadienes results from hyperconjugative aromaticity and antiaromaticity, a concept that describes the hyperconjugative interactions of the C_5-X bonds and the termini of the diene π-system resulting in aromaticity (6π electron) or antiaromaticity (4π electron).

We have explored the role of hyperconjugative aromaticity on the reactivity of 5-substituted cyclopentadienes in the Diels–Alder reaction. We show how the stabilization through hyperconjugative interactions reduces the reactivity by increasing the energy to distort the cyclopentadiene to the transition state geometry while negative hyperconjugation destabilizes the cyclopentadiene and increases reactivity. Burnell earlier reported an extensive study on the Diels–Alder cycloadditions of 5-X-substituted cyclopentadienes with a focus on the syn and anti stereoselectivity. He noted the role of

distortion energies (called deformation energies) on the selectivity.[3] We have also explored this type of stereoselectivity using modern density functional theory (DFT), and those results will be reported at a later time (Zou et al., in preparation). We are delighted to honor Paul Schleyer by showing how a concept he created explains a very large and surprising substituent effect on reactivity.

The high reactivity and thermal reversibility of cyclopentadiene in the Diels–Alder reaction have been exploited in a variety of applications including the immobilization of biomolecules, protecting groups, functionalization of materials, and thermally responsive polymers.[4] Replacement of the C5 carbon center in cyclopentadiene with an O, N, or S heteroatom results in aromaticity and limited Diels–Alder reactivity compared to cyclopentadiene (Scheme 1a).[5,6] For example, the Diels–Alder reactions of thiophenes with highly reactive dienophiles such as maleic anhydride require extreme conditions.[5d] Pyrroles require activation through the installation of electron-withdrawing groups on the nitrogen atom to favor the [4 + 2] cycloaddition over the competing Michael addition.[5c,7] Scheme 1b shows the Diels–Alder reactivity of 5-(trimethyl)silylcyclopentadiene and 5-fluorocyclopentadiene.[6] With electronically similar dienophiles, 5-fluorocyclopentadiene is more reactive than 5-(trimethyl)silylcyclopentadiene.

Scheme 2.1 a) Diels‑Alder reactions of maleic anhydride with cyclopentadiene, furan, pyrrole, and thiophene.[5] b) Diels‑Alder reactions of dimethyl acetylenedicarboxylate (DMAD) with 5-fluorocyclopentadiene and dimethyl maleate with (trimethyl)silylcyclopentadiene.[6]

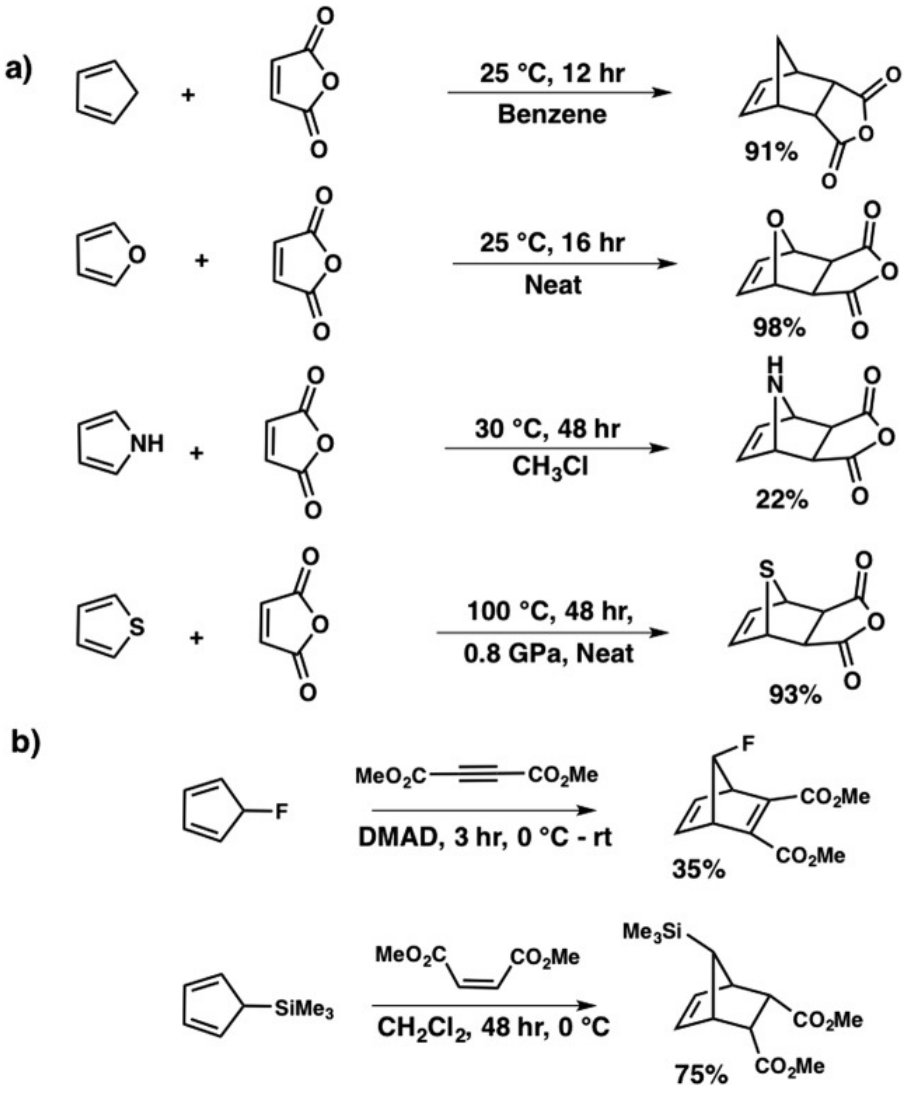

To compare the reactions of aromatic dienes to 5‑substituted cyclopentadienes, the activation energies for the Diels–Alder reactions of 5,5‑difluorocyclopentadiene (1), 5‑

fluorocyclopentadiene (2), cyclopentadiene (3), 5-silylcyclopentadiene (4), and 5,5-disilylcyclopentadiene **(**5**)** with ethylene and maleic anhydride have been explored here using DFT. We have compared these dienes to the aromatic dienes: furan **(**6**)**, thiophene **(**7**)**, and pyrrole **(**8**)**, to probe and understand the effect of hyperconjugative aromaticity and antiaromaticity on the Diels–Alder reactivity.

2.2 Computational Methods

All quantum mechanical calculations were performed with Gaussian 09.[8] Geometries were optimized using the M06-2X[9] density functional with the 6-31G(d) basis set. Normal mode analysis confirmed that all reactants and products are minima and that the transition states are first-order saddle points. Thermal corrections and enthalpies were computed from unscaled M06-2X/6-31G(d) frequencies at 298 K. Single-point energies were calculated with the 6-311++G(d,p) basis set.

2.3 Influence of the 5-substitutent on Ground State Stability

The aromatic stabilization energy (ASE) of each diene was calculated using the isodesmic reaction shown in Figure 1a, proposed by Schleyer to assess the aromatic stabilization energies (ASE).[2] This relates the stability of the potentially cyclic delocalized cyclopentadiene to nonconjugated molecules with the same number and types of double bonds, but no cyclic delocalization. Schleyer reported B3LYP values earlier.[2] The calculated reaction enthalpy for the isodesmic reaction with cyclopentadiene is unfavorable by 3.6 kcal/mol, indicative of the stabilization by conjugation. The reaction enthalpies for 5,5-difluorocyclopentadiene and 5-fluorocyclopentadiene are

favorable: −8.9 kcal/mol and −3.9 kcal/mol, respectively. This is a result of ground state destabilization associated with negative hyperconjugation that leads to hyperconjugative antiaromaticity. The reaction enthalpies of 5,5-disilylcyclopentadiene and 5-silylcyclopentadiene are unfavorable: 10.3 kcal/mol and 7.4 kcal/mol, respectively. The unfavorable reaction enthalpies result from the ground state stabilization associated with hyperconjugative aromaticity. The fluorines are hyperconjugatively electron withdrawing giving the cyclopentadiene 4-electron cyclic delocalization, that is, antiaromaticity. Electron donation from the silyl groups leads to 6-electron aromatic character.

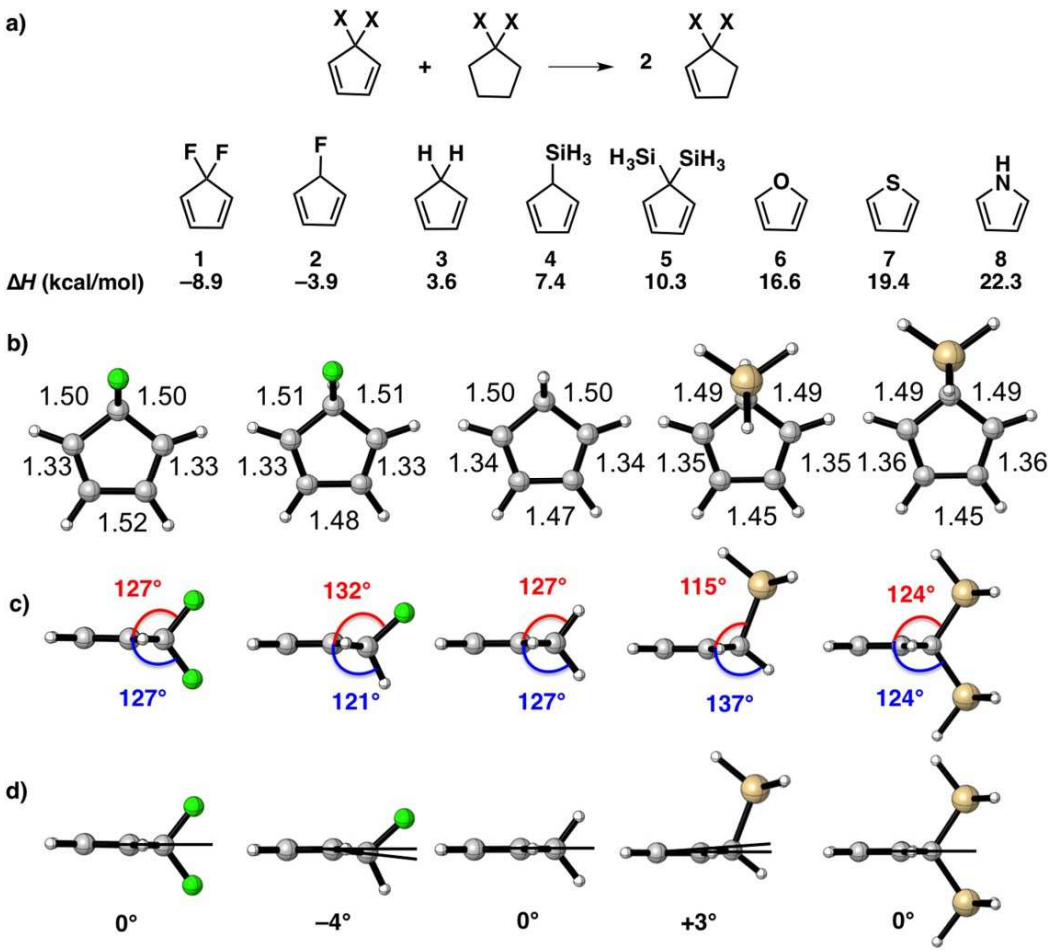

Figure 2.1 a) Isodesmic equation and ASE of dienes 1–8. b) Calculated bond lengths in the ground states of dienes 1–5 reported in Ångstroms. c) $\theta_{C5\text{-}X}$, the angle between the C_5-X bonds and the plane of the diene. d) θ_{C5}, the angle between the $C_1C_4C_5$ plane and the C_1C_4 plane.

Figures 1b–1d show that the C_5 substituents also influence the diene geometries. The equalization of bond lengths due to the cyclic electron delocalization is a structural measure of aromaticity.[2,10] As the 5-substituent on cyclopentadiene becomes a stronger hyperconjugative donor, the diene bond lengths equalize. That is, the C_2-C_3 bonds shorten from 1.52 to 1.45 Å and the C_1=C_2 bonds elongate from 1.33 to 1.36 Å between **1** and **5** (Fig. 2b). In the bond localization index,[11] maximum deviation of the diene C-C bond lengths ranges from 0.019 Å with **1** to 0.09 Å with **5**. The symmetrically substituted dienes: 5,5-difluorocyclopentadiene, cyclopentadiene, and 5,5-disilylcyclopentadiene, are planar with C_{2v} symmetry. The C_5-X and C_5-H bonds of 5-fluorocyclopentadiene and 5-silylcyclopentadiene are distorted relative to the plane of the diene (Fig. 2c). $\theta_{C5\text{-}X}$ describes the angle between the C_5-X bond and the $C_1C_4C_5$ plane of the diene. The C_5-F bond of 5-fluorocyclopentadiene distorts away from the plane of the diene to minimize the unfavorable overlap of the σ* C_5-F bond with the cyclopentadiene π-system that results in hyperconjugative antiaromaticity. To maximize the effect of hyperconjugative aromaticity in 5-silylcycopentadiene, the C_5-

SiH_3 bond distorts toward the plane of the diene. The distortion of the C_5-X bond is accompanied by the raising or lowering of C_5 carbon atom from the plane of the diene into an envelope conformation (Fig. 2d). θ_{C5} is the angle of the $C_1C_4C_5$ plane with regards to the C_1-C_4 plane. In 5-silylcyclopentadiene the inward rotation of the C_5-SiH_3 bond distorts the C_5 carbon 3° in an endo direction. There is an opposite 4° exo distortion of the C_5 carbon in 5-fluorocyclopentadiene.

2.4 Reactivity Trends of 5-substituted Cyclopentadienes

Figure 2 shows the transition state geometries with the activation free and reaction free energies for the reactions of dienes 1–5 with ethylene. There are two possible transition states for the reactions of 5-fluorocyclopentadiene and 5-silylcyclopentadiene with ethylene. The cycloaddition can occur on the face syn or anti to the C_5-X substituent. As noted earlier, Burnell and coworkers established that the π-facial selectivity of cycloadditions involving 5-substituted cyclopentadienes is controlled by the deformation, or distortion energy.3 Consistent with experimental and computational studies, the syn transition state of 5-fluorocyclopentadiene and the anti transition state of 5-silylcyclopentadiene are the favored transition states.[6] More details on the stereoselectivities of these and other 5-substituted cyclopentadienes will be reported in a future paper (Zou et al., in preparation).

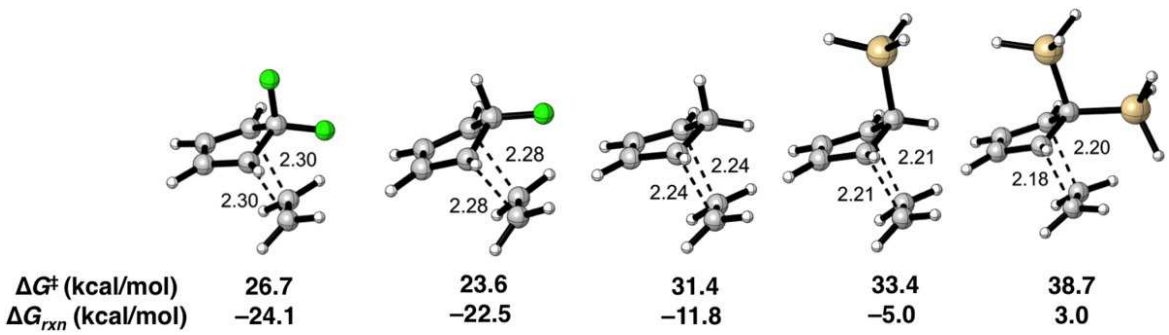

Figure 2.2 Transition structures for the reaction of dienes 1–5 with ethylene. The forming bond lengths are reported in Ångstroms.

The activation free energy for the reaction of cyclopentadiene with ethylene is 31.4 kcal/mol. Fluorination lowers the activation free energies to 26.7 and 23.6 kcal/mol for 5,5-difluorocyclopentadiene and 5-fluorocyclopentadiene, respectively. Silylation raises the activation free energies to 33.4 and 38.7 kcal/mol for 5-silylcyclopentadiene and 5,5-disilylcyclopentadiene, respectively. The activation energy for the reaction of 5,5-disilylcyclopendaiene is comparable to that of the aromatic dienes 6–8, with activation free energies between 35.1 and 43.0 kcal/mol (S1). The Diels–Alder reactions of the 5-substituted cyclopentadienes with the electron-deficient dienophile, maleic anhydride, show similar reactivity patterns as ethylene (discussed later), with activation barriers 7–12 kcal/mol lower. We analyze the ethylene reactions here to avoid complications due to interactions of the dienophile substituents and the diene.

Figure 3a shows a plot of the ASE versus the activation free energies of reactions with ethylene. Interestingly, the differences in ΔGrxn are about 1.4 times the ΔASE, indicating that substituents also have a significant effect on product stability. The Diels–

Alder adduct from the reaction of 5,5disilylcyclopentadiene with ethylene is endergonic by 3.0 kcal/mol. The Diels–Alder reactions of dienes 1–4 with ethylene are exergonic by −4.5 to −24.1 kcal/mol.

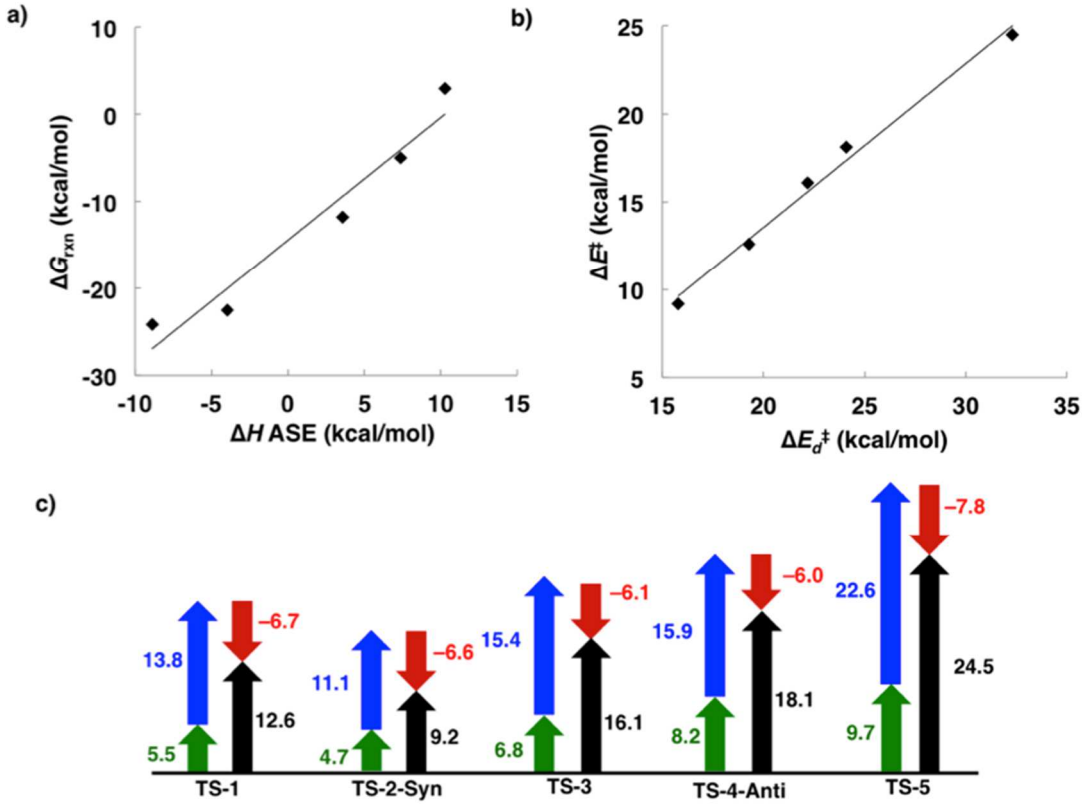

Figure 2.3 a) Plot of the ASE (ΔH) versus free energy of reaction (ΔG_{rxn}), $\Delta G_{rxn} = 1.4\ \Delta_{ASE} - 14.4$, $r^2 = 0.95$. b) Plot of the activation energy ($\Delta E^{‡}$) versus distortion energy ($\Delta E^{‡}_{d}$), $\Delta E^{‡} = 0.93\Delta E^{‡}_{d} + 5.0$, $r^2 = 0.99$. c) Plots of the distortion, interaction, and activation energies for the transition states involving dienes **1**–**5** with ethylene (black, activation energy; green, distortion energy of the dienophile; blue, distortion energy of the diene; red, interaction energy;inkcal/mol).

To understand the origin of the reactivity differences in the series of 5substituted cyclopentadienes, the activation energies (ΔE‡) have been analyzed with the distortion/interaction model.[12] The distortion/interaction model relates the activation energy to the energy required to geometrically distort the reactant ground state structures

into the corresponding transition state structures ($\Delta E^{\ddagger}_{d}$). The interaction energy ($\Delta E^{\ddagger}_{i}$) results from all interactions between the distorted reactants in the transition state, including charge transfer (e.g., HOMO□LUMO), electrostatic, polarization, and closed□ shell repulsion. Figure 4b shows a plot of the activation energy versus the distortion energy. The energy required to distort the diene and ethylene into the transition state geometry controls the reactivity, and the interaction energy changes are much less across the series.

Figure 4c shows the results from the distortion interaction analysis. The interaction energies range from −6 to −8 kcal/mol and are strongest in transition states with a substituent syn to ethylene. The dienophile distortion ranges from 5 to 10 kcal/mol. Part of this difference is related to the shift from an earlier transition state for 5,5□ difluorocyclopentadiene with forming C-C bond lengths of 2.30 Å to the later transition state of 5,5□disilylcyclopentadiene with forming C-C bond lengths of 2.18 and 2.20 Å. The largest differences in distortion occur in the diene, and range from 11 to 23 kcal/mol.

The distortion of each diene is associated with changes in $\theta_{C5\text{-}X}$ and θ_{C5} between the ground and transition states. Figures 4a and 4b show the values of in $\theta_{C5\text{-}X}$ and θ_{C5} in the transition states of dienes 1–5 with ethylene. In $\theta_{C5\text{-}X}$ is larger for the substituent syn to ethylene compared to the substituent anti to ethylene in the transition state. The differences between in $\theta_{C5\text{-}X}$ in the transition states of substituted cyclopentadienes results

from the staggering of the syn $C_{5\text{-}X}$ bond with the C_1-H, C_4-H, and the forming bonds in the transition state (Fig. 5).

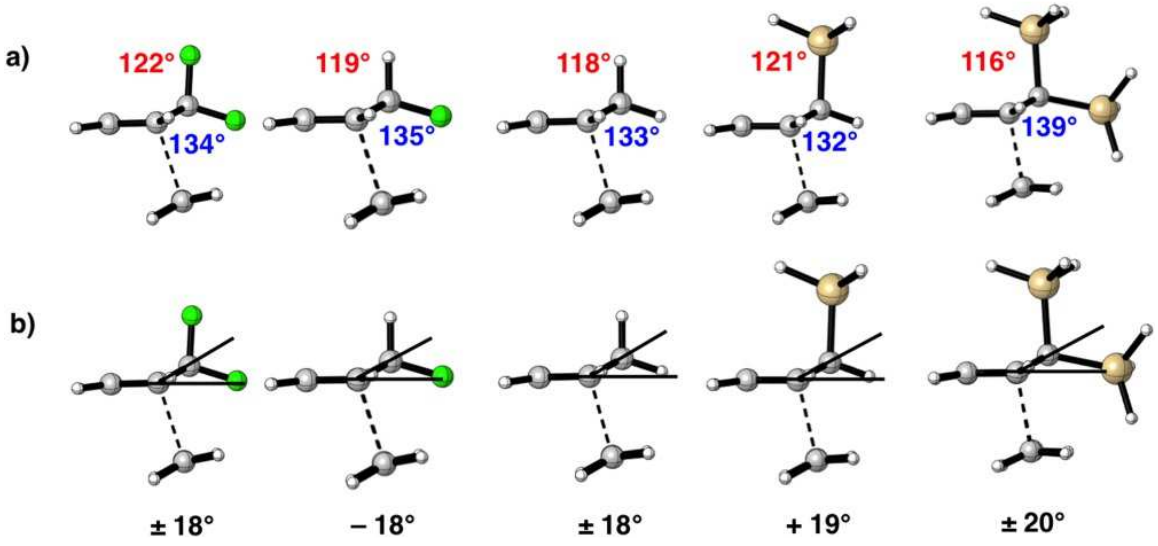

Figure 2.4 a) in $\theta_{C5\text{-}X}$ and θ_{C5} in the Diels–Alder transition states of dienes 1–5 with ethylene. θC5 - X is the angle between the $C_{5\text{-}x}$ bond and the $C_1C_4C_5$ plane. b) θ_{C5} for Diels–Alder transition states of dienes 1–5 with ethylene. θ_{C5} is the angle between the $C_1C_4C_5$ plane and the C_1C_4 plane.

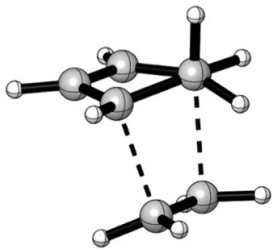

Figure 2.5 Newman projection along the C_1-C_5 bond in the cyclopentadiene - ethylene transition state showing staggering of the bonds to C_5 and to C_1.

The reactivities of cyclopentadienes are controlled by the energy required to distort the diene from a planar to envelope geometry,13 and the change in $\theta_{C5\text{-}X}$ that accompanies this change. In the transition states of dienes 1–6, θ_{C5} ranges from 17 to 20°.

These slight differences in θ_{C5} result from the differences in the positions of the transition states along the reaction coordinate. Figure 7 shows the energetic cost of distorting the $C_1C_4C_5$ plane from the C_1C_4 plane to adopt the envelope geometry of the transition state. For planar dienes (1, 3, 5, and 6) the difficulty of this distortion parallels the aromatic character of diene. Predistortion of 5-fluorocyclopentadiene and 5-silylcyclopentadiene toward the envelope geometry of the transition state lessens the diene distortion and increases the reactivity by a few tenths of a kcal/mol. The $\Delta\theta_{C5}$ from the ground state to transition state geometry, however, differs among the dienes from 14 to 20°. The change in θC5 for 5-fluorocyclopentadiene is only 14°, compared to 18° for 5,5-difluorocyclopentadiene, and the change in $\theta_{C5\text{-}X}$ for 5-fluorocyclopentadiene is only 5° compared to 12° for 5,5-difluorocyclopentadiene. The accelerated reactivity of 5-fluorocyclopentadiene compared to the highly destabilized hyperconjugative antiaromatic 5,5-difluorocyclopentadiene is the result of less distortion about θ_{C5} and $\theta_{C5\text{-}X}$.

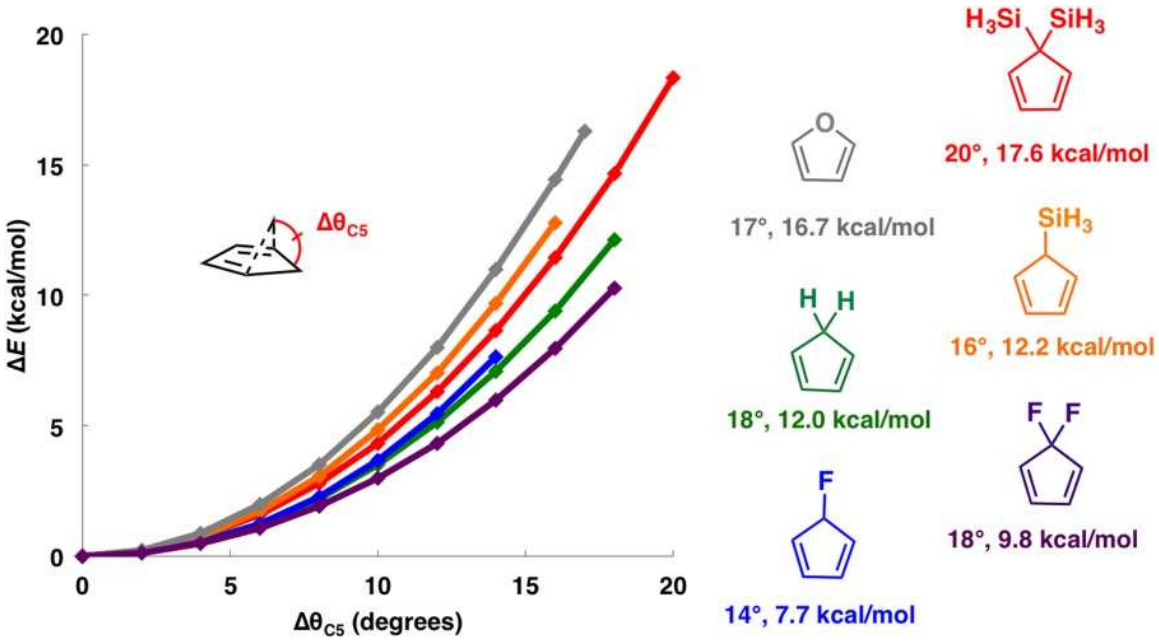

Figure 2.6 M06-2X/6-31G(d) deformation energy (relative to fully optimized diene) for the out-of-plane motion of the C5atom between the ground and transition state geometries.

The endo transitions states for the Diels–Alder reactions of maleic anhydride with dienes 1–5 are shown in Figure 8a. The activation free energies range from 14.7 to 29.3 kcal/mol and are 7 to 12 kcal/mol lower than with ethylene as the dienophile. The distortion/interaction analysis for the transition states of dienes 1–5 with maleic anhydride is shown in Figure 8b. The diene distortions of 1–5 with maleic anhydride are nearly identical as in reactions with ethylene, differing 1 kcal/mol at most. Maleic anhydride is slightly more difficult to distort into the transition state geometry than ethylene by 0.4–2.6 kcal/mol.

The lower activation barriers in the Diels–Alder reactions of dienes 1–5 with maleic anhydride are a result of the interaction energies, which are 9–15 kcal/mol more favorable than the interaction energies with ethylene. A consequence of the electron deficiency of maleic anhydride and the favorable secondary orbital interactions present in

the endo transition state. The interaction energies in the transition states of dienes 1–5 with maleic anhydride range from −15 to −23 kcal/mol, and increase as the 5substituent becomes a better donor. Calculations indicated that the HOMOs of the 5substituted dienes range from −9.4 to 8.4 eV (HOMO energies calculated at the HF/6 311++G(d,p)//M06 2X/6 31G(d) level). The general trend is that the HOMO energy increases as the 5substituent becomes a stronger donor resulting in a smaller HOMO LUMO gap between the 5substituted diene and maleic anhydride.

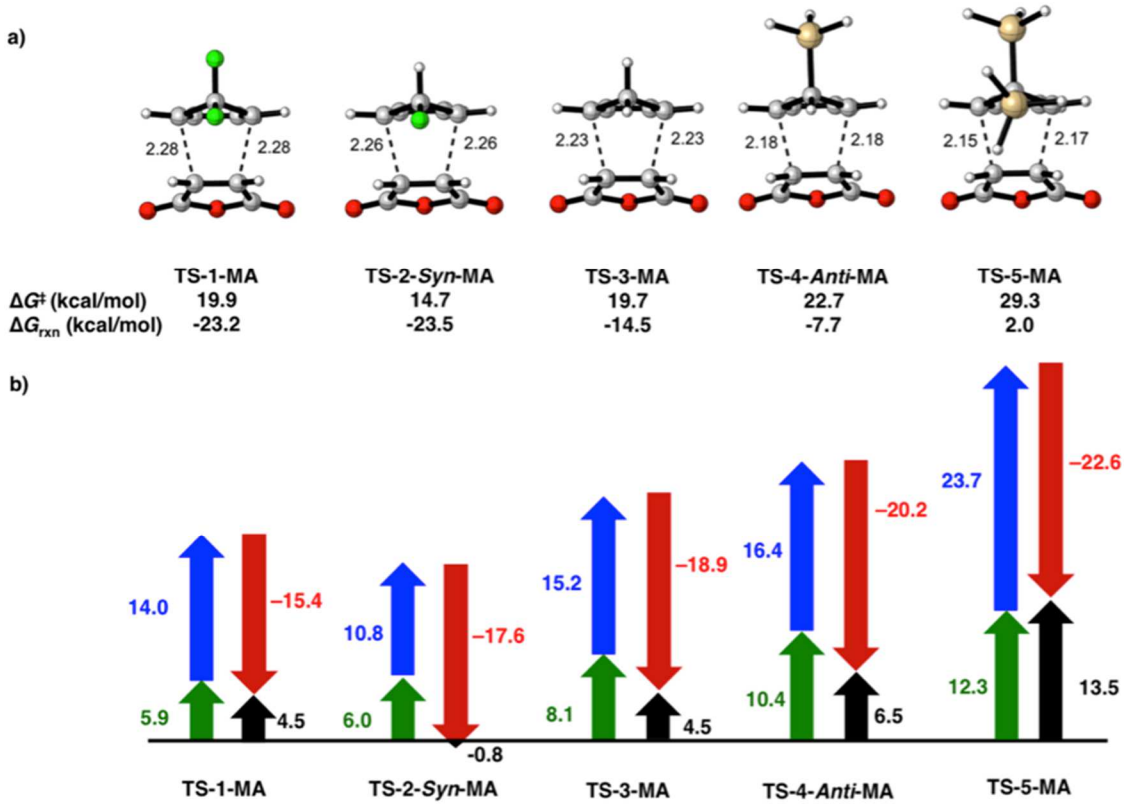

Figure 2.7 a) Endo transition structures for the reaction of dienes 1–5 with maleic anhydride. The forming bond lengths are reported in Ångstroms. b) Plots of the distortion, interaction, and activation energies for the transition states involving dienes 1–

5 with ethylene (black, activation energy; green, distortion energy of the dienophile; blue, distortion energy of the diene; red, interaction energy; in kcal/mol).

2.5 Conclusions

Substitution at the 5-position of cyclopentadiene is predicted to result in over a billionfold variation in the relative reaction rates with ethylene or maleic anhydride at room temperature in the gas phase. The differences in reactivity arise from hyperconjugative aromaticity and antiaromaticity. Negative hyperconjugation destabilizes the cyclopentadiene and increases reactivity, while donors stabilize the cyclopentadiene and decrease reactivity. In unsymmetrically 5-substituted cyclopentadienes, hyperconjugation of the C_5 substituents and the cyclic π-system results in geometrical distortion of the diene. To increase hyperconjugative aromaticity, the $C_{5\text{-}X}$ bond distorts toward the plane of the diene and the cyclopentadiene adopts an envelope geometry with the C_5 atom endo to the $C_{5\text{-}X}$ substituent. The $C_{5\text{-}X}$ bond of hyperconjugative acceptors distorts away from the diene plane to minimize hyperconjugation with the π-system, and the cyclopentadiene adopts an envelope geometry with the C_5 atom exo to the $C_{5\text{-}X}$ substituent. The role of these distortions on π-facial stereoselectivity will be the focus of an upcoming paper from our lab (Zou et al., in preparation).

2.6 References

1. A. R. Katritzky, D. C. Oniciu, A. T. Balaban, *Chem. Rev*. **2004**, 104, 2777.

2. (a) L. Nyulászi, P. v. R. Schleyer, *J. Am. Chem. Soc*. **1999**, *121*, 6872; (b) L. Nyulászi, T. Kárpáti, P. v. R. Schleyer, *Eur. J. Org. Chem*. **2003**, *10*, 1923; (c) I. Fernandez, J. I. Wu, P. v. R. Schleyer, J. *Org. Lett***. 2013**, *15*, 2990.

3. (a) Z. Valenta, D. J. Burnell, *J. Chem. Soc., Chem. Commun*. **1985**, *18*, 1247; (b) F. K. Brown, K. N. Houk, D. J. Burnell, Z. Valenta, *J. Org. Chem.* **1987**, *52*, 3050; (c) L. C. Burry, J. N. Bridson, D. J. Burnell, *J. Org. Chem*. **1995**, *60*, 5931; (d) M. A. Wellman, L. C. Burry, J. E. Letournea, J. N. Bridson, D. O. Miller, D. J. Burnell, *J. Org. Chem*. **1997**, *62*, 939; (e) J. D. Xidos, R. A. Poirier, C. C. Pye, D. J. Burnell, *J. Org.Chem*. **1998**, *63*, 105; (f) L. C. Burry, O. D. Miller, D. J. Burnell, *J. Chem. Soc., Perkin Trans. 1*, **1998**, 22, 3825.

4. (a) J. S. Kron, J. H. Huh, M. Mrksich, B. T. Houseman, *Nat. Biotechnol*. **2002**, *20*, 270; (b) S. H. Jung, G. S. Hwang, S. Lee, D. H. Ryu, *J. Org. Chem*. **2012**, *77*, 2513; (c) S. Bian, A. M. Scott, Y. Cao, Y. Liang, S. Osuna, K. N. Houk, A. B. Braunschweig, *J. Am. Chem. Soc*. **2013**, *135*, 9240; (d) A. V. Samoshin, C. J. Hawker, R. Read de Alaniz, *ACS Macro Lett*. **2014**, *3*, 753.

5. (a) C. A. Citron, S. M. Wickel, B. Schulz, S. Draeger J. S. Dickschat, *Eur. J. Org. Chem*. **2012**, *33*, 6636; (b) J. Chola, I. B. Masesane, *Tetrahedron Lett*. **2008**, *49*, 5680; (c) S. V. Leont'eva, O. S. Manulik, E. M. Evstigneeva, E. N. Bobkova, V. R. Flid, *Kinet. Catal*. **2006**, *47*, 384; (d) K. Kumamoto, I. Fukada, H. Kotsuki, *Angew. Chem. Int. Ed*. **2004**, *43*, 2015.
6. (a) M. A., McClinton, V. J. Silk*, J. Chem. Soc., Perkin Trans. 1*, **1992**, *15*, 1891; (b) R. Lin, C. Wu, C. J. Chern, H. J. Wu, J. *Chin. Chem. Soc.* **1996**, *43*, 289.

7. (a) R. M. Acheson, J. M. Vernon, *J. Chem. Soc.* **1962**, 1148; (b) C. S. Hahn Chang, K. Lee, *J. Org. Chem*. **1978**, *43*, 3727.

8. M. J. Frisch, G. W. Trucks, H. B. Schlegel, G. E. Scuseria, M. A. Robb, J. R. Cheeseman, G. Scalmani, V. Barone, B. Mennucci, G. A. Petersson, H. Nakatsuji, M. Caricato, X. Li, H. P. Hratchian, A. F. Izmaylov, J. Bloino, G. Zheng, J. L. Sonnenberg, M. Hada, M. Ehara, K. Toyota, R. Fukuda, J. Hasegawa, M. Ishida, T. Nakajima, Y. Honda, O. Kitao, H. Nakai, T. Vreven, J. A. Montgomery, Jr., J. E. Peralta, F. Ogliaro, M. Bearpark, J. J. Heyd, E. Brothers, K. N. Kudin, V. N. Staroverov, R. Kobayashi, J. Normand, K. Raghavachari, A. Rendell, J. C. Burant, S. S. Iyengar, J. Tomasi, M. Cossi, N. Rega, J. M. Millam, M. Klene, J. E. Knox, J. B. Cross, V. Bakken, C. Adamo, J. Jaramillo, R. Gomperts, R. E. Stratmann, O. Yazyev, A. J. Austin, R. Cammi, C. Pomelli, J. W. Ochterski, R. L. Martin, K. Morokuma, V. G. Zakrzewski, G. A. Voth, P. Salvador, J. J. Dannenberg, S. Dapprich, A. D. Daniels, Ö. Farkas, J. B. Foresman, J. V. Ortiz, J. Cioslowski, and D. J. Fox, Gaussian 09, Revision D.01; Gaussian, Inc: Wallingford, CT, 2009.

9. Y. Zhao, D. G. Truhlar, *Theor. Chem. Acc*. **2008**, *120*, 215.

10. H. Jiao, P. v. R. Schleyer, *Pure Appl. Chem*. **1996**, *68*, 209.

11. M. Nendel, B. Goldfuss, B. Beno, K. N. Houk, *Pure Appl. Chem*. **1999**, *71*, 221. 12(a) D. H. Ess, K. N. Houk, *J. Am. Chem. Soc.* **2007**, *129*, 10646; (b) D. H. Ess, K. N. Houk, *J. Am. Chem. Soc*. **2008**, *130*, 10187; (c) A. E. Hayden, K. N. Houk, J. *Am. Chem. Soc.* **2009**, *131*, 4084; (d) W. J. van Zeist, F. M. Bickelhaupt, *Org. Biomol. Chem*. **2010**, 8, 3118; (e) F. Liu, R. S. Paton, S. Kim, Y. Liang, N. Houk, *J. Am. Chem. Soc*. **2013**, *135*, 15642; (f) I. Fernandez, *Phys. Chem. Chem. Phys*. **2014**, *16*, 7662; (g) I. Fernandez, F. M. Bickelhaupt, *Chem. Soc. Rev*. **2014**, *43*, 4953; (h) F. Liu, Y. Liang, K. N. Houk, *J. Am. Chem. Soc.* **2014**, *136*, 11483. 13 B. J. Levandowski, K. N. Houk, *J. Org. Chem.* **2015**, *80*, 3530.

14 C. Y. Legault, CYLview, 1.0b; Université de Sherbrooke: Sherbrooke, QC, Canada, 2009. Available at: http://www.cylview.org

Chapter 3. *Syn* and *Anti* π-facial Selectivity in Diels-Alder reactions of 5-substituted Cyclopentadienes

3.1 Introduction to Cyclopentadiene π-facial Stereoselectivity

Cyclopentadiene is a highly reactive diene in the Diels-Alder reaction.[1,2] 5-substituted cyclopentadienes (C_5-X) are asymmetric, and depending on the substituent, will react on either the *syn* or *anti* face of the cyclopentadiene with regard to the C_5-X substitutent. As shown in Scheme 1, the π-facial stereoselectivity of the cycloaddition is considered *syn* when the dienophile (Y=Z) reacts on the same face of the C_5-X substituent, whereas addition to the face opposite of the C_5-X substituent is considered *anti*.

Scheme 3.1 *Syn* and *anti* Diels-Alder π-facial selectivity to a C_5-X cyclopentadiene with the X=Y dienophile.

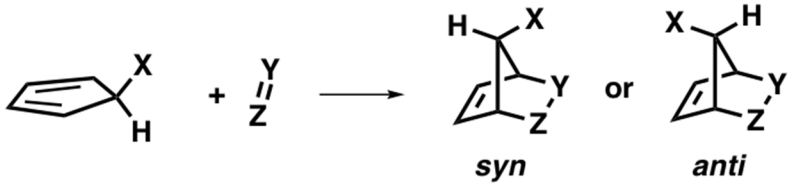

Winstein and Woodward reported the first contrasteric (*syn*) Diels-Alder reaction of 5-acetoxycyclopentadiene (C_5-OAc) with ethylene (Scheme 2) during their seminal studies on 7-norbornenyl cations.[4] Similar constrasteric cycloadditions have since been reported. Scheme 3 shows the π-facial selectivity in the Diels-Alder reactions of C_5-F, C_5-Cl, and C_5-Br with dimethyl acetylenedicarboxylate (DMAD).[5,6] C_5-F reacts with *syn* π-facial stereoselectivity, C_5-Cl forms a mixture of *syn* and *anti* adducts, and C_5-Br reacts with *anti* π-facial stereoselectivity.

Scheme 3.2 Reaction of C_5-OAc with ethylene exclusively forms the *syn* adduct.[4]

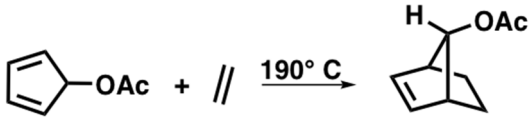

Scheme 3.3 *Syn* and *anti* π-facial stereoselectivity in the Diels-Alder reactions of C_5-F, C_5-Cl, and C_5-Br with DMAD.[5,6]

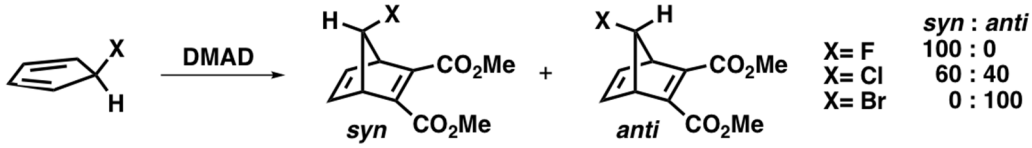

Control of π-facial selectivity is crucial in the synthesis of aconitine alkaloids. Scheme 4 shows the reaction of cyclopentadiene **1** and cyclopropene **2** proceeds predominantly with *syn* selectivity to yield the desired intermediate **3a** in the David Gin synthesis of neofinaconitine shown in Scheme 3.[3] The late David Gin visited our group in

early 2011 and he brought the subject of π-facial stereoselectivity in cyclopentadienes to our attention.

Scheme 3.4 Gin's exploitation of π-facial stereoselectivity in the total synthesis of neofinaconitine.[3]

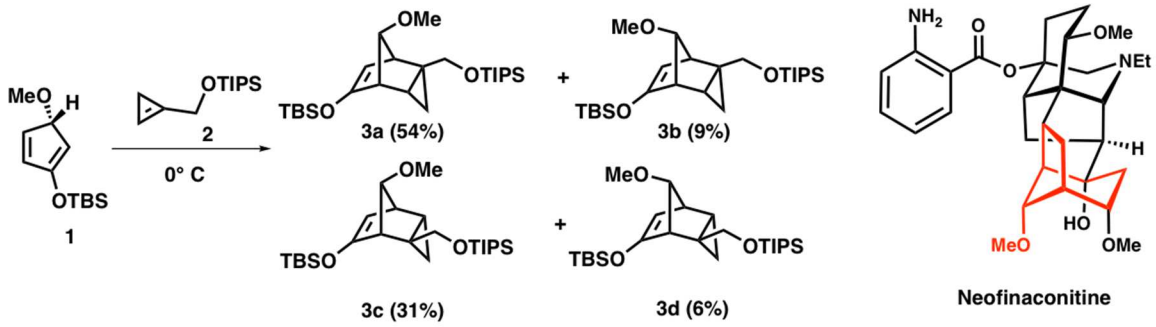

3.2 Previous explanations of the *syn* and *anti* π-favial selectivity

Many explanations have been offered, and it seems that the the origin of π-facial stereoselectivity in 5-substituted cyclopentadiene cycloadditions remains unsettled.[7] Cieplak proposed that the stereoselectivity for a number of nucleophilic reactions can be explained through the hyperconjugative stabilization of an incipient □*-bond by an antiperiplanar donor □-bond in the transition state.[8] Fallis and Macaulay applied the Cieplak effect to the Diels-Alder reactions of 5-substituted cyclopentadienes to rationalize the *syn* and *anti* π-facial stereoselectivity.[9] They proposed that the cycloaddition occurs *anti* to the C_5-X bond that is the better □-donor. Scheme 5 shows the $□_{C5\text{-}X}$-□* hyperconjugative interaction of the antiperiplanar C_5-X bond with the incipient bonds. *Anti* stereoselectivity is predicted when the C_5-X substituent is a stronger □-donor than the hydrogen atom of the C_5-H bond, while a C_5-X substituent that is a worse □-donor is predicted to give *syn* selectivity.

Scheme 3.5 Hyperconjugative stabilization of the incipient □* bonds by the antiperiplanar C_5-X □ bond (Cieplak effect).

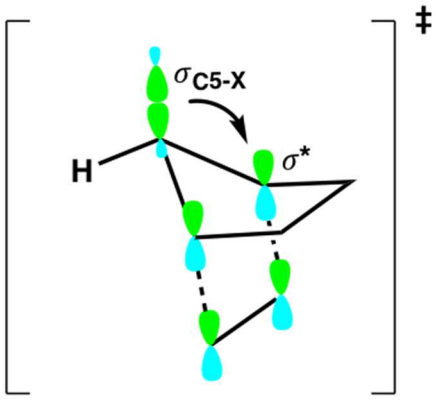

Burnell and coworkers studied computationally the π-facial selectivities of C_5-X cyclopentadienes.[10,11] They concluded that the π-facial stereoselectivity is controlled by the energy required to deform the diene into the transition state geometry. They associated the deformation with the change about the C_1-C_5-X angle between the ground and transition state geometries.

We have recently reported cyclopentadienes as potential bioorthogonal reactions and that the C_5-X substituent has a very large effect on the Diels-Alder reactivity.[12,2] Understanding the reactivity and stereoselectivity trends in 5-substituted cyclopentadienes will be of use in the expansion of the bioorthogonal cyclopentadiene toolbox. To understand how the reactivity and the *syn* and *anti* π-facial stereoselectivity trends relate to the C_5-X substituent, we have investigated a wide scope of C_5-X cyclopentadienes (Scheme 6) with the distortion/interaction-activation strain model.[13]

Scheme 3.6 C_5-X cyclopentadienes studied in this work.

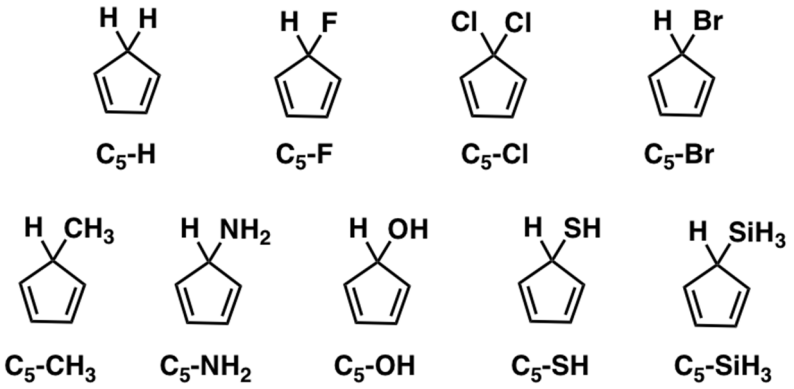

3.3 Computational Methods

All calculations were performed with Gaussian 09.[14] Geometry optimizations and frequency calculations were calculated with the M06-2X[15] functional and the 6-31G(d) basis set. The M06-2X functional has been found to accurately reproduce experimental trends in the reactivity and selectivity of Diels-Alder reactions.[16] Normal mode analysis of each structure verified that each stationary point is either a first-order saddle-point or a minimum. Single point energies were computed at the 6-311++G(d,p) level of theory.

3.4 Revisiting the reactivity of 5-substituted cyclopentadienes

The *anti* and *syn* transition structures and the activation free energies ($\Delta \boldsymbol{G}^{\ddagger}$) for the Diels-Alder reactions of the 5-substituted cyclopentadienes with ethylene are shown in Figure 1.

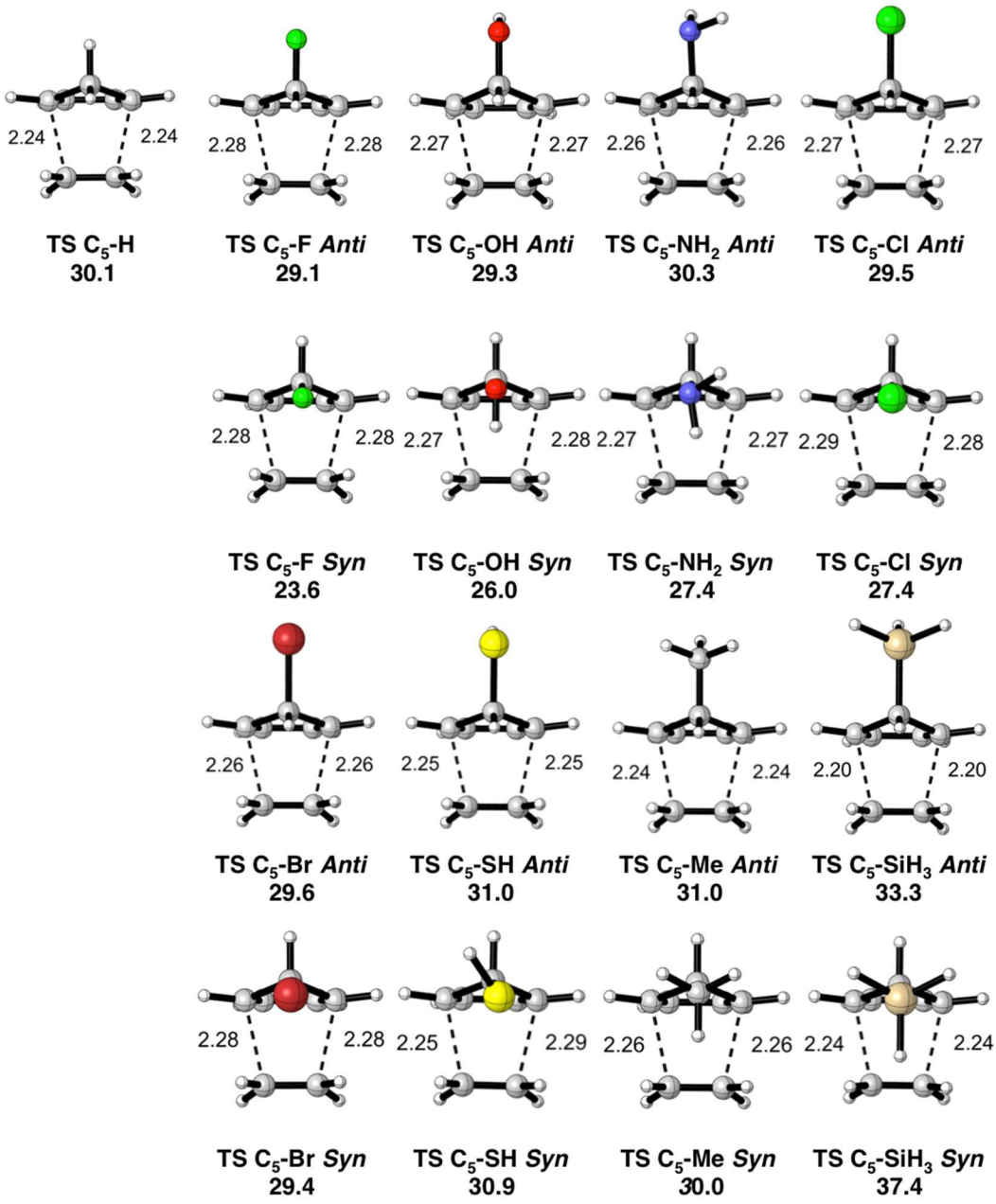

Figure 3.1 Transition state structures with forming bond lengths reported in Å and activation free energies ($\Delta G^{\ddagger}$) in kcal/mol for the *syn* and *anti* Diels-Alder reactions of the 5-substituted cyclopentadienes with ethylene.

Syn π-facial stereoselectivity is favored when the C_5 substituent is F, OH, NH_2 or Cl. Poor π-facial selectivity is predicted when the substituent is Br, SH, or Me. *Anti* π-facial stereoselectivity is favored when the C_5-X substituent is SiH_3. The activation free energies of the *syn* and *anti* transition states range from 24 to 38 and from 29 to 33

kcal/mol, respectively. There is a correlation between the electronegativity of the C_5-X substituent and the activation barriers, as observed earlier by Burnell.[10,11] Electron-withdrawing substituents accelerate the reactivity and electron-donating substituents decrease the reactivity.

Extensive computational and experimental studies by the late Schleyer group on the aromaticity of cyclic π-systems with a saturated linkage (cyclopropene, cyclopentadiene, and cycloheptatriene) show that the substituents at the saturated linkage contribute to the π-electron count as pseudo π-donors or π-acceptors via hyperconjugative interactions with the π-system.[17] The effect of the C_5-X substituent on the stability on the cyclopentadiene was estimated with the isodesmic equation shown in Figure 2. This isodesmic equation measures the aromatic stabilization enthalpy (H_{ASE}) of the cyclopentadiene relative to non-conjugated cyclopentadienes for which the electron delocalization of the π-bonds is not possible. A positive reaction enthalpy in the isodesmic equation indicates that cyclic delocalization of the π-electrons via hyperconjugation is stabilizing. The weak hyperconjugative donors, C_5-H and C_5-Me, are stabilized by 2-3 kcal/mol, which arises mostly from the favorable π-conjugation. Silyl substitution further stabilizes the cyclopentadiene to 7.4 kcal/mol, whereas fluorine substitution destabilizes the cyclopentadiene to -3.4 kcal/mol in the isodesmic equation. When the C_5-X substituent is a □-acceptor the hyperconjugative π-□*$_{C5-X}$ interaction destabilizes the cyclopentadiene by giving it pseudo 4π electron antiaromatic character. When the C_5-X substituent is a □-donor the □$_{C5-X}$-π hyperconjugative interaction stabilizes the cyclopentadiene by giving it pseudo 6π electron aromatic character.

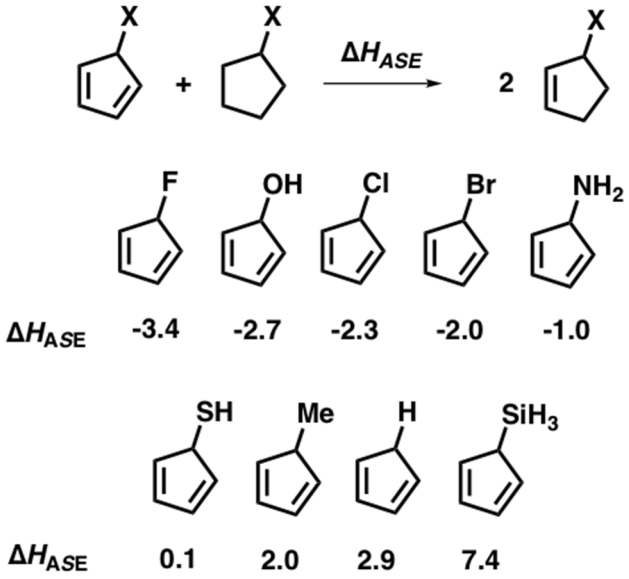

Figure 3.2 Isodesmic equation and calculated aromatic stabilizations enthalpies of the cyclopentadienes.

Figure 3a shows a plot of ΔH of reaction for the reactions of the C_5-X cyclopentadienes vs. the aromatic stabilization energy (ΔH_{ASE}) of the diene. The the linear correlation suggests that the exothermicities of these cycloadditions are related to the stabilities of the C_5-X cyclopentadienes. The *syn* adducts are more stable than the *anti* adduct with the exception of C_5-SiH_3. The norbene π-bond donates into the antiperiplanar □*$_{C5\text{-}X}$ bond of the *syn* and *anti* adducts.[18] As the C_5-X substituent becomes a stronger □-acceptor the *syn* adduct becomes increasingly favored as a result of the stronger π-□*$_{C5\text{-}X}$ interaction.

Figure 3b shows a plot of the $\Delta H^{\ddagger}$ for the C_5-X cycloadditions with ethylene against the diene aromatic stabilization energies. Here the correlations are quite different for the *syn* and *anti* reactions with slopes of 1.1 and 0.33, respectively. Formation of the *syn* adducts are clearly favored for electron-withdrawing substituents while the silyl-substituted cyclopentadiene reacts with a strong preference for the *anti* adduct.

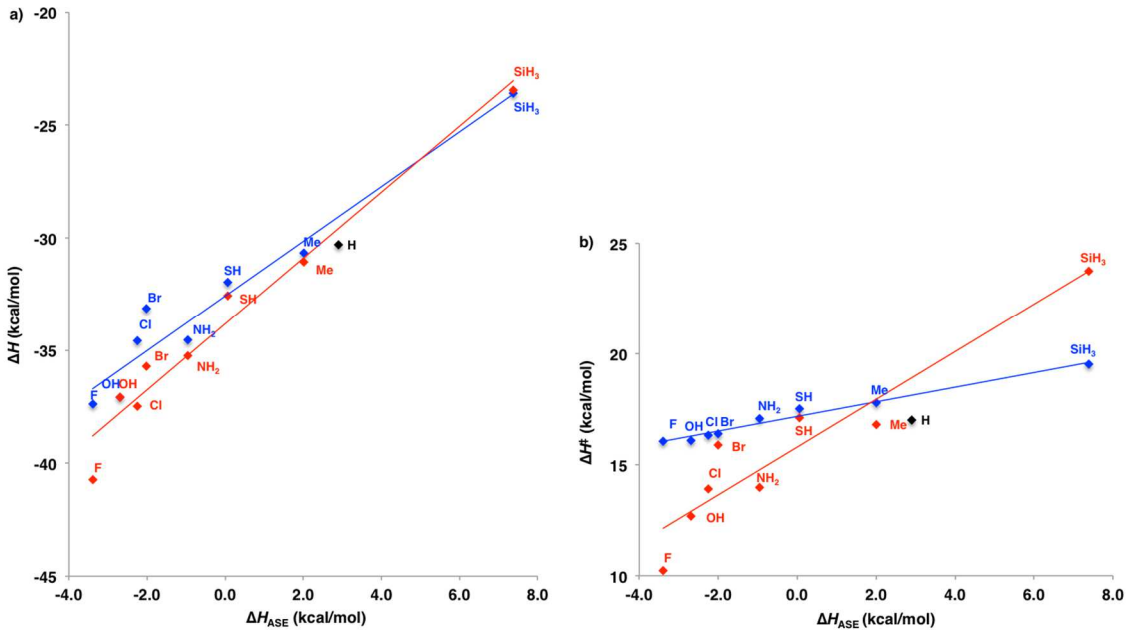

Figure 3.3 Plots of the reaction enthalpies (a) and activation enthalpies (b) against the calculated aromatic stabilization enthalpies. *Syn*: red, (a) $\Delta H = 1.2\ \Delta H_{ASE} - 33$, $r^2 = 0.95$ (b) $\Delta H^{\ddagger} = 1.1\Delta H_{ASE} + 16$, $r^2 = 0.90$. *Anti*: blue, (a) $\Delta H = 1.5\Delta H_{ASE} - 34$, $r^2 = 0.95$ (b) $\Delta H^{\ddagger} = 0.33\Delta H_{ASE} + 17$, , $r^2 = 0.98$.

To further understand the origins of the reactivity differences and of the *syn* and *anti* π-facial stereoselectivity in Diels-Alder reactions of 5-substituted cyclopentadienes we applied the distortion/interaction-activation strain analysis.[12] This analysis dissects the electronic activation energies in the distortion and interaction energies of the reaction. The distortion energy (ΔE_d) is the energy required to deform the reactants into the corresponding transition structures, and the interaction energy (ΔE_i) comprises the interactions that occur between the diene and dienophile at the transition geometry. Figure 4 shows the results of the distortion/interaction-activation strain analysis for the stereochemically preferred Diels-Alder reactions of C_5-F(*syn*), C_5-H, and C_5-SiH_3(*anti*) with ethylene and maleic anhydride. The analysis is performed from the reactant complexes with average C--C bond forming distances of 2.8 Å to the geometry of the corresponding transition states. Each line ends at the stereochemically preferred

geometries of the corresponding transition state. The distortion energies are similar along the reaction coordinates with C_5-F and C_5-SiH_3 requiring less distortion relative to C_5-H reaction. This is a result of the C_5-F being pre-distorted towards the *syn* transition state geometry and C_5-SiH_3 being pre-distorted towards the *anti* transition state geometry, which we discuss in further detail later on. The differences in the reactivities of the 5-substituted cyclopentadienes results from the differences in the interaction energies, which strongly favor the C_5-F reaction over the C_5-SiH_3 and C_5-H reactions.

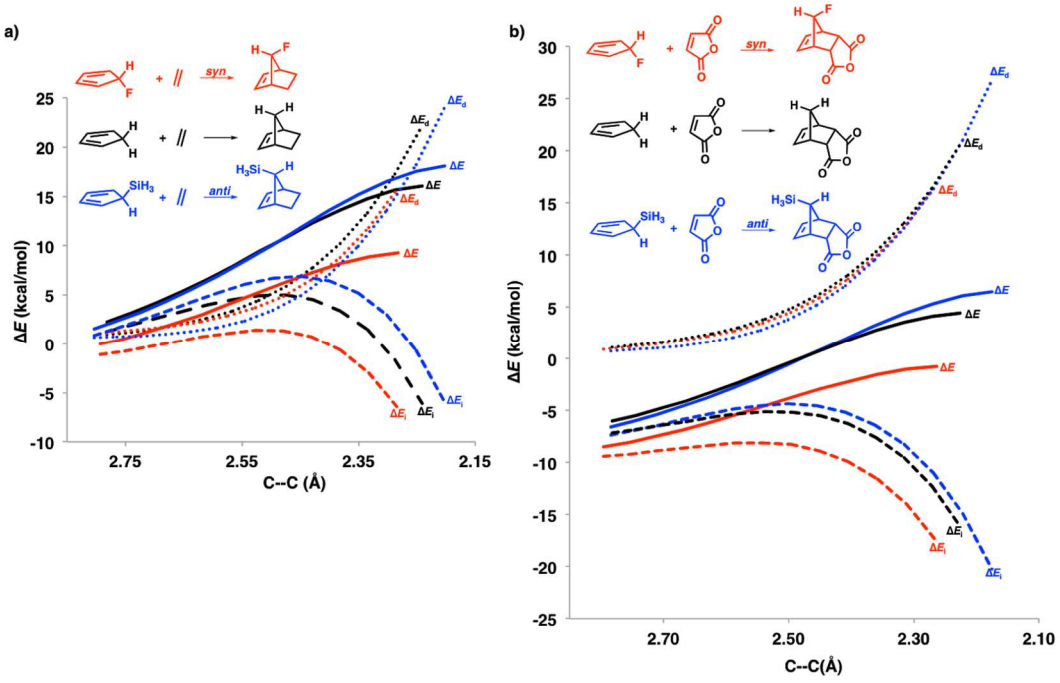

Figure 3.4 Distortion/Interaction-Activation Strain analysis for the Diels-Alder reactions of C_5-F (red, *syn* reaction), C_5-H (black), and C_5-SiH_3 (blue, *anti* reaction) with ethylene and maleic anhydride. Interaction energies (ΔE_i, dashed), electronic energies (ΔE, solid), and distortion energies (ΔE_d, dotted) are shown along the intrinsic reaction coordinate defined by the average lengths of the forming bonds.

Diels-Alder reactions of the 5-substituted cyclopentadienes with ethylene and maleic anhydride proceed through the normal electron-demand Diels-Alder mechanism where the highest occupied molecular orbital (HOMO) of the 5-substituted cyclopentadiene interacts with the lowest unoccupied molecular orbital (LUMO) of the

dienophile. The frontier molecular orbitals were calculated at the HF/6-311++G(d,p) level of theory for the reactions of the substituted cyclopentadienes with maleic anhydride and are shown in Figure 5. The HOMO energies of C_5-F, C_5-H and C_5-SiH_3 are -8.9, -8.4, and -8.5 electron volts (eV), respectively. The trend in the reactivities and interaction energies of the 5-substituted cyclopentadienes cannot be explained by frontier molecular orbital (FMO) theory. In fact, FMO theory incorrectly predicts that C_5-F would be the least reactive of the 5-substituted cyclopentadiene series.

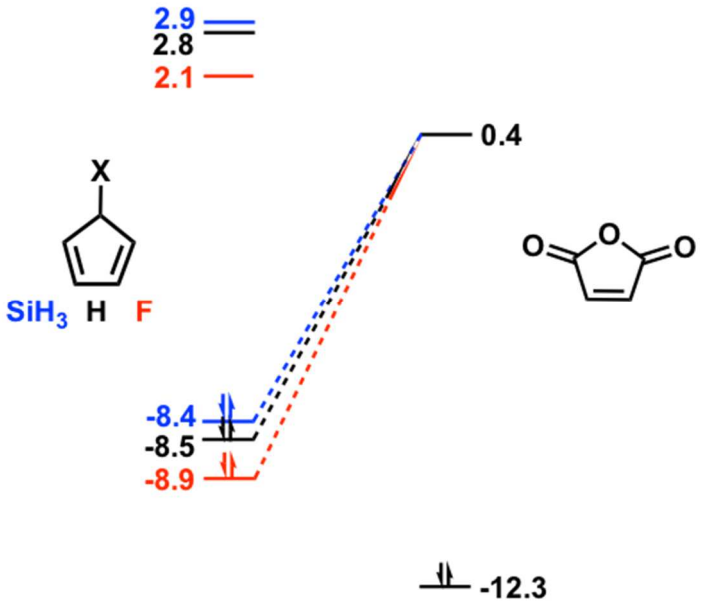

Figure 3.5 Frontier molecular orbitals interactions in the Diels-Alder reactions of C_5-F(red), C_5-H(black) and C_5-SiH_3(blue) with maleic anhydride. The HOMO and LUMO energies are provided in electron volts (eVs).

Schleyer probed computationally for aromatic properties in the transition state for the Diels-Alder reaction of butadiene with ethylene and found that the transition state is aromatic with a highly delocalization structure and large resonance stabilization as predicted by Evans and Warhurst in 1938.[19] The reactivity trends in the series of C_5-X substituted cyclopentadiene can be understood by the aromaticity of the transition states. When the C_5-X substituent is a strong σ-acceptor the ground state resembles an

antiaromatic 4π system that rapidly reacts with the 2π system of ethylene through a stabilizing aromatic 6π transition state. Conversely, positive hyperconjugation of the C_5-X bond to the cyclopentadiene π-system invokes an aromatic 6π system that reacts with the 2π system of ethylene through a destabilizing 8π antiaromatic electron transition state. The reactivity of the 5-substituted cyclopentadiene and the aromatic stabilization of the transition state increase as the C_5-X substituent becomes a stronger σ-acceptor, and decreases as the C_5-X substituent becomes a σ-donor. The reversal of aromaticity along a reaction coordinate where aromatic systems react through an antiaromatic transition state and an antiaromatic systems react through aromatic transition states has been identified in the conformational interconversion of homotropylium cations.[20] Aromatic homotropylium cation introconverts between conformers through an antiromatic transition state with a barrier of 22 kcal/mol. Substitution of the methylene hydrogen atoms in the homotropylium cation with fluorine atoms results in an antiaromatic homotropylium cation that interconverts through an aromatic transition state with a lower barrier of 17 kcal/mol. The reversal of aromaticity between the ground and transition states explains the linear correlation shown in Figure 3b between $\Delta H^{\ddagger}$ and ΔH_{ASE}.

3.4 Origin of the *syn* and *anti* π-facial stereoselectivity

Figure 6 shows a plot of the stereoselectivity measured as the difference in the *anti* and *syn* electronic activation energies ($\Delta E^{\ddagger}$(*syn*) - $\Delta E^{\ddagger}$(*anti*)) with the difference in

the distortion ($\Delta E_d^{\ddagger}$(*syn*) - $\Delta E_d^{\ddagger}$(*anti*)) required to achieve the *anti* and *syn* transition states.

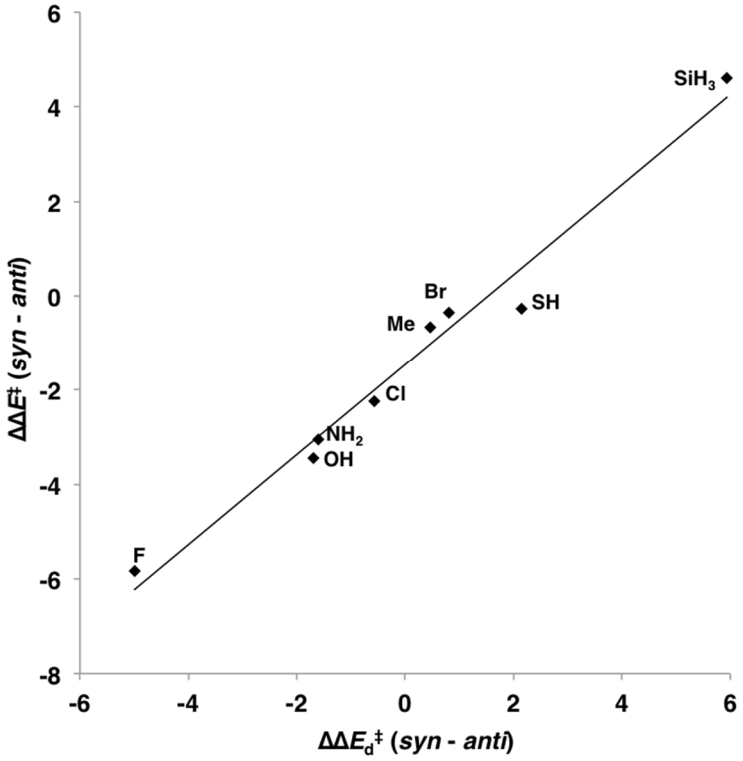

Figure 3.6 Plot of π-facial selectivity ($\Delta\Delta E^{\ddagger}$ (*syn-anti*)) against the differences in the distortion energies ($\Delta\Delta E_d^{\ddagger}$ (*syn-anti*)). ($\Delta\Delta E^{\ddagger}$ = 0.95 $\Delta\Delta E_d^{\ddagger}$ – 1.5, r^2 = 0.98).

The excellent linear correlation suggests that the π-facial selectivity results from differences in the energies required to distort the reactants into the *syn* and *anti* geometries as proposed by Burnell.[10,11] We also performed the distortion/interaction-activation strain analysis along the intrinsic reaction coordinate defined by the length of the forming C--C bonds. These plots are provided in the Supplementary Information section. When the forming bond lengths of the stereoisomers in the transition state are similar, performing the distortion/interaction-activation strain analysis at the TS and along the IRC lead to the same conclusion that the *syn* and *anti* stereoselectivity is distortion controlled.

As shown in Figure 7, the cyclopentadiene (C_5-H) ground state is planar. The electronic nature of the C_5-X substituent pre-distorts the cyclopentadiene into an envelope geometry. The angle θ_{env} is defined as the angle that the C_5 atom of the cyclopentadiene puckers above or below the plane of the cyclopentadiene. The value of θ_{env} is negative when the C_5 atom extends below the plane and positive when it extends above the plane of the cyclopentadiene. When C_5-X is a □-donor, the C_5 atom distorts above the plane of the cyclopentadiene. This distortion aligns C_5-X bond with the cyclopentadiene π-system to increase the stabilizing $□_{C5\text{-}X}$-π* interaction that provides the diene with Schleyer's hyperconjugative aromaticity.[2,17] For the □-donor C_5-SiH_3, the C_5 atom is distorted 3° above the plane of the cyclopentadiene. When C_5-X is a □-acceptor, the C_5 atom distorts below the plane of the cyclopentadiene to minimize the overlap and destabilizing effect of hyperconjugative aromaticity brought by the cyclopentadiene π-$□^*_{C5\text{-}X}$ bond interaction. For □-acceptors, C_5-F, C_5-OH, and C_5-Cl the C_5 atom is predistorted 2 to 4° below the plane of the cyclopentadiene ring. The poor □-donors/acceptors, C_5-Br, C_5-CH_3, C_5-SH and C_5-NH_2 are nearly planar with the C_5 atom predistorted less than 2° relative to the plane of the cyclopentadiene.

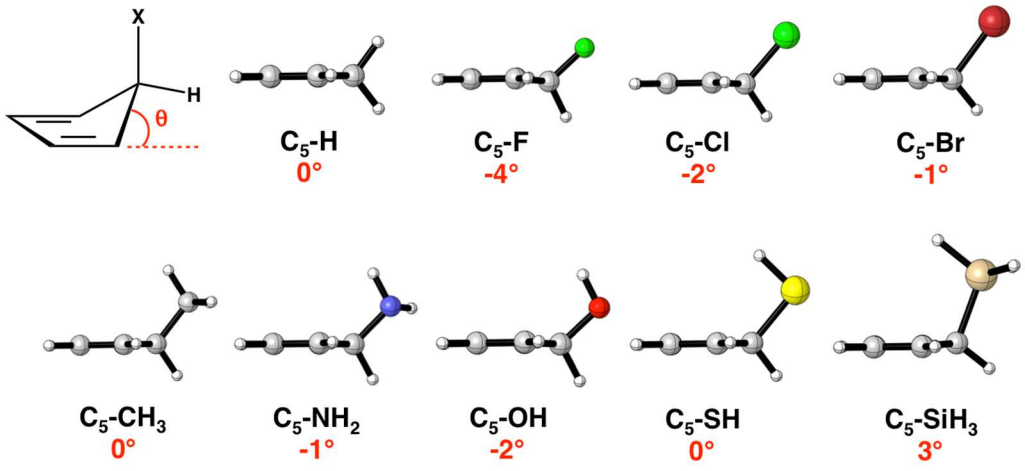

Figure 3.7 Optimized M06-2X/6-31G(d) ground state geometries of the C_5-X cyclopentadienes with θ_{env}, the angle measuring the out of plane distortion of the C_5 atom, reported in degrees.

In the *syn* and *anti* transition structures θ_{env} ranges from -18° to -19° and from 16° to 19°, respectively. Figure 8 shows θ_{env} for the *syn* and *anti* Diels-Alder reactions of C_5-F, C_5-Br, and C_5-SiH_3 with ethylene. The *syn* selective C_5-F requires a 14° change about θ_{env} to achieve the *syn* transition state geometry and a change of 21° to achieve the *anti* transition state geometry. To achieve the *syn* and *anti* transition state geometries, θ_{env} in C_5-Br distorts 17° and -18°, respectively. For the *syn* selective C_5-SiH_3, the change about θ_{env} to achieve the *syn* and *anti* transition state geometries is 16° and -21° from the ground state geometry, respectively.

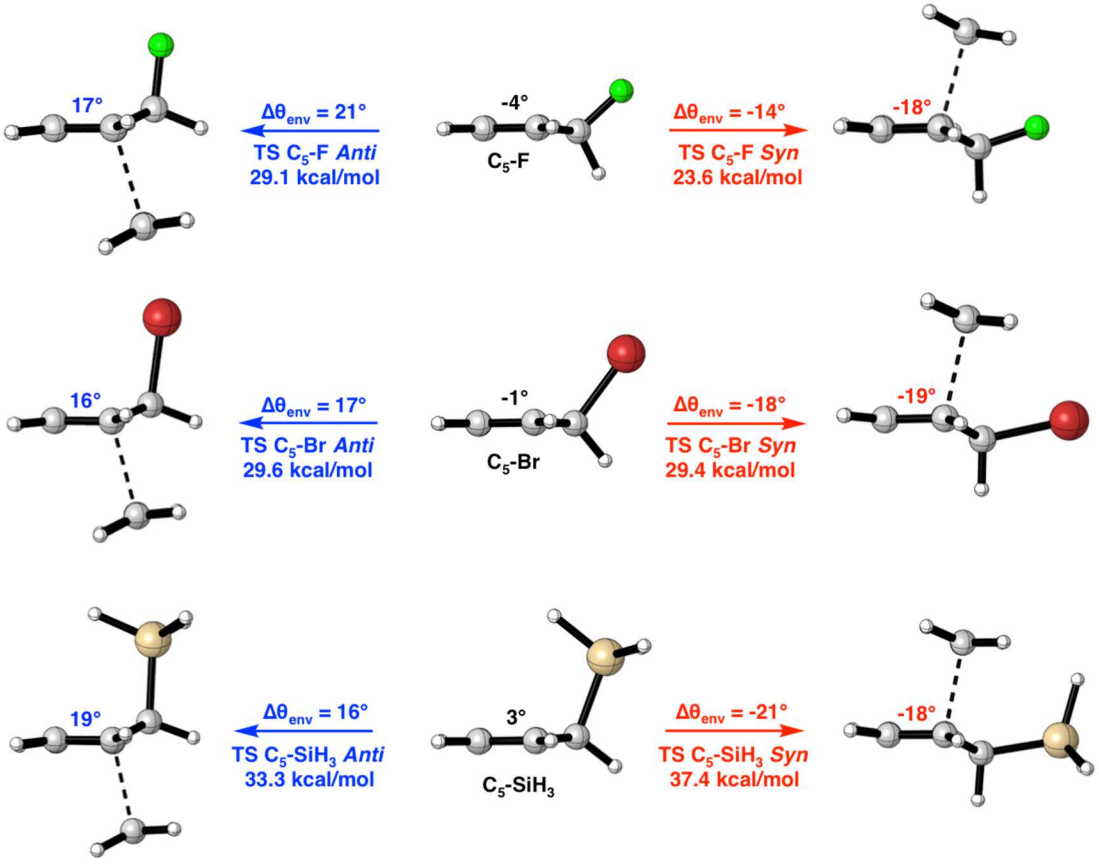

Figure 3.8 Ground and *syn* and *anti* transition state structures of C_5-F, C_5-Br, and C_5-SiH_3 with θ_{env} shown in degrees.

Figure 8a shows a strong linear correlation when the difference in the diene distortion energies is plotted against the change in the cyclopentadiene envelope angle, θ_{env}, required to achieve the *syn* and *anti* transition state geometries. The stereoselectivity of C_5-X cyclopentadiene Diels-Alder reactions is determined by the distortion energies, which are related to how the C_5-X cyclopentadiene is predistored in the ground state. When the substituent is a □-donor, the ground state is pre-distorted into an envelope geometry that resembles the *anti* transition state to maximize the stabilizing $\square_{C5\text{-}X}$-π* interaction, while □-acceptors cause the ground state to pre-distort into an envelope geometry that resembles the *syn* transition state to minimize the destabilizing π-$\square^*_{C5\text{-}X}$ interaction. The transition state that requires less distortion of θ_{env} is the stereoselectively observed reaction.

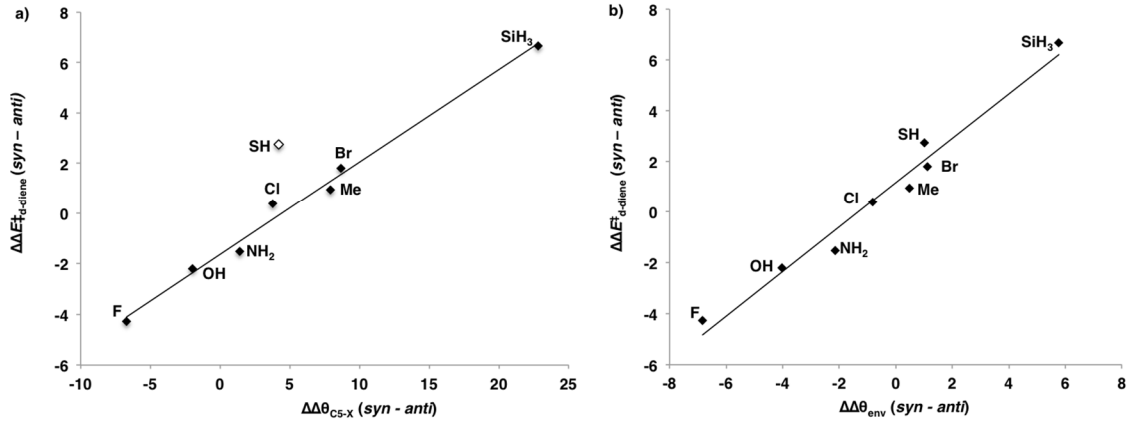

Figure 3.9 a) Plot of differences in the diene distortion energies ($\Delta\Delta E_{d\text{-}diene}^{\ddagger}$ (*syn* - *anti*)) against the change in the bending of the $C_{5\text{-}X}$ bond required to achieve the *syn* and *anti* transition state geometries ($\Delta\Delta E_{d\text{-}diene}^{\ddagger}$ = 0.37 $\Delta\Delta\theta_{C5\text{-}X}$ - 1.6, r^2 = 0.99) b) Plot of differences in the diene distortion energies ($\Delta\Delta E_{d\text{-}diene}^{\ddagger}$ (*syn* - *anti*)) against the change in the envelope angle required to achieve the *syn* and *anti* transition state geometries $\Delta\Delta\theta_{env}$ (*syn* - *anti*). ($\Delta\Delta E_{d\text{-}diene}^{\ddagger}$ = 0.88 $\Delta\Delta\theta_{env}$ + 1.2, r^2 = 0.97).

We have also considered the contribution of the in-plane bending (rocking) of the C_5-X bond to the distortion energy as proposed by Burnell.[11] The C_5-X ($\theta_{C5\text{-}X}$) bond angle is measured relative to a the plane of the cyclopentadiene defined by the $C_1C_4C_5$ atoms. Figure 9b shows a plot of the differences in the diene distortion energies against the difference in the bending of the C_5-X ($\theta_{C5\text{-}X}$) bond from the plane of the cyclopentadiene between the *syn* and *anti* transition state. There is a strong linear correlation between the diene distortion and the bending of the C_5-X bond from the plane of the diene with the exception of the outlier C_5-SH. The x-intercept shows that for diene distortion of the *syn* and *anti* transition states to be equal ($\Delta\Delta E_{\text{d-diene}}^{\ddagger} = 0$), an additional 5° distortion of the C_5-X bond towards the *anti* transition state is required about the C_5-X bond. Figure 9a shows the plot of the difference in the diene distortion energies against the difference in θ_{env} between the *syn* and *anti* transition states. There is only a 1° difference between the envelope geometry of the *syn* and *anti* transition states when the distortion energy of the *syn* and *anti* transition states are equal ($\Delta\Delta E_{\text{d-diene}}^{\ddagger} = 0$).

The difficulty of distorting a bond is related to the strength of the bending force constants. Table 1 summarizes the computed force constants associated with the bending of the C_5-X bond and the C_5 carbon relative to the plane of the cyclopentadiene in the C_5-X cyclopentadiene ground states. The force constants for the bending of the C_5-X bonds range from 118-188 *v* and are significantly lower than the out-of-plane bending force constants associated with the out-of-plane bending of the C_5 carbon atom, which range from 772-857 *v*. The differences in the bending of the C_5-X alkyl bonds required to achieve the *syn* and *anti* transition state structures contributes less to the differences in the distortion energies of the *syn* and *anti* transition states than the distortion associated with

the bending of the C_5 carbon from the plane of the cyclopentadiene as the envelope geometry is adopted, and as a result has less influence on the stereoselectivity.

Table 3.1 Vibrational modes computed at the M06-2X/6-31G(d) level of theory for bending of the C_5-X bonds and for the out-of-plane bending of the C_5 atom from the plane of the cyclopentadiene.

C_5-X	Bending of C_5-X bond (ν)	Out-of-plane bending of C_5 atom (ν)
C_5-F	188	857
C_5-Cl	146	848
C_5-Br	126	809
C_5-CH_3	164	795
C_5-NH_2	167	832
C_5-OH	174	848
C_5-SH	139	772
C_5-SiH_3	118	816

The strength of the hyperconjugation interaction between the π-system and the C_5-X substituent determines the extent of the predistortion. The electronegativity of the

C_5-X substituent correlates with the envelope angle θ_{env} in the ground state geometries of the C_5-X cyclopentadienes (Figure 10a) and is a useful way to predict the π-facial stereoselectivity in Diels-Alder reactions of C_5-X cyclopentadiene with ethylene (Figure 10b). As the C_5-X substituent becomes a stronger σ-acceptor it predistorts more towards the envelope conformation of the *syn* transition state and becomes increasingly selective for the *syn* reaction.

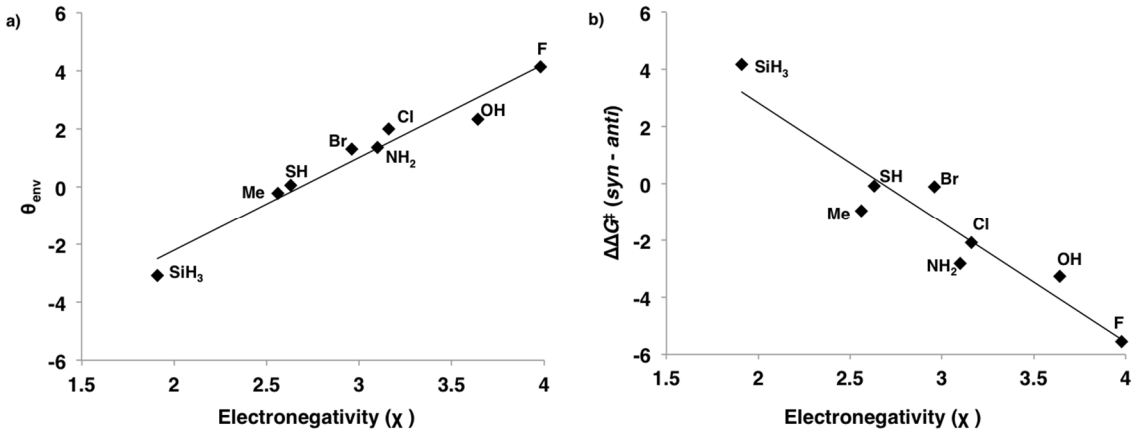

Figure 3.10 a) Plot of θ_{env} in the ground state of the C_5-X cyclopentadienes against the electronegativity of the C_5-X substituent (C_5-X = 3.2□ - 8.7, r^2 = 0.96). b) Plot of π-facial selectivity against the electronegativity of the C_5-X substituent ($\Delta\Delta G^{\ddagger}$ = -4.2□ + 11.2, r^2 = 0.90).

The influence of the dienophile on the π-facial stereoselectivity was investigated by calculating the Diels-Alder stereoselectivities with maleic anhydride (MA), tetracyanoethylene (TCNE), 1,2,4-triazoline-3,5-dione (TAD), and acetylene. Figure 11 summarizes the *syn* and *anti* π-facial stereoselectivity of the C_5-X cyclopentadienes with these dienophiles.

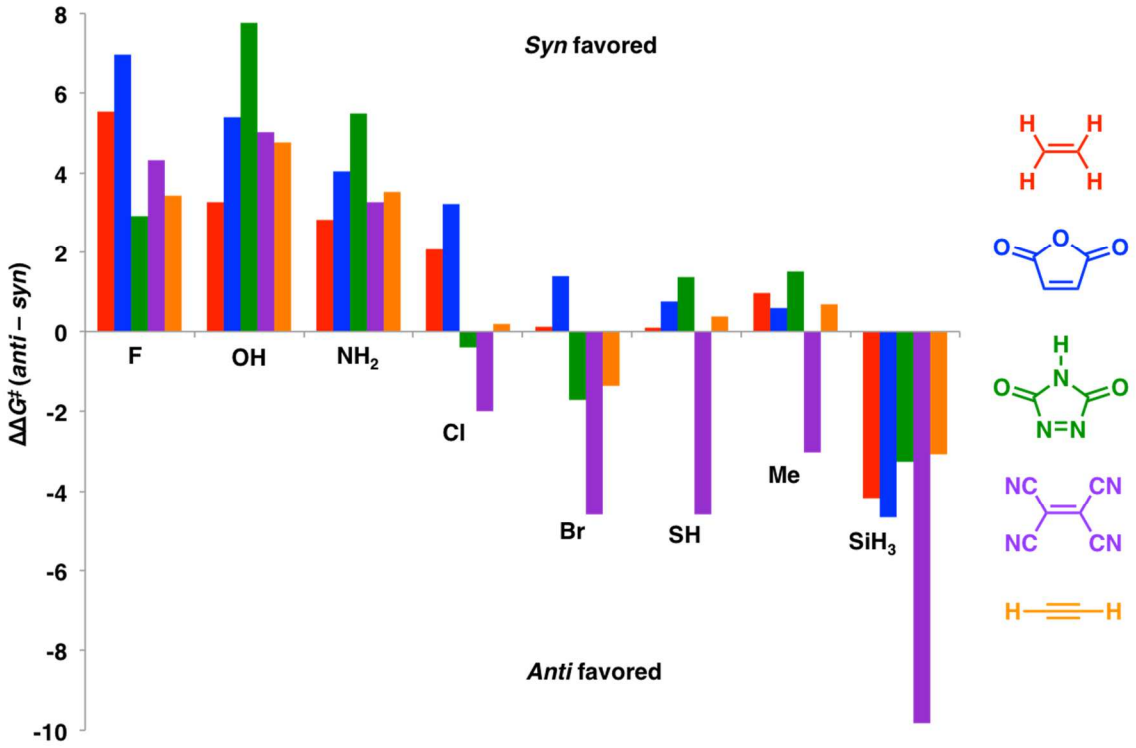

Figure 3.11 Histogram showing the *syn* and *anti* π-facial stereoselectivity in the Diels-Alder reactions of the C_5-X cyclopentadienes with ethylene (red), maleic anhydride (blue), 1,2,4-triazoline-3,5-dione (green), tetracyanoethylene (purple), and acetylene (orange).

The Diels-Alder reaction of C_5-SiH_3 is *anti* with all dienophiles. For C_5-Cl, C_5-Br, C_5-SH ,and C_5-Me, which are poor sigma donor/acceptors, the π-facial stereoselectivity is dependant on the dienophile. Steric interactions destabilize the *syn* transition state when TCNE is the dienophile and *anti* π-facial stereoselectivity becomes favored for C_5-Cl, C_5-Br, C_5-SH ,and C_5-Me. Lone pair repulsions between the nitrogens of TAD with the halogen lone pair on the Cl and Br destabilizes the *syn* transition state and results in poor stereoselectivity for the Diels-Alder reaction of C_5-Cl with TAD and *anti* stereoselectivity in the reaction of C_5-Br with TAD. The predistortion of the C_5-F, C_5-OH, and C_5-NH_2 ground states towards the *syn* transition state geometry is strong enough to overcome any destabilizing interactions with the dienophile in the *syn*

transition states and *syn* π-facial stereoselectivity is favored with all of the studied dienophiles.

3.6 Conclusions

The π-facial selectivity of C_5-X cyclopentadienes is distortion controlled. When the C_5-X substituent is a strong σ-acceptors (X = F, OH, and NH_2) the cyclopentadiene adopts an envelope geometry with the C_5 distorted to minimizes the π-□*$_{C5-X}$ hyperconjugative interaction that provides the cyclopentadiene with antiaromatic character. This distortion causes the cyclopentadiene to resemble the envelope geometry of the *syn* transition and lessens the distortion energy required of the *syn* cycloaddition. Conversely, when the C_5-X substituent is a σ-donor (X = SiH_3) the C_5 atom distorts to maximize the effect of the stabilizing □$_{C5-X}$-π* hyperconjugative interaction that provides the cyclopentadiene with aromatic character. This distortion of the ground state causes the cyclopentadiene to resemble the envelope geometry of the *anti* transition state, and *anti* π-facial selectivity is favored. When the C_5-X substituent is a poor σ-acceptor/donor (X = Cl, Br, SH, and Me), the π-facial selectivity is sensitive to the nature of the dienophile.

3.6 References

1. Levandowski, B. J.; Houk, K. N. *J. Org. Chem.* **2015**, *80*, 3530

2. Levandowski, B. J.; Zou, L.; Houk, K. N. *J. Comput. Chem.* **2016**, *37*, 117.

3. Shi, Y.; Wilmot, J. T.; Nordstrøm, L. U.; Tan, D. S.; Gin, D. Y. *J. Am. Chem. Soc.* **2013**, *135*, 14313.

4. Winstein, S.; Shatavsky, M.; Norton, C.; Woodward, R. B. *J. Am. Chem. Soc.* **1955**, *77*, 4183.

5. McClinton, M. A.; Silk, V. J.; *J. Chem. Soc., Perkin Trans. 1*, **1992**, *15*, 1891.

6. Franck-Neumann, M.; Sedrati, M. *Tetrahedron Lett.*, **1983**, *24*, 1391.

7. Ishida, M.; Inagaki, S. In Topics in Current Chemistry; Inagaki, S., Ed.; Springer: **2010**; *289*, 183-218.

8. Cieplak, A. S. *Chem. Rev.* **1999**, *99*, 1265.

9. Macaulay, J. B.; Fallis, A. G. *J. Am. Chem. Soc.* **1990**, *112*, 1136.

10. Xidos, J. D.; Poirier, R. A.; Pye, C. C.; Burnell, D. J. *J. Org. Chem.* **1998**, *63*, 105.

11. Xidos, J. D.; Poirier, R. A.; Burnell, D. J. *Tetrahedron Lett.* **2000**, *41*, 995.

12. Levandowski, B. J.; Gamache, R. F.; Murphy, J. M. Houk, K. N. *J. Am. Chem.* **2018**, 140, 20, 6426.

13. Bickelhaupt, F. M.; Houk, K. N. *Angew. Chem., Int. Ed.* **2017**, *56*, 2.

14. Frisch, M. J.; Trucks, G. W.; Schlegel, H. B.; Scuseria, G. E.; Robb, M. A.; Cheeseman, J. R.; Scalmani, G.; Barone, V.; Mennucci, B.; Petersson, G. A.; Nakatsuji, H.; Caricato, M.; Li, X.; Hratchian, H. P.; Izmaylov, A. F.; Bloino, J.; Zheng, G.; Sonnenberg, J. L.; Hada, M.; Ehara, M.; Toyota, K.; Fukuda, R.; Hasegawa, J.; Ishida, M.; Nakajima, T.; Honda, Y.; Kitao, O.; Nakai, H.; Vreven, T.; Montgomery, J. A., Jr.; Peralta, J. E.; Ogliaro, F.; Bearpark, M.; Heyd, J. J.; Brothers, E.; Kudin, K. N.; Staroverov, V. N.; Kobayashi, R.; Normand, J.; Raghavachari, K.; Rendell, A.; Burant, J. C.; Iyengar, S. S.; Tomasi, J.; Cossi, M.; Rega, N.; Millam, M. J.; Klene, M.; Knox, J. E.; Cross, J. B.; Bakken, V.; Adamo, C.; Jaramillo, J.; Gomperts, R.; Stratmann, R. E.; Yazyev, O.; Austin, A. J.; Cammi, R.; Pomelli, C.; Ochterski, J. W.; Martin, R. L.; Morokuma, K.; Zakrzewski, V. G.; Voth, G. A.; Salvador, P.; Dannenberg, J. J.; Dapprich, S.; Daniels, A. D.; Farkas, Ö.; Foresman, J. B.; Ortiz, J. V.; Cioslowski, J.; Fox, D. J. *Gaussian 09*, Revision D.01; Gaussian, Inc.: Wallingford CT, 2009.

15. Zhao, Y.; Truhlar, D. G. *Theor. Chem. Acc.* **2008**, *120*, 215.

16. (a) Pieniazek, S. N.; Clemente, F. R.; Houk, K. N. *Angew. Chem., Int. Ed.* **2008**, 47, 7746. (b) Lan, Y.; Zou, L.; Cao, Y.; Houk, K. N. *J. Phys. Chem. A* **2011**, *115*, 13906. (c) Levandowski, B. J.; Hamlin, T. A.; Bickelhaupt, F. M.; Houk, K. N. *J. Org. Chem.* **2017**, *82*, 8668−8675. (d) Levandowski, B. J.; Hamlin, T. A.; Helgeson, R. C.; Bickelhaupt, F. M.; Houk, K. N. *J. Org. Chem.* 83, 6, 3164-3170

17. (a) Nyulászi, L.; Schleyer, P. v. R. *J. Am. Chem. Soc.* **1999**, *121*, 6872. (b) Fernandez, I.; Wu, J. I.; Schleyer, P. v. R. J. Org. Lett. 2013, 15, 2990. (c) Levandowski, B. J.; Houk, K. N. *J. Am. Chem. Soc.* **2016**, *138*, 16731.

18. (a) Adcock, W.; Angus, D. I.; Lowe, D. A. Magn. Reson. Chem. 1996, 34, 675. (b) Levandowski, B. J.; Herath, D.; Gallup, N. M.; Houk, K. N. *J. Org. Chem.* **2018**, *83*, 2611.

19. (a) M. G. Evans and E. Warhurst. *Trans. Faraday Soc.* **1938**, *34*, 61 (b) H. Jiao, P. von R. Schleyer, *J. Phys. Org. Chem.* **1998**, *11*, 655 (c) Schleyer, P. v. R.; Wu, J. I.; Cossío, F. P.; Fernandez, I. *Chem. Soc. Rev.* **2014**, *43*, 4909.

20. Gibson, C. M.; Havenith, R. W. A.; Fowler, P. W.; Jenneskens, L. W. P. *J. Org. Chem.* **2015**, *80*, 1395.

Chapter 4. Application of Cyclopentadienes to Bioorthogonal Chemistry

4.1 Introduction to Bioorthogonal Chemistry

Bioorthogonal reactions enable the study of biomolecules in living systems for the elucidation of biological processes.[1] The strain-promoted 3+2 azide-alkyne cycloaddition (SPAAC) developed by Bertozzi,[2] and the inverse-electron demand tetrazine *trans*-cyclooctene Diels-Alder reaction introduced by Fox[3] are bioorthogonal cycloadditions that have been utilized to study complex interactions within biological settings. These reactions take place rapidly and selectively under physiological conditions while avoiding reactions with nucleophiles present in cellular systems.

Research focused on improving the reactivity of the SPAAC and the inverse-electron demand Diels-Alder (IED-DA) reactions has mostly centered around modifications of the two-π-electron (dienophile or dipolarophile) component. Scheme 1 shows the reactivity of benzyl azide (**1**) with some of the cyclooctynes developed for bioorthogonal applications. The introduction of a propargylic fluoride (MOFO)[4] on the cyclooctyne scaffold doubles the reactivity of the cyclooctyne, while incorporation of a second electron deficient fluorine atom at the propargylic position (DIFO)[5] results in a 30-fold increase in reactivity. Negative hyperconjugation involving the $\sigma^*_{C\text{-}F}$ stabilizes the transition state.[6,7]

Theoretical work by the Alabugin group guided the design of SNO-OCTs (sulfur, nitrogen, and oxygen containing heterocyclic cyclooctynes) where the propargylic heteroatom is endocyclic and antiperiplanar to the alkyne π-bond to maximize the stabilizing effect of the π-σ* hyperconjugative interaction.[8,9] Tomooka and coworkers synthesized several cyclooctynes with endocyclic heteroatoms and confirmed that the rate

enhancement associated with an endocyclic propargyl heteroatom exceeds that of exocyclic propargyl substitution.[8] The hyperconjugative interaction involving the endocyclic heteroatom in SNO-OCTS is stronger because it is antiperiplanar to the reactive π-bond, while the heteroatoms in MOFO and DIFO are gauche.[8] While modulating the electronic properties of the cycloalkyne has improved reactivity, the most reactive cyclooctynes are highly strained multi-cyclic cyclooctynes such as dibenzocyclooctyne (DIBO),[10] biarylazacyclooctynone (BARAC)[11], dibenzoazacyclooctyne (DIBAC)[12] and *endo* 9-hydroxymethylbicyclo[6.1.0]nonyne (BCN).[13] Optimization of the azide cyclooctyne cycloaddition has led to rate constants that have leveled off near 1 M^{-1} s^{-1}. For more rapid rate constants, the tetrazine ligation can be used.[3]

Scheme 4.1 Cyclooctynes and second order-rate constants (M^{-1} s^{-1}) for reactions with benzyl azide (**1**). Reaction rates were measured in acetonitrile (CD_3CN)[a], methanol (CD_3OD)[b], or 3:1 CD_3CN/D_2O[c] at ambient temperature.

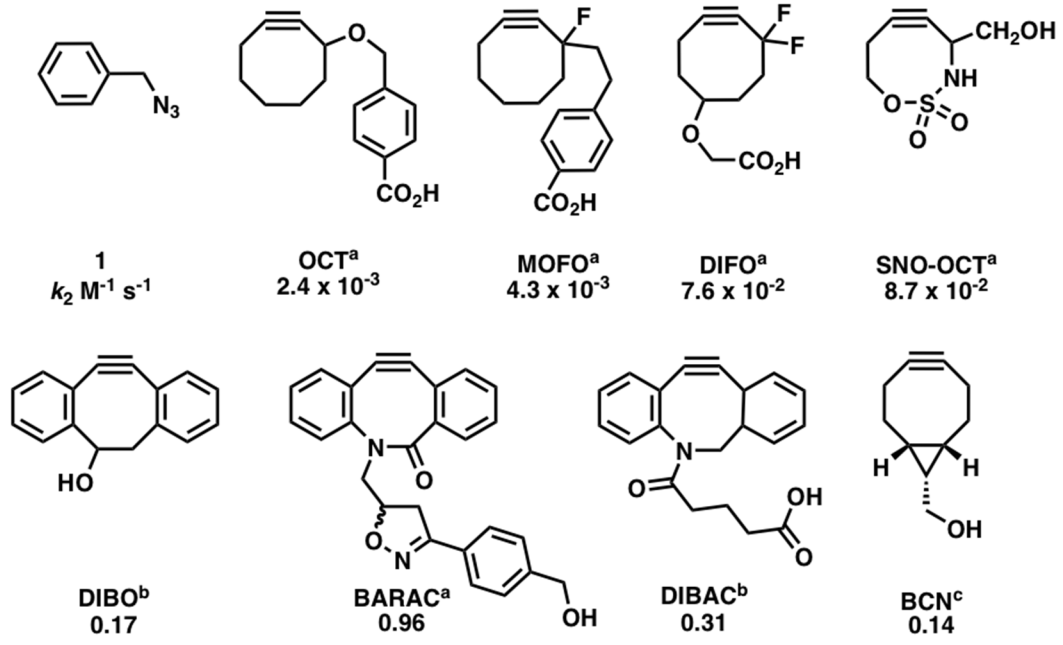

Tetrazines are electron-deficient, highly reactive dienes that undergo IED-DA reactions with strained dienophiles to label biomolecules of interest.[14,15] The rate constants for IED-DA reactions of 3,6-di-2-pyridyl-1,2,4,5-tetrazine (**2**) with a series of dienophiles are shown in Scheme 2. In the IED-DA reaction, the low-lying LUMO of the highly electrophilic tetrazine interacts with the HOMO of the nucleophilic and strained dienophile. Dienophiles with higher lying HOMOs are more reactive towards tetrazines. For example, *trans*-cyclooctene has a higher HOMO energy than cyclooctyne and is more reactive.[16] An interesting exception is in the series of cycloalkenes. From cyclopropene to cyclohexene the reactivity diminishes despite the increasing HOMO energies in the series.[14,15,17] Recent analyses by our group and the Bickelhaupt group showed that differences in the strength of the secondary orbital interactions, which are especially strong with cyclopropene and weaken with increasing cycloalkene ring size, overcome the differences in primary orbital interactions.[18,19]

The tetrazine-*trans*-cyclooctene reactions are among the fastest bioorthogonal cycloadditions, with rates exceeding 10^4 M^{-1} s^{-1}.[3] Cyclooctynes,[16] norbornenes,[20] and cyclopropenes[21,22] have been paired with tetrazines when a more stable dienophile is required, but these reactions are considerably slower (Scheme 2). Bulky dienophiles, such as 3,3-disubstituted cyclopropenes[23] and 3,3,6,6-tetramethylthiacycloheptynes (TMTH),[24] react poorly with tetrazines. These bulky dienophiles react with azides and allow for tandem labeling studies studies with tetrazine-*trans*-cyclooctene reactions for multi-target imaging.[25] The use of tetrazines in bioorthogonal chemistry is hampered by their bulkiness and vulnerability to nucleophilic attack from biological nucleophiles.[26] To address these issues the Prescher group has developed bioorthogonal reactions with the

less reactive 1,2,4-triazine scaffold.[27]

Scheme 4.2 Dienophiles and their second-order rate constants for reactions with 3,6-di-2-pyridyl-1,2,4,5-tetrazine (**2**). Reactions rates are measures in 9:1 MeOH/H_2O[a] or MeOH[b] at ambient temperature. N/R indicates no reaction.

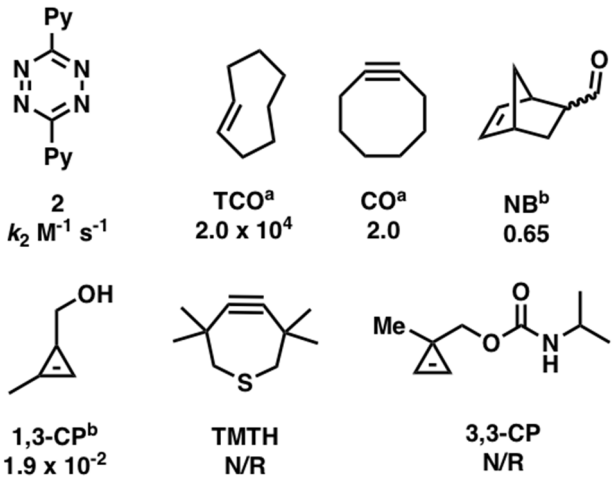

New reactions are continually being developed that enable rapid, selective ligations to study molecules in a chemically complex environment.[28,29] Cyclopentadiene is a classic diene that was used by Diels and Alder in their seminal 1928 publication on the Diels-Alder reaction.[30] Substituted cyclopentadienes have since enjoyed much success in synthesis,[31,32] material functionalization,[33,34] bioconjugation,[35] and chemical trapping,[36,37] yet their potential in bioorthogonal chemistry remains unexplored. We have used computational screening to probe the reactivity of cyclopentadienes with bioorthogonal 2π cycloaddends to design a cyclopentadiene-based bioorthogonal reaction. This method of screening reduces the toil of tedious large-scale reactivity screenings in the laboratory and vastly accelerates the discovery of new bioorthogonal reactions by providing a short list of promising cyclopentadiene-based bioorthogonal reactions to study experimentally.

4.2 Summary of cyclopentadiene Diels-Alder reactions

Cyclopentadiene reacts as both a diene and a dienophile in the Diels-Alder reaction and readily dimerizes at room temperature.[38] Highly substituted cyclopentadienes, such as hexachlorocyclopentadiene, are reactive as dienes, but do not readily dimerize at room temperature.[39,40] This lack of self-reactivity is referred to as "self-orthogonal". Substituents at the 1,2 and 3,4 positions of cyclopentadiene sterically impede dimerization by clashing with the substituents at the 5-position of the cyclopentadiene. Extensive experimental and computational studies by the Schleyer group on the stability of 5-substituted cyclopentadienes demonstrate that electronegative substituents destabilize the cyclopentadiene by inducing 4π antiaromatic electron delocalization, whereas electropositive substituents stabilize the cyclopentadiene by creating 6π aromatic character.[41,42,43] Our group expanded upon Schleyer's work with a computational study that predicts that the Diels-Alder reactivity of the cyclopentadiene is tunable through substitution at the 5-position, and that electronegative substituents accelerate the reactivity.[44,45]

Sauer's pioneering studies on the synthesis and reactivity of 1,2,4,5-tetrazines with many dienophiles have been a variety of inspiration for the design of reactions in bioorthogonal chemistry.[14,15] Sauer's detailed reports on the synthesis and reactivities of substituted cyclopentadienes, however, have gone relatively unrecognized.[39,40] The highly reactive, self-orthogonal, and ambiphilic properties of the tetrachlorocyclopentadiene ketal (TCK) shown in scheme 3 and described by Sauer, attracted our attention as a potential bioorthogonal diene.[39,40] TCK is stable at room

temperature and requires heating to 80 °C in toluene for 11 days to form 71% yield of the TCK Diels-Alder dimer.[37] TCK is ambiphilic and reacts with both electron-deficient dienophiles such as maleic anhydride and electron-rich dienophiles such as (1*Z*,5*Z*)-cycloocta-1,5-diene.[46]

Scheme 4.3 Tetrachlorocyclopentadiene ketal (TCK)

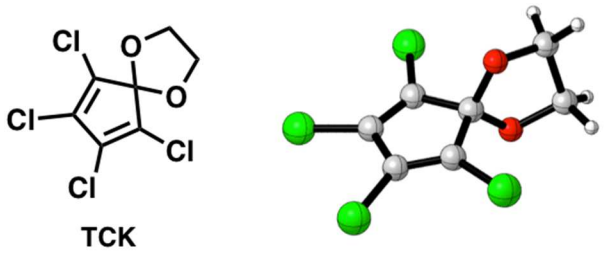

4.3 Reactivity Screening of TCK with known Bioorthogonal Cycloaddends

We have probed computationally the bioorthogonal potential of the TCK with bioorthogonal 2π scaffolds. The M06-2X[47] functional with the 6-31G(d) basis set was used for geometry optimizations. Single point energies were calculated with the 6-311++G(d,p) basis set and solvation effects of water were included through use of the conductor-like polarizable continuum model (CPCM).[48,49] Figure 1 shows the computed transition state structures and activation free energies for the Diels-Alder reactions of TCK with the bioorthogonal cycloaddends of *trans*-cyclooctene (**TS-TCO**), bicyclononyne (**TS-BCN**), cyclooctyne (**TS-CO**), norbornene (**TS-NB**), 3,3-dimethylcyclopropene (**TS-3,3-CP**), and dibenzocyclooctyne (**TS-DIBO**). For the reactions of TCK with *trans*-cyclooctene, dibenzocyclooctyne, and cyclooctyne, the computational screening reveals activation free energies of 18.1 – 20.6 kcal/mol, indicating potential as viable partners with TCK in bioorthogonal cycloadditions. By contrast, the activation free energies for the Diels-Alder reactions of TCK with

norbornene, 3,3-dimethyl cyclopropene, and dibenzocyclooctyne range from 23.1 – 27.7 kcal/mol, and are too high for bioorthogonal applications. These latter scaffolds are highly reactive with some 1,3-dipoles, providing an opportunity to develop mutually orthogonal cycloadditions.

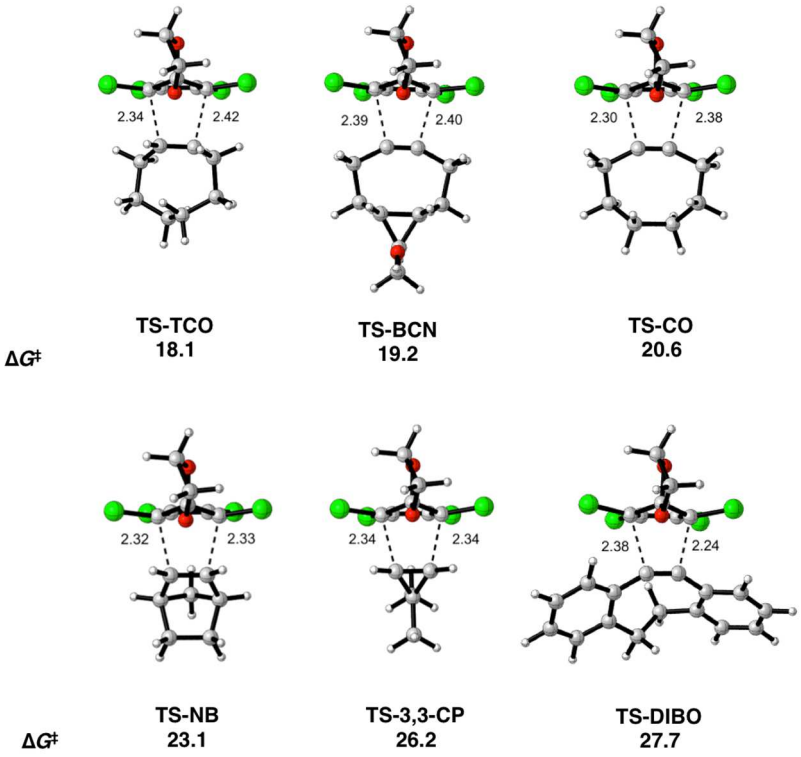

Figure 4.1 Transition state structures and activation free energies in kcal/mol for the Diels-Alder reactions of TCK with bioorthogonal cycloaddends.

4.4 Kinetics of and preparation of TCK

To test our *in-silico* predictions and evaluate the potential of TCK as a bioorthogonal reaction partner, the second-order rate constants of TCK with BCN and TCO cycloaddends were measured exerimentally. We chose BCN and TCO as the cycloaddends because they were predicted to be the most reactive bioorthogonal dienophiles towards TCK from the computational screening (Figure 1). TCK was prepared from commercially available hexachlorocyclopentadiene according to Chang's

protocol shown in Scheme 4.[46] Hexachlorocyclopentadiene **3** was treated with potassium hydroxide (KOH) and ethylene glycol to yield TCK. TCK undergoes a rapid 4+2 cycloaddition with BCN and the axial 5-hydroxy *trans*-cyclooctene (TCO-OH) stereoisomer to give cycloadducts **4** and **5**, respectively. The reactions of TCK with BCN and TCO-OH give a mixture of four and two stereoisomers, respectively.

Scheme 4.4 Synthesis of TCK and cycloaddition rates with TCO-OH and BCN.

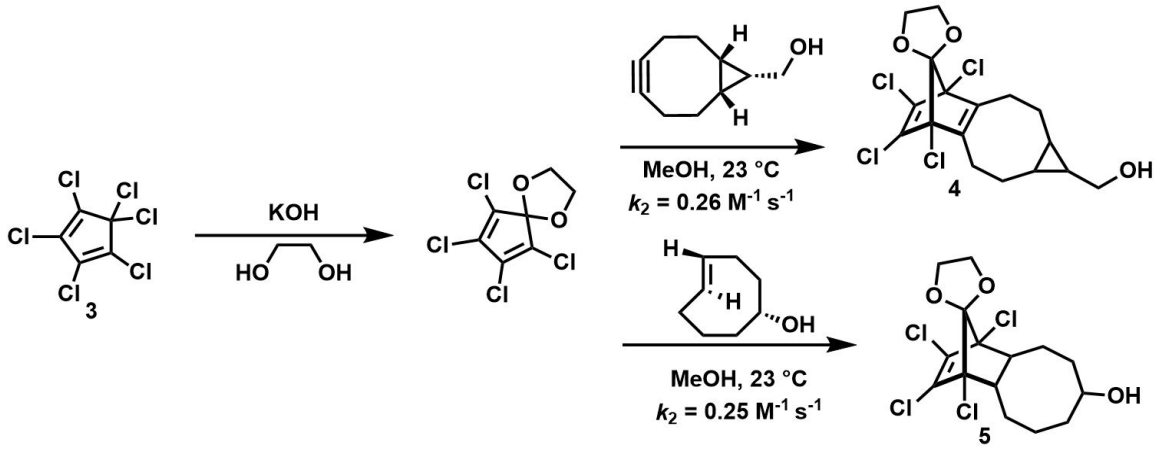

Rate constants were measured with ultraviolet visible (UV/Vis) spectroscopy by monitoring the disappearance of the TCK absorption peak under *pseudo*-first order conditions. The experimentally observed second-order rate constants for the Diels-Alder reactions of TCK with BCN and TCO-OH in methanol are 0.26 M^{-1} s^{-1} and 0.25 M^{-1} s^{-1}, respectively (Figure 2). These rate constants are comparable to previously reported SPAAC bioorthogonal labeling approaches shown in Scheme 1.

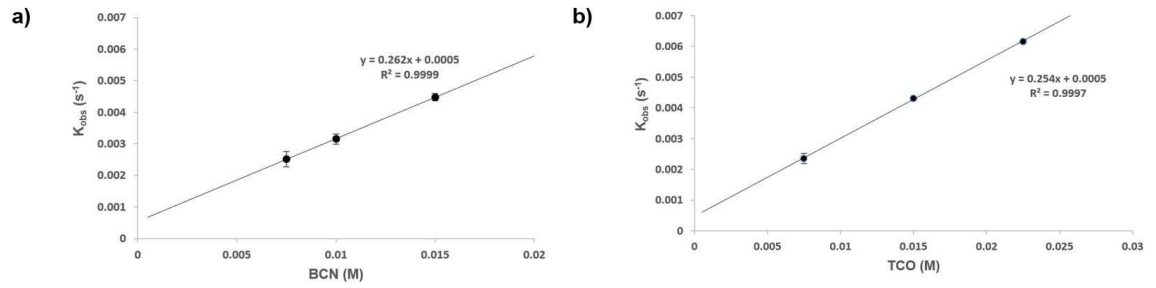

Figure 4.2 a) Plot of rate observed vs. concentration of BCN with the slope taken as the second-order rate constant. b) Plot of rate observed vs. concentration of TCO-OH with the slope taken as the second-order rate constant.

Mutually orthogonal bioorthogonal reactions allow for dual labeling studies that monitor multi-component biological processes by targeting multiple biomolecules.[22] Computational screening predicts that DIBO derivatives will react poorly with TCK. To test this prediction, TCK and DIBAC were stirred together for 20 hours at room temperature, and no cycloaddition products were observed. 1,3-dipoles such as azides react quickly with DIBAC, and poorly with TCO derivatives as shown in Scheme 5.[12,50] Scheme 5 outlines these findings and demonstrates how tandem labeling is possible with the mutually orthogonal TCK-TCO and benzyl azide-DIBAC reactions.

Scheme 4.5 Mutual orthogonality between the TCK TCO-OH and benzyl azide-DIBAC reactions.

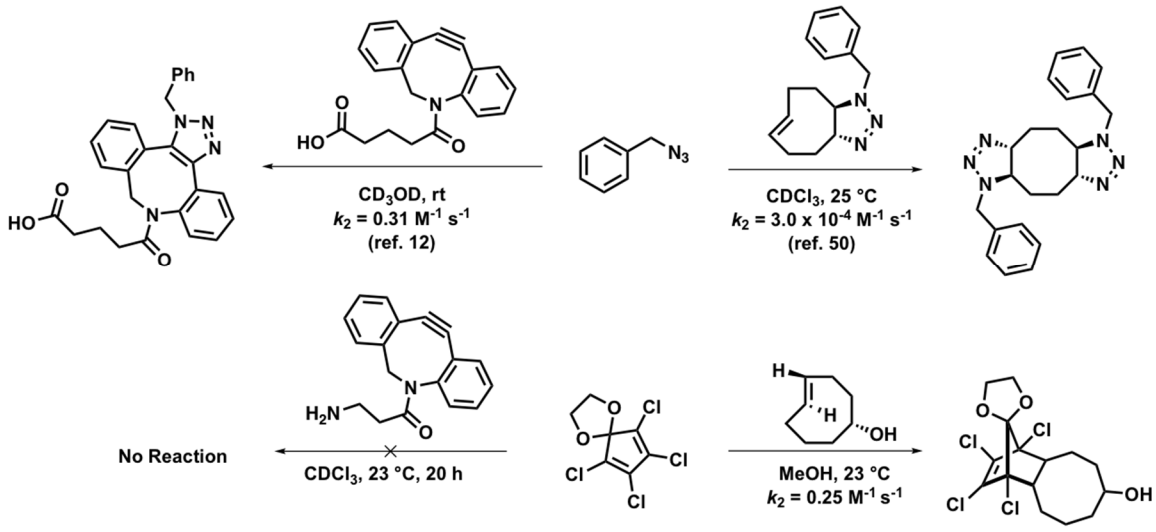

4.5 Labeling of Peptides with TCK

Scheme 6 illustrates a three-step protocol for the synthesis of a *N*-hydroxysuccinimide functionalized TCK to enable bioconjugation to primary amines. Ketalization of hexachlorocyclopentadiene **3** was carried out with (±)-1,2,4-butanetriol to yield the intermediate alcohol **6**. Oxidation to the corresponding carboxylic acid **7** and subsequent coupling to *N*-hydroxysuccinimide under standard conditions afforded the desired activated ester **8**.

Scheme 4.6 Synthesis of TCK succinimidyl ester **9** for bioconjugation to primary amines.

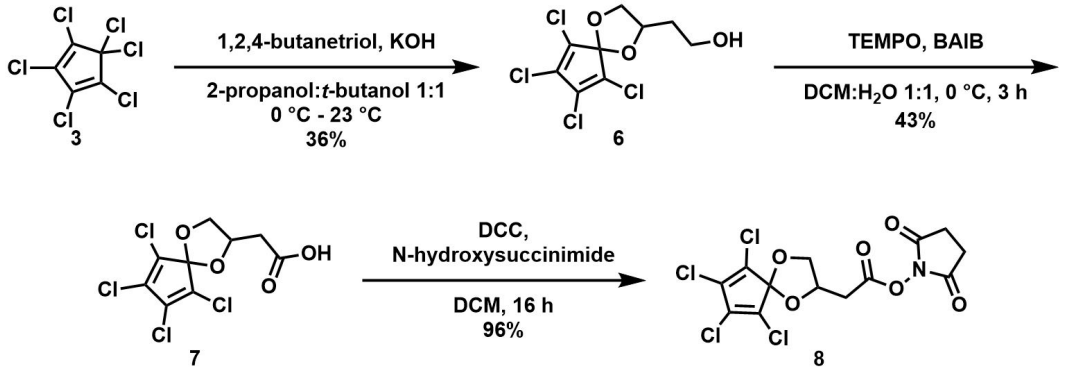

To validate the biocompatibility of the reaction, the commercial neuropeptide used to prevent neuronal damage against hypoxic or ischemic induced brain injury, [D-Ala^2, D-Leu^5]-Enkephalin, was chosen for initial labeling experiments.[51] Activated diene **8** was readily conjugated to [D-Ala^2, D-Leu^5]-Enkephalin via the succinimidyl ester to afford cyclopentadiene-peptide conjugate **9.** Peptide-conjugate **9** efficiently underwent the Diels-Alder cycloaddition with Cy5-TCO in ambient temperature to afford the fluorescent peptide **10**, as shown in Scheme 7.

Scheme 4.7 Bioconjugation and fluorescence labeling of [D-Ala^2, D-Leu^5]-Enkephalin.

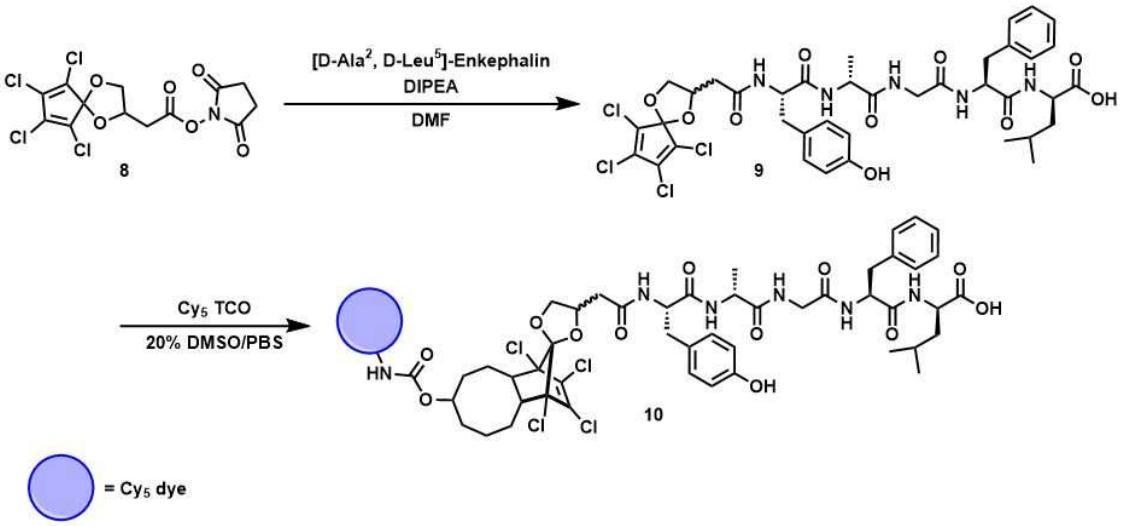

Many bioorthogonal reagents are sensitive to air or light, react with biological endogenous nucleophiles such as thiols, or are unstable as a result of strain making prolonged labeling studies and storage difficult.[11,28,52] TCK can be stored at room temperature as a white solid with a melting point range of 64.5-65.5 °C. No decomposition or dimerization of TCK was observed by proton NMR after 63 hours of incubation at 37 °C in a 1:1 CD_3CN:D_2O mixture with cysteine. TCK displays high stability under biological conditions and is inert to the nucleophilic thiol cysteine.

4.6 Conclusions

We report TCKs as a new class of bioorthogonal reagents with reaction rates towards *endo*-BCN and TCO-OH that are practical for biological labeling studies. Proof of fluorescence peptide labeling with TCK is demonstrated using a commercial neuropeptide and the near-infrared cyanine dye, Cy5. The enduring stability of TCK is ideal for long-term applications and our computational studies suggest future tandem labeling with azide reactions is plausible. TCK is readily synthesized from inexpensive starting materials and stable at room temperature. The dynamic reactivity, accessibility,

and stability found in TCKs are essential for adoption as a bioorthogonal reagent.

4.7 References

1. Sletten, E. M.; Bertozzi, C. R. *Angew. Chem. Int. Ed Engl.* **2009**, *48*, 6974.

2. Agard, N. J.; Prescher, J. A.; Bertozzi, C. R. *J. Am. Chem. Soc.* **2004**, *126*,15046.

3. Blackman, M. L.; Royzen, M.; Fox, J. M. *J. Am. Chem. Soc.* **2008**, *130*, 13518.
4. Agard, N. J.; Baskin, J. M.; Prescher, J. A.; Lo, A.; Bertozzi, C. R. *ACS Chem. Biol.* **2006**, *1*, 644.

5. Baskin, J. M.; Prescher, J. A.; Laughlin, S. T.; Agard, N. J.; Chang, P. V.; Miller, I. A.; Lo, A.; Codelli, J. A.; Bertozzi, C. R. *Proc. Natl. Acad. Sci. U. S. A.* **2007**, *104*, 16793.

6. Schoenebeck, F.; Ess, D. H.; Jones, G. O.; Houk, K. N. *J. Am. Chem. Soc.* **2009**, *131*, 8121.
7. Gold, B.; Shevchenko, N. E.; Bonus, N.; Dudley, G. B.; Alabugin, I. V. *J. Org. Chem.* **2012**, *77*, 75.
8. Ni, R.; Mitsuda, N.; Kashiwagi, T.; Igawa, K.; Tomooka, K. *Angew. Chem. Int. Ed Engl.* **2015**, *54*, 1190.

9. Burke, E. G.; Gold, B.; Hoang, T. T.; Raines, R. T.; Schomaker, J. M. *J. Am. Chem. Soc.* **2017**, *139*, 8029.

10. Ning, X.; Guo, J.; Wolfert, M. A.; Boons, G.-J. *Angew. Chem. Int. Ed Engl.* **2008**, *47*, 2253.

11. Jewett, J. C.; Sletten, E. M.; Bertozzi, C. R. *J. Am. Chem. Soc.* **2010**, *132* , 3688.

12. Debets, M. F.; van Berkel, S. S.; Schoffelen, S.; Rutjes, F. P. J. T.; van Hest, J. C. M.; van Delft, F. L. *Chem. Commun.* **2010**, *46*, 97.

13. Dommerholt, J.; Schmidt, S.; Temming, R.; Hendriks, L. J. A.; Rutjes, F. P. J. T.; van Hest, J. C. M.; Lefeber, D. J.; Friedl, P.; van Delft, F. L. *Angew. Chem. Int. Ed Engl.* **2010**, *49*, 9422.

14. Thalhammer, F.; Wallfahrer, U.; Sauer, J. *Tetrahedron Lett.* **1990**, *31*, 6851.

15. Sauer, J.; Heldmann, D. K.; Hetzenegger, J.; Krauthan, J.; Sichert, H.; Schuster, J. *Eur. J. Org. Chem.* **1998**, *1998*, 2885.

16. Chen, W.; Wang, D.; Dai, C.; Hamelberg, D.; Wang, B. *Chem. Commun.* **2012**, *48*, 1736.
17. Rademacher, P. *Chem. Rev.* **2003**, *103*, 933.

18. Levandowski, B. J.; Hamlin, T. A.; Bickelhaupt, F. M.; Houk, K. N. *J. Org. Chem.* **2017**, *82*, 8668.

19 Levandowski, B. J.; Houk, K. N. *J. Am. Chem. Soc.* **2016**, *138*, 16731.

20 Wang, D.; Chen, W.; Zheng, Y.; Dai, C.; Wang, K.; Ke, B.; Wang, B. *Org. Biomol. Chem.* **2014**, *12* (23), 3950.

21.Yang, J.; Šečkutė, J.; Cole, C. M.; Devaraj, N. K. *Angew. Chem. Int. Ed Engl.* **2012**, *51*, 7476.

22. Patterson, D. M.; Nazarova, L. A.; Xie, B.; Kamber, D. N.; Prescher, J. A. *J. Am. Chem. Soc.* **2012**, *134*, 18638.
23. Kamber, D. N.; Nazarova, L. A.; Liang, Y.; Lopez, S. A.; Patterson, D. M.; Shih, H.-W.; Houk, K. N.; Prescher, J. A. *J. Am. Chem. Soc.* **2013**, *135*, 13680.

24. Kamber, D.; Nguyen, S.; Liang, Y.; Liu, F.; Briggs, J.; Shih, H.-. W.; Houk, K. N.; Prescher, J. Isomeric 1,2,4-triazines exhibit distinct profiles of bioorthogonal reactivity. (Unpublished)

25. Karver, M. R.; Weissleder, R.; Hilderbrand, S. A. *Angew. Chem. Int. Ed Engl.* **2012**, *51*, 920.

26. Karver, M. R.; Weissleder, R.; Hilderbrand, S. A. *Bioconjug. Chem.* **2011**, *22*, 2263.

27. Kamber, D. N.; Liang, Y.; Blizzard, R. J.; Liu, F.; Mehl, R. A.; Houk, K. N.; Prescher, J. A. *J. Am. Chem. Soc.* **2015**, *137*, 8388.

28. Patterson, D. M.; Nazarova, L. A.; Prescher, J. A. *ACS Chem. Biol.* **2014**, *9*, 592.

29. McKay, C. S.; Finn, M. G. *Chem. Biol.* **2014**, *21*, 1075.

30. Diels, O.; Alder, K. *Justus Liebigs Ann. Chem.* **1928**, *460*, 98.

31. Paquette, L. A.; Wyvratt, M. J. *J. Am. Chem. Soc.* **1974**, *96*, 4671.

32. Horton, D.; Machinami, T.; Takagi, Y.; Bergmann, C. W.; Christoph, G. C. *J. Chem. Soc. Chem. Commun.* **1983**, 1164.

33. Pang, L. S. K.; Wilson, M. A. *J. Phys. Chem.* **1993**, *97*, 6761.

34. Bian, S.; Scott, A. M.; Cao, Y.; Liang, Y.; Osuna, S.; Houk, K. N.; Braunschweig, A. B. *J. Am. Chem. Soc.* **2013**, *135*, 9240.

35. Yousaf, M. N.; Mrksich, M. *J. Am. Chem. Soc.* **1999**, *121*, 4286.

36. Binger, P.; Wedemann, P.; Goddard, R.; Brinker, U. H. *J. Org. Chem.* **1996**, *61*, 6462.
37. Wiberg, K. B.; Bartley, W. J. *J. Am. Chem. Soc.* **1960**, *82*, 6375.

38. Khambata, B. S.; Wassermann, A. *Nature* **1936**, *137*, 496.

39. Eibler, E.; Burgemeister, T.; Höcht, P.; Prantl, B.; Roßmaier, H.; Schuhbauer, H. M.; Wiest, H.; Sauer, J. *Liebigs Ann./Recl.* **1997**, *1997*, 2451.

40. Eibler, E.; Höcht, P.; Prantl, B.; Roßmaier, H.; Schuhbauer, H. M.; Wiest, H.; Sauer, J. *Liebigs Ann./Recl.* **1997**, *1997*, 2471.

41. Nyulászi, L.; Schleyer, P. von R. *J. Am. Chem. Soc.* **1999**, *121*, 6872.

42. von Ragué Schleyer, P.; Nyulászi, L.; Kárpáti, T. *Eur. J. Org. Chem.* **2003**, *2003*, 1923.

43. Fernández, I.; Wu, J. I.; Schleyer, P. von R. *Org. Lett.* **2013**, *15*, 2990.

44. Levandowski, B. J.; Houk, K. N. *J. Org. Chem.* **2015**, *80*, 3530.

45. Levandowski, B. J.; Zou, L.; Houk, K. N. *J. Comput. Chem.* **2016**, *37*, 117.

46. Chang, W.-H. *J. Chem. Soc.* **1965**, *0*, 2305.

47. Zhao, Y.; Truhlar, D. G. *Theor. Chem. Acc.* **2008**, *120*, 215.

48. Cossi, M.; Rega, N.; Scalmani, G.; Barone, V. *J. Comput. Chem.* **2003**, *24*, 669.

49. Barone, V.; Cossi, M. *J. Phys. Chem. A* **1998**, *102*, 1995.

50. Stöckmann, H.; Neves, A. A.; Day, H. A.; Stairs, S.; Brindle, K. M.; Leeper, F. J. *Chem. Commun.* **2011**, *47*, 7203.

51. Su, T. P. *J. Biomed. Sci.* **2000**, *7*, 195.

52. Murrey, H. E.; Judkins, J. C.; am Ende, C. W.; Ballard, T. E.; Fang, Y.; Riccardi, K.; Di, L.; Guilmette, E. R.; Schwartz, J. W.; Fox, J. M.; Johnson, D. S. *J. Am. Chem. Soc.* **2015**, *137*, 11461.

Chapter 5. *Syn* and *Anti* π-facial Selectivity in Thiophene 1-oxide Cycloadditions

5.1 Introduction to Thiophene 1-oxide Cycloadditions

The high reactivities, selectivities, and yields of thiophene 1-oxide cycloadditions warrant their classification as click reactions, alongside the useful and well studied inverse electron-demand Diels–Alder reactions of tetrazines.[1]Thiophene 1-oxides react with electron-rich, electron-neutral, and electron-deficient dienophiles in the Diels–Alder reaction with exclusive *syn* π-facial stereoselectivity, as shown in Scheme 1[2-10] *Syn* refers to the reaction where the dienophile adds *syn* to the oxygen.

Scheme 5.1. *Syn* stereoselectivity in Diels-Alder reactions of thiophene 1-oxides with three dienophiles.

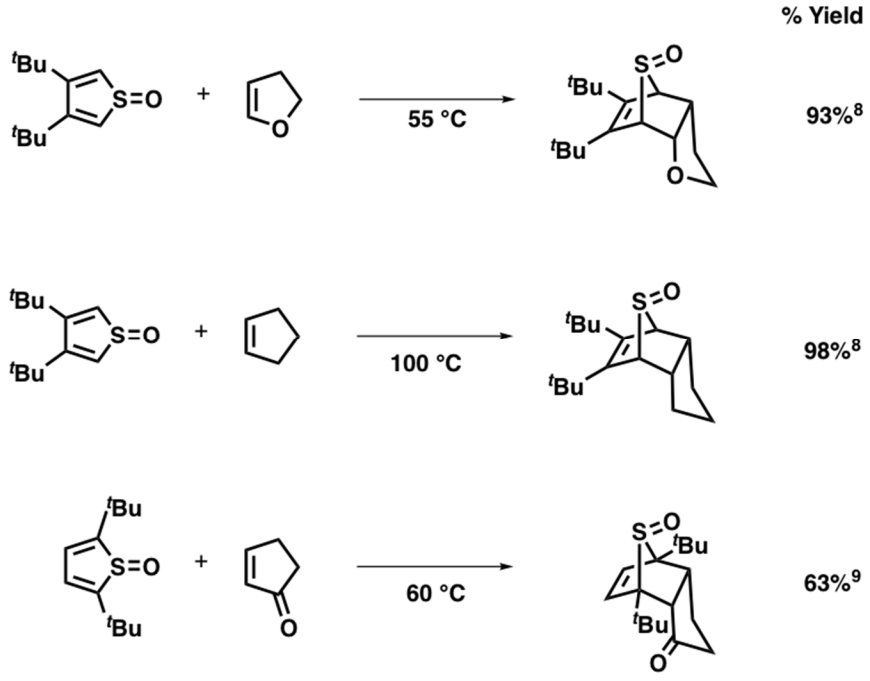

Previously proposed explanations for the *syn* π-facial stereoselectivity in thiophene 1-oxide Diels–Alder reactions are summarized in Scheme 2. Fallis et al. reported X-ray crystal structures for the thiophene 1-oxide adducts with a series of dienophiles and attributed the *syn* π-facial stereoselectivity to the Cieplak Effect.[2] In the

Cieplak model, stereoselectivity is controlled by hyperconjugation between an antiperiplanar donor orbital and the σ* acceptor orbitals of the incipient bonds in the transition state.[11,12] The lone pair on sulfur in thiophene 1-oxide is a stronger donor compared to the S═O bond of the sulfoxide moiety. The Cieplak model correctly predicts that dienophiles will attack *anti* to the sulfur lone pair and *syn* to the sulfoxide oxygen (Scheme 2A).

Scheme 5.2. Previous explanations for the *syn* π-facial stereoselectivity of thiophene 1-oxide Diels-Alder reactions.

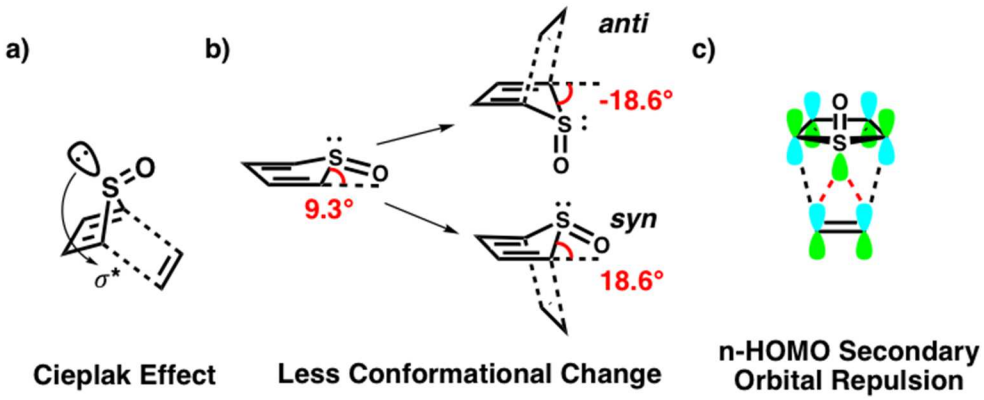

An extensive experimental and computational study by Nakayama showed that thiophene 1-oxide Diels–Alder reactions are inverse electron-demand reactions with electron-rich, electron-neutral, and electron-deficient dienophiles.[8] They computed the *syn* and *anti* transition state geometries and reported that the envelope geometry of the thiophene 1-oxide ground state requires less geometrical change of the S═O bond about the plane of the diene to achieve the *syn* transition state geometry (Scheme 2b). Additionally, a destabilizing interaction in the *anti* transition state involving the nonbonding sulfur lone pair with the HOMO of the dienophile was proposed as a potential factor disfavoring the *anti* transition state (Scheme 2c).[10c] Because of our theoretical interest in the reactivity and stereoselectivity of 5-X-cyclopentadienes[13] and

heterocyclic analogues,[14] and of the distortion/interaction activation-strain[15] method of analysis, we have reinvestigated this phenomenon. We have found that hyperconjugative antiaromaticity in the thiophene 1-oxide ground state and distortion energies control stereoselectivity.

5.2 Computational Methods

Computations were performed in Gaussian 09, revision D.0.1.[16] with the M06-2X density functional that provides accurate energies for cycloaddition reactions.[17] Geometry optimizations and single point energies reported here were computed with the 6-31+G(d) and 6-311++G(d,p) basis sets, respectively. Truhlar's quasiharmonic correction was applied by setting all positive frequencies below 100 cm^{-1} to a value of 100 cm^{-1}.[18]

5.3 Origin of the *Syn* Kinetic Preference

Figure 1 shows the activation free energies ($\Delta G^{\ddagger}$) for the *syn*- and *anti-endo* Diels–Alder reactions of thiophene 1-oxide with cyclopentene (**1**), cyclopentenone (**2**), and 2,3-dihydrofuran (**3**). The *syn-endo* reactions are favored by 7–8 kcal/mol relative to the *anti-endo* transition state. The activation free energies for the *syn-exo* and *anti-exo* reactions are 4–5 and 2 kcal/mol higher in energy than the *syn-endo* and *anti-endo* reactions, respectively.

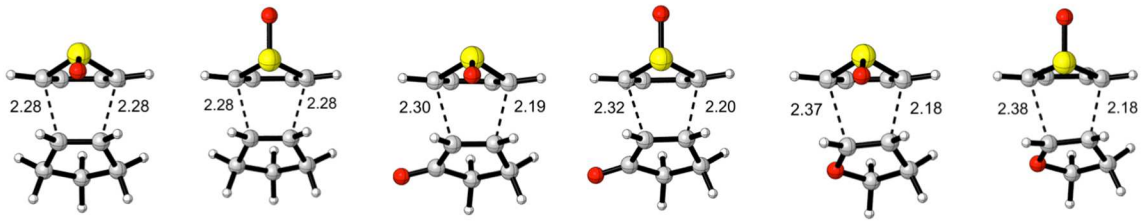

Figure 5.1 Activation free energies in kcal/mol for the *syn* and *anti endo* Diels-Alder reactions of thiophene 1-oxide with cyclopentene (**TS-1**), cyclopentenone (**TS-2**), and 2,3-dihydrofuran (**TS-3**).

We computed the *syn* and *anti* transition structures and adducts for the Diels–Alder reaction with the simplest dienophile, ethylene (Figure 2) to study the intrinsic selectivity of thiophene 1-oxide. The Diels–Alder transition structures for both the *anti* and *syn* transition states with ethylene are synchronous with forming bond lengths of 2.29 Å. The *syn* reaction is favored kinetically and thermodynamically. The reactions are exothermic with reaction free energies of −32 and −25 kcal/mol for the *syn* and *anti* adducts, respectively. The activation free energies are 19 and 27 kcal/mol for the *syn* and *anti* transition states, respectively.

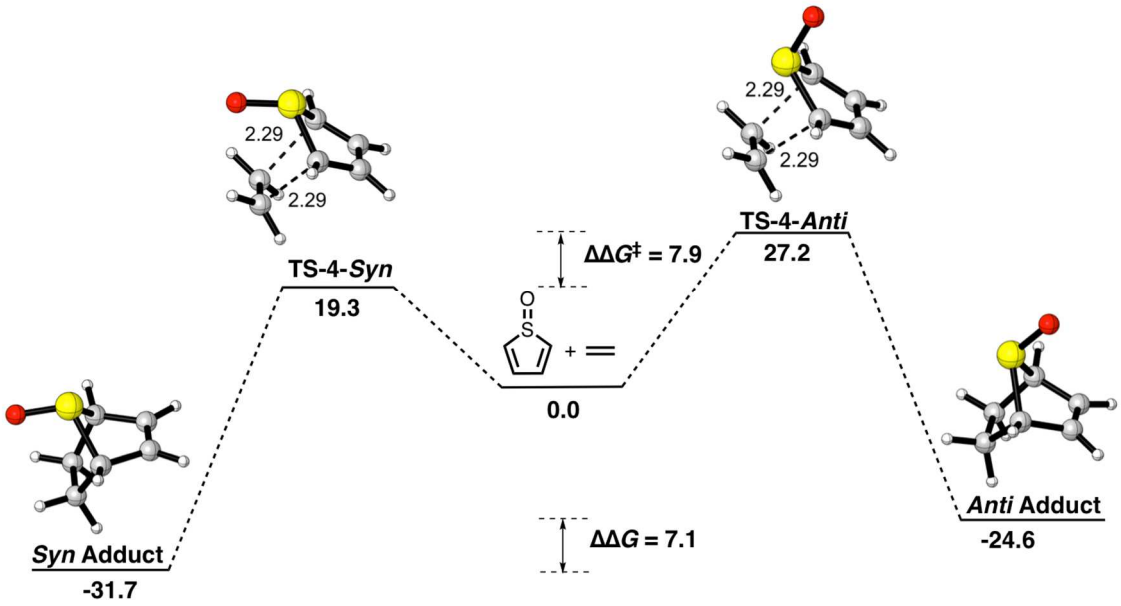

Figure 5.2 Computed reaction profile for the *syn* and *anti* Diels-Alder reactions of thiophene 1-oxide with ethylene. Bond lengths are reported in Ångstroms and free energies are reported in kcal/mol.

We have analyzed the differences in the transition state energies with the distortion/interaction activation-strain model.[15] This model dissects the activation energy into two energetic terms: distortion energy ($\Delta E^{\ddagger}_{d}$) is the energy required to geometrically deform the ground state geometries of the reacting diene and dienophile into their

respective transition state geometries; interaction energy ($\Delta E^{\ddagger}_{i}$) is calculated as the difference between the activation energy ($\Delta E^{\ddagger}$) and the distortion (strain) energy ($\Delta E^{\ddagger}_{i} = \Delta E^{\ddagger} - \Delta E^{\ddagger}_{d}$) and represents the strength of the interactions between the distorted diene and dienophile at the transition state. The interaction energies include the effects of electrostatic interactions, closed shell repulsions (steric effects), dispersion, and charge transfer between the occupied orbitals (HOMO) of one reacting species with the unoccupied orbitals (LUMO) of the other reacting species.[19]

The distortion/interaction analysis was performed on the *syn* and *anti* transition states of the thiophene 1-oxide Diels–Alder reaction with ethylene. Figure 3 shows that the 8 kcal/mol preference for the *syn* transition state results from the difference in the diene distortion energies. It requires 17 kcal/mol to distort the thiophene 1-oxide into the geometry of the *anti* transition state, whereas the *syn* transition state requires only 11 kcal/mol. The interaction and dienophile distortion energies of the *syn* and *anti* transition states each exhibit a 1 kcal/mol preference for the *syn* addition.

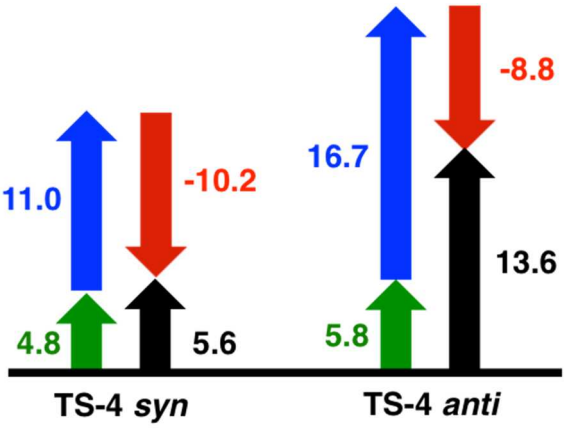

Figure 5.3 Distortion/interaction analysis for the *syn* and *anti* transition structures for the Diels-Alder reaction of thiophene 1-oxide with ethylene. (black, activation energy; green, distortion energy of the dienophile; blue, distortion energy of the diene; red, interaction energy; in kcal/mol).

Figure 4 shows a side view of the thiophene 1-oxide ground state and of the *syn* and *anti*transition states with ethylene. The π–σ* hyperconjugative interaction between the diene π-bonds and the σ^*_{SO} bond destabilizes the thiophene-1-oxide by inducing the 4π antiaromatic character in the diene.[20] The sulfur lone pair interaction with the diene is a stabilizing 6π interaction, but the sulfur atom is tetrahedral with the lone pair mainly *s* in character and not appreciably overlapping with the diene π-system.[21] To minimize the destabilizing effect of the hyperconjugative antiaromaticity, the S═O bond distorts away from the plane of the diene and the thiophene 1-oxide adopts an envelope geometry with CSC plane folded 8° above the plane of the diene. The same predistortion has been observed in 5-fluorocyclopentadiene to minimize the destabilizing π–σ^*_{CF}bond interaction.[13b]

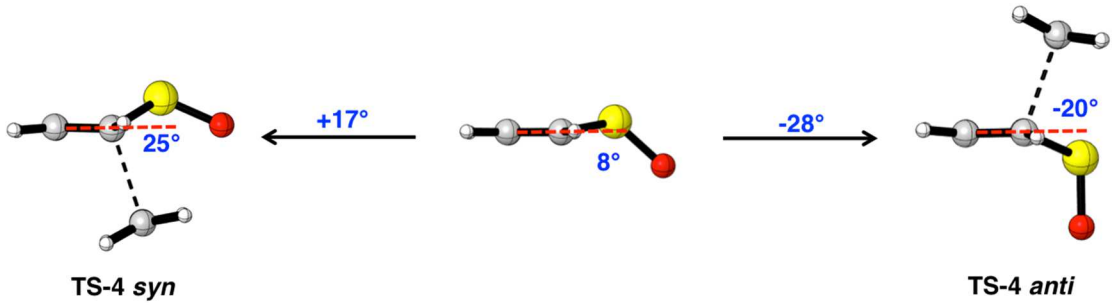

Figure 5.4 Side view of the thiophene 1-oxide ground state and the *syn* and *anti* transition states with ethylene. The out-of-plane bending of the sulfur atom from the plane of the diene is shown in degrees. The plane of the diene is represented by the red dashed line.

The difference in the distortion energies of the *syn* and *anti* transition states controlling the π-facial stereoselectivity is consistent with Nakayama's explanation involving the conformational change of the thiophene 1-oxide.[8] In the *syn* and *anti* transition state structures, the CSC plane is distorted 25° and −20° relative to the plane of the diene, respectively. As a result of the 8° predistortion toward

the *syn* envelope geometry, the *anti* transition state requires an additional distortion of 11° about the CSC plane compared to the *syn* transition state (see Figure 4).

5.4 Origin of the *Syn* Thermodynamic Preference

The origin of the 7 kcal/mol difference between the stabilities of the *syn* and *anti* adducts has not been resolved in literature. Lemal et al. computationally investigated the differences in product stabilities through an isodesmic reaction that relates the energies of the *syn* and *anti* adducts to a saturated analogue.[22] The isodesmic reaction suggests the presence of a stabilizing interaction in the *syn* adduct, but they were unable to identify the nature of the stabilizing interaction.

Scheme 3 shows the hydrogenation enthalpies (ΔH) for the addition of H_2 across the double bond of the *syn* and *anti* adducts and a dioxide analogue for reference. This analysis points to the presence of a 3–4 kcal/mol stabilizing interaction involving the π-bond of the *syn* adduct and a 3–4 kcal/mol destabilizing interaction involving the π-bond of the *anti* adduct. Figure 5a shows a stabilizing hyperconjugative π–σ* interaction between the alkene π-bond and the σ* of the S–O bond in the *syn* adduct that accounts for the *syn* thermodynamic preference. The π–σ* hyperconjugative interaction is not present in the *anti* adduct because the π-bond and the σ^*_{SO} are not antiperiplanar. The natural bonding orbitals (NBOs) of the discussed π_{CC} and σ^*_{SO} orbitals are shown in Figure 5b,c. We used second-order perturbation theory calculations provided by Natural Bond Orbital (NBO 3.1)[23] analysis to quantify the strength of the π_{CC}–σ^*_{SO} interaction. The NBO analysis calculated the strength of the π_{CC}–σ^*_{SO} interaction to be 2.9 kcal/mol in the *syn* adduct, consistent with our prediction from the hydrogenation reactions.

Scheme 5.3 Enthalpies of hydrogenation (ΔH) in kcal/mol for the *syn* and *anti* Diels-Alder adducts and an oxidized analog.

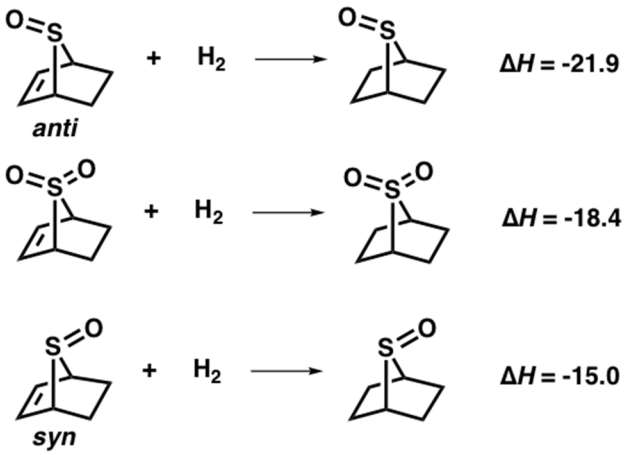

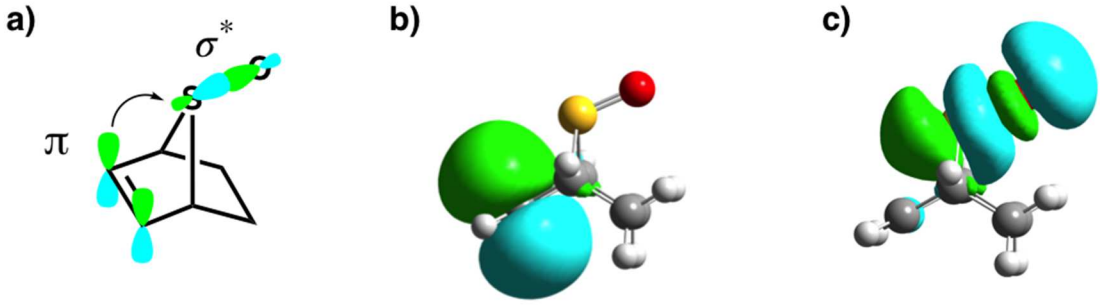

Figure 5.5 a) Stabilizing π-σ^*_{so} interaction in the *syn* adduct b) Visualized π_{cc} NBO c) Visualized σ^*_{so} NBO

Evidence of π–σ^* interactions have been spectroscopically observed in norbornen-7-yl fluorides.[24] When the double bond is *anti* to the C–F bond in the norbornen-7-yl fluoride, the π–σ^*_{CF} interaction causes a large downfield fluoride shift. Figure 6 shows a repulsive *n*–π interaction between the nonbonding oxygen lone pair of the sulfoxy moiety and the $\pi_{C=C}$ bond that is destabilizing in the *anti* adduct. The combination of the stabilizing π–σ^* interaction in the *syn* adduct and the destabilizing repulsive *n*–π interaction in the *anti* adduct result in the 7 kcal/mol thermodynamic preference for the *syn* adduct.

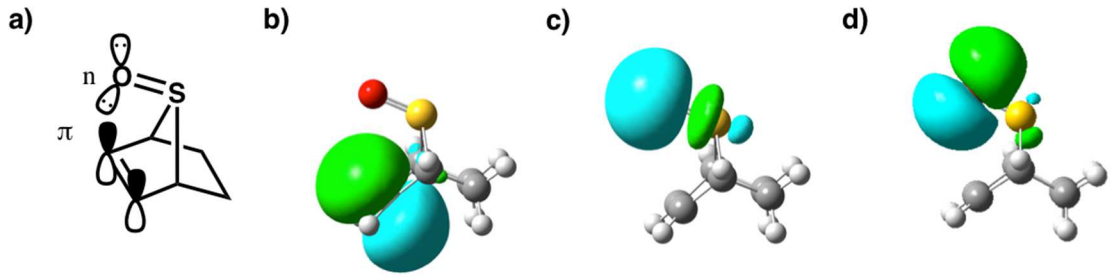

Figure 5.6 a) Repulsive n-π interaction that destabilizes the *anti* adduct b) Visualized π_{cc} NBO c) *s*-type lone pair of sulfoxide oxygen d) *p*-type lone pair of sulfoxide oxygen

5.5 Reactivity of thiophene 1,1-dioxide relative to thiophene 1-oxide

Lemal reported that thiophene 1-oxides rapidly dimerize, while thiophene 1,1-dioxides are less prone to dimerization.[22,25] The free energy profile for the Diels–Alder reaction of thiophene 1,1-dioxide with ethylene is shown in Figure 7. The activation free energy barrier is 26 kcal/mol, similar to the barrier of the thiophene 1-oxide *anti* cycloaddition. Comparatively, the *syn* reaction of thiophene 1-oxide with ethylene has a lower barrier of only 19 kcal/mol (see Figure 2).

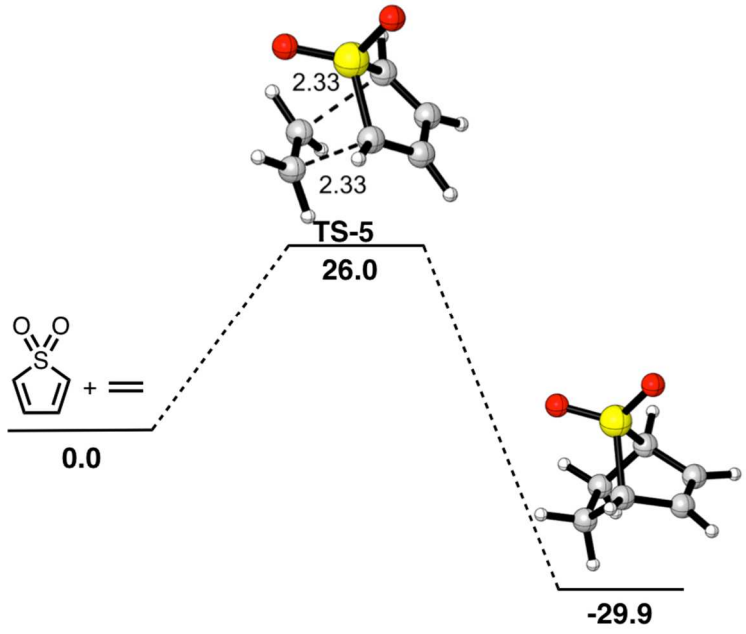

Figure 5.7 Free energy profile for the Diels-Alder reaction of thiophene 1,1-dioxide with ethylene. Forming bond lengths are reported in Å, end energies in kcal/mol.

The frontier molecular orbital (FMO) analysis of thiophene 1-oxide and thiophene 1,1-dioxide with ethylene is shown in Figure 8. Both dienes are inverse electron-demand where the principal interaction is the HOMO of ethylene and the LUMO of the diene. FMO theory predicts that thiophene 1-oxide with a larger FMO gap should be less reactive than thiophene 1,1-dioxide in the inverse electron-demand Diels–Alder reaction with ethylene.

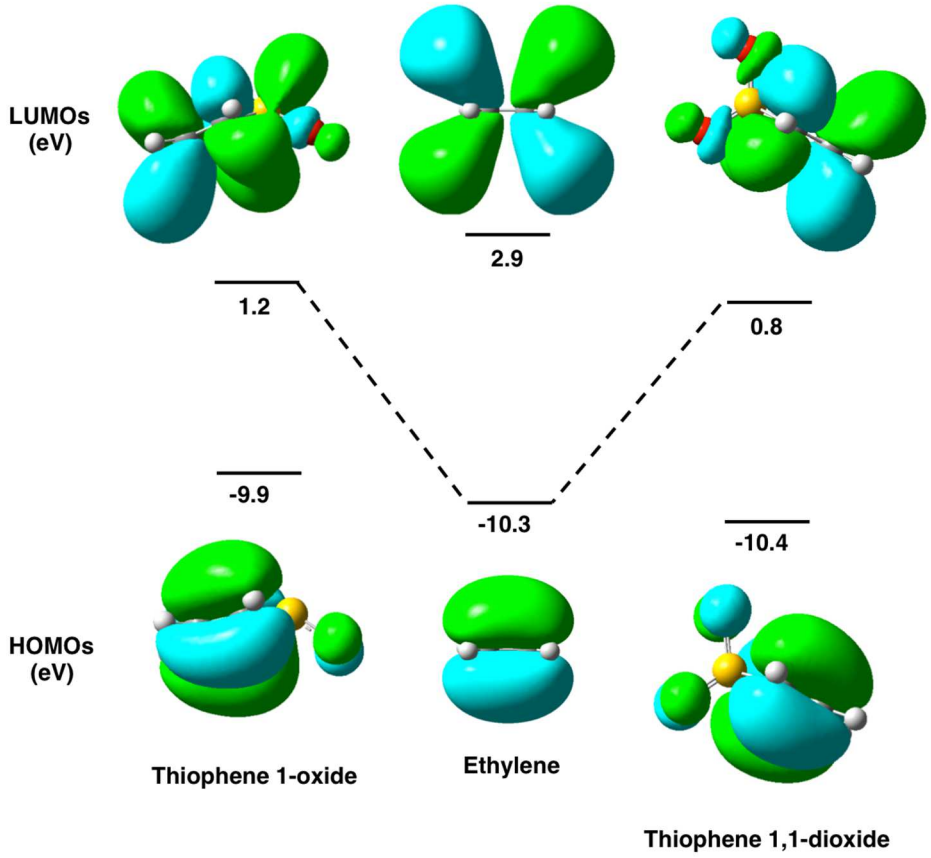

Figure 5.8 Frontier molecular orbitals of thiophene 1-oxide, thiophene 1,1-dioxide, and ethylene with energies reported in electron volts (Ev). Frontier molecular orbital energies computed at the HF/6-311++G(d,p)//M06-2X/6-31+G(d) level of theory.

To understand why thiophene 1-oxide is more reactive than thiophene-1,1-dioxide in the Diels–Alder reaction with ethylene, we analyzed the reaction pathways from a reaction complex with average carbon–carbon bond forming lengths of 2.8 Å to the

transition state geometries using the distortion/interaction-activation strain model.[15] Figure 9 shows that the differences in the Diels–Alder reactivities of thiophene 1-oxides and thiophene 1,1-dioxides result from differences in the distortion energies.

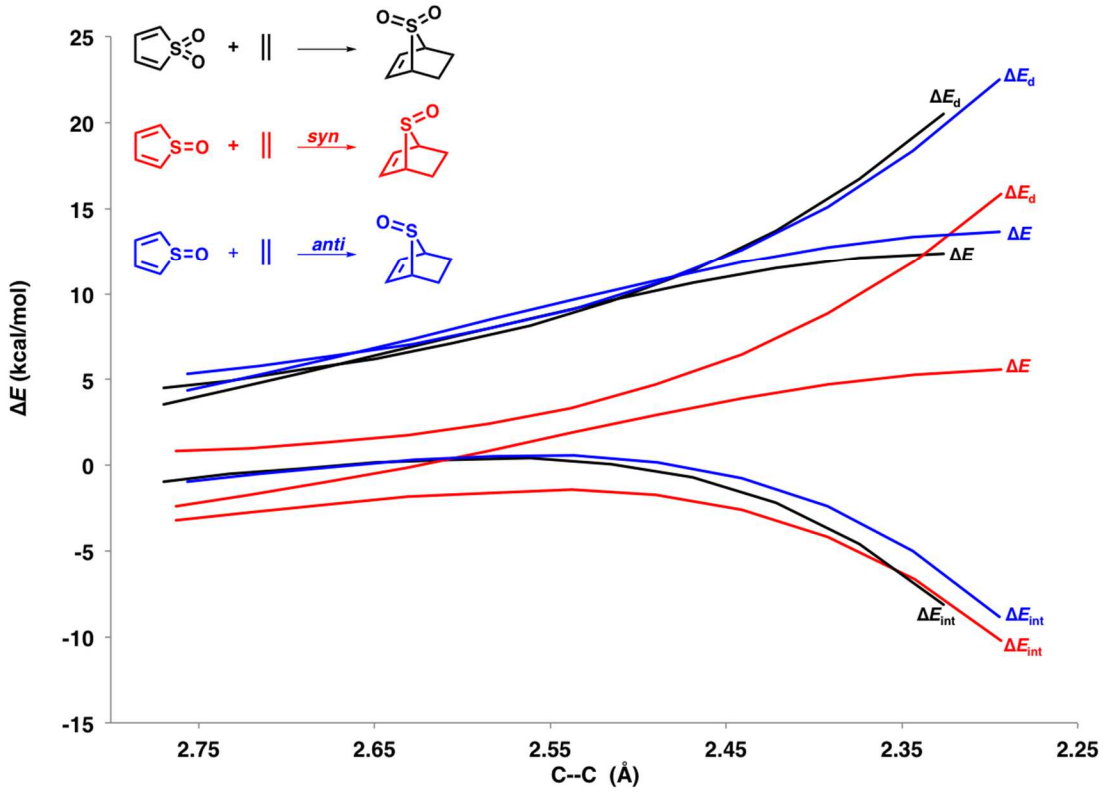

Figure 5.9 Distortion/Interaction-activation strain analysis for the *syn* (red) and *anti* (blue) Diels-Alder reactions of thiophene 1-oxide with ethylene and the Diels-Alder reaction of thiophene 1,1-dioxide with ethylene (black). Electronic activation energies (ΔE), distortion energies (ΔE_d), and interaction energies (ΔE_i).

As shown in Figure 10, the ground state geometry of the thiophene 1,1-dioxide is planar and requires a folding of 22° to achieve the envelope geometry of the transition state. Thiophene 1-oxides are more reactive than thiophene 1,1-dioxides because the ground state geometries of thiophene 1-oxides are predistorted toward the envelope geometries of the *syn* transition states. This is consistent with our previous prediction that

5-fluorocyclopentadiene, which adopts an envelope geometry in the ground state to minimize the effect of the π–σ^*_{CF} antiaromatic hyperconjugative interaction, is more reactive than the planar 5,5-difluorocyclopentadiene in Diels–Alder reactions.[13b]

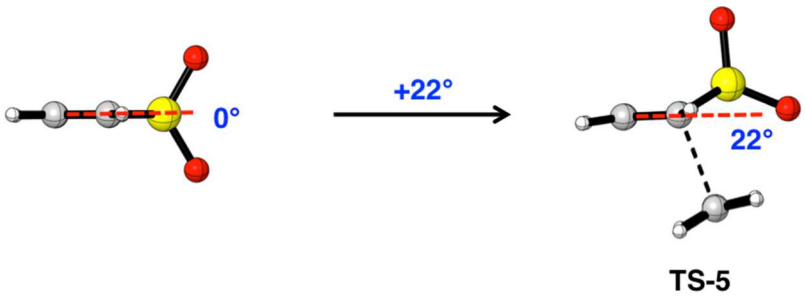

Figure 5.10. Planar geometry of the thiophene 1,1-dioxide and envelope geometry of the thiophene 1,1-oxide transition state with ethylene. The plane of the diene is represented with a red line.

5.6 Conclusions

Analysis of the *syn* and *anti* Diels–Alder reactions with the distortion/interaction-activation strain model reveals that the kinetic preference for the *syn* adduct parallels the differences in the thiophene 1-oxide distortion energies. To reduce the destabilizing effect of hyperconjugative aromaticity, the thiophene 1-oxide is predistorted into an envelope geometry that more closely resembles the envelope geometry of the *syn* transition state. This effect results in the observed *syn* stereoselectivity and high reactivity of thiophene 1-oxide Diels–Alder reactions. The thermodynamic preference for the *syn* adduct is the result of a stabilizing π–σ^*_{SO} interaction in the *syn* adduct and a destabilizing *n*–π interaction in the *anti* adduct.

5.7 References

(1) (a) Jewett, J. C.; Bertozzi, C. R. *Chem. Soc. Rev*. **2010**, *39*, 1272. (b) Liu, F.; Liang, Y.; Houk, K. N. *Acc. Chem. Res*. **2017**, *50*, 2297.

(2) Naperstkow, A. M.; Macaulay, J. B.; Newlands, M. J.; Fallis, A. G. *Tetrahedron Lett.* **1989**, *30*, 5077.

(3) Treiber, A.; Dansette, P. M.; Amri, H. E.; Girault, J. P.; Ginderow, D.; Mornon, J. P.; Mansuy, D. J. *J. Am. Chem. Soc.* **1997**, *119*, 1565.

(4) Li, Y.; Thiemann, T.; Sawada, T.; Mataka, S.; Tashiro, M. *J. Org. Chem.* **1997**, *62*, 7926.

5. Furukawa, N.; Zhang, S.-Z.; Horn, E.; Takahashi, O.; Sato, S. *Heterocycles* **1998**, *47*, 793.

6. Li, Y. Q.; Thiemann, T.; Mimura, K.; Sawada, T.; Mataka, S.; Tashiro, M. Eur. *J. Org. Chem*. **1998**, 1841.

7. Otani, T.; Takayama, J.; Sugihara, Y.; Ishii, A.; Nakayama, J. *J. Am. Chem. Soc*. **2003**, *125*, 8255.

8. J. Takayama, Y. Sugihara, T. Takayanagi, J. Nakayama *Tetrahedron Lett*., **2005**, *46*, 4165.

9. Thiemann, T.; Iniesta, J.; Walton, D. J. Phosphorus, *Sulfur Silicon Relat. Elem*., **2016**, *191*, 876.

10. For reviews, see: (a) Nakayama, J.; Sugihara, Y. *Sulfur Reports*, **1997**, *19*, 349. (b) Nakayama, J.; *Sulfur Reports*, **2000**, *22*, 123. (c) Ishida, M.; Inagaki, S. Orbitals in Chemistry; Inagaki, S., Ed.; Springer-Verlag: Berlin, 2009; Vol. 289, p 183.

(11) (a) Cieplak, A. S. *J. Am. Chem. Soc*. **1981**, *103*, 4540. (b) Cieplak, A. S.; Tait, B. D.; Johnson, C. R. *J. Am. Chem. Soc*. **1989**, 111, 8447.

(12) (a) Macaulay, J. B.; Fallis, A. G. *J. Am. Chem. Soc.* **1990**, *112*, 1136. (b) Coxon, J. M.; McDonald, D. Q. *Tetrahedron Lett*. **1992**, *33*, 651.

(13) (a) Levandowski, B. J.; Hamlin, T. A.; Bickelhaupt, F. M.; Houk, K. N. *J. Org. Chem*. **2017**, *82*, 866. (b) Levandowski, B. J.; Zou, L.; Houk, K. N. *J. Comput. Chem.* **2016**, *37*, 117. (c) Levandowski, B. J.; Houk, K. N. *J. Org. Chem*. **2015**, *80*, 3530.
(14) Fell, J. S.; Martin, B. M.; Houk, K. N. *J. Org. Chem*. **2017**, *82*, 1912−1919.

(15) Bickelhaupt, F. M.; Houk, K. N. *Angew. Chem., Int. Ed*. **2017**, *56*, 2.

(16) Frisch, M. J.; Trucks, G. W.; Schlegel, H. B.; Scuseria, G. E.; Robb, M. A.; Cheeseman, J. R.; Scalmani, G.; Barone, V.; Mennucci, B.; Petersson, G. A.; Nakatsuji, H.; Caricato, M.; Li, X.; Hratchian, H. P.; Izmaylov, A. F.; Bloino, J.; Zheng, G.; Sonnenberg, J. L.; Hada, M.; Ehara, M.; Toyota, K.; Fukuda, R.; Hasegawa, J.; Ishida, M.; Nakajima, T.; Honda, Y.; Kitao, O.; Nakai, H.; Vreven, T.; Montgomery, J. A., Jr.; Peralta, J. E.; Ogliaro, F.; Bearpark, M.; Heyd, J. J.; Brothers, E.; Kudin, K. N.; Staroverov, V. N.; Kobayashi, R.; Normand, J.; Raghavachari, K.; Rendell, A.; Burant, J. C.; Iyengar, S. S.; Tomasi, J.; Cossi, M.; Rega, N.; Millam, M. J.; Klene, M.; Knox, J. E.;

Cross, J. B.; Bakken, V.; Adamo, C.; Jaramillo, J.; Gomperts, R.; Stratmann, R. E.; Yazyev, O.; Austin, A. J.; Cammi, R.; Pomelli, C.; Ochterski, J. W.; Martin, R. L.; Morokuma, K.; Zakrzewski, V. G.; Voth, G. A.; Salvador, P.; Dannenberg, J. J.; Dapprich, S.; Daniels, A. D.; Farkas, Ö.; Foresman, J. B.; Ortiz, J. V.; Cioslowski, J.; Fox, D. J. Gaussian 09, revision D.01; Gaussian, Inc.: Wallingford, CT, 2009.

(17) Zhao, Y.; Truhlar, D. G. *Theor. Chem. Acc*. **2008**, *120*, 215.

(18) Zhao, Y.; Truhlar, D. G. *Phys. Chem. Chem. Phys*. **2008,** *10*, 2813.

(19) Levandowski, B. J.; Houk, K. N. *J. Am. Chem. Soc*. **2016**, *138*, 16731.

(20) L. Nyulászi, P. v. R. Schleyer, *J. Am. Chem. Soc.* **1999**, *121*, 6872 b) L. Nyulászi, T. Kárpáti, P. v. R. Schleyer, Eur. *J. Org. Chem.* **2003**, *10*, 1923.

(21) (a) Mock, W. L. *J. Am. Chem. Soc.* **1970**, *92*, 7610. (b) Pouzet, P.; Erdelmeier, I.; Ginderow, D.; Mornon, J.-P.; Dansette, P.; Mansuy, D. *J. Chem. Soc., Chem. Commun.* **1995**, *0*, 473. (c) Pouzet, P.; Erdelmeier, I.; Ginderow, D.; Mornon, J.-P.; Dansette, P.; Mansuy, D. J. *Heterocycl. Chem.* **1997**, *34*, 1567. (d) Nakayama, J.; Yu, T.; Sugihara, Y.; Ishii, A. *Chem. Lett*. **1997**, *26*, 499.

(22) Lemal, D. M.; Akashi, M.; Lou, Y.; Kumar, V. *J. Org. Chem.* **2013**, *78*, 12330.

(23) NBO Version 3.1, E. D. Glendening, A. E. Reed, J. E. Carpenter, and F. Weinhold.

(24) Adcock, W.; Angus, D. I.; Lowe D. A. *Magn. Reson. Chem.*, **1996**, *34*, 675.

(25) Lemal, D. M. *J. Org. Chem.* **2016**, *81*, 4931.

Chapter 6. Diels-Alder Reactivities of Cyclic Alkenes

6. 1. Introduction to Cycloalkene Diels-Alder Reactions

The exceptional stability and high reactivity of cyclopropenes is of great value for bioorthogonal chemistry.[1] The results of a pioneering kinetic study by Sauer *et al.* on the reactivity of a strained cycloalkene series, from cyclopropene to cyclohexene, with 3,6-bis(trifluoromethyl)tetrazine are shown in Scheme 1.[2] The reactivities of the strained cycloalkene series span 6 orders of magnitude and decrease as the ring size of the cycloalkene increases. The cyclopropene cycloaddition with the electron-deficient 3,6-bis(trifluoromethyl)tetrazine is extremely rapid, while cyclobutene, the second most strained cycloalkene, reacts 100 times more slowly than cyclopropene.

Scheme 6.1 Reactivities of strained cycloalkenes in the inverse electron-demand Diels-Alder reaction with 3,6-bis(trifluoromethyl)tetrazine.

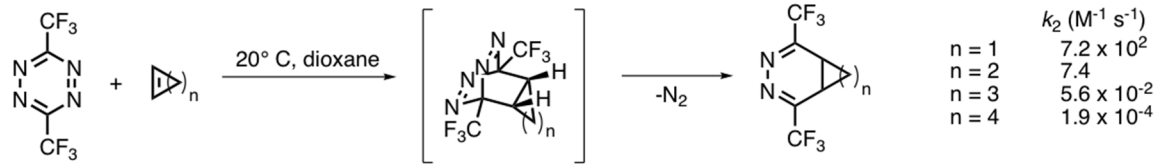

	k_2 (M^{-1} s^{-1})
n = 1	7.2×10^{2}
n = 2	7.4
n = 3	5.6×10^{-2}
n = 4	1.9×10^{-4}

The trend in reactivity of the strained cycloalkenes has been rationalized previously in terms of the differences in distortion energies for different cycloalkenes.[3] Liu *et al.* analyzed the reactivity of cycloalkenes with 1,3-dimethoxybutadiene, cyclopentadiene, 3,6-bis(dimethyl)tetrazine, and 3,6-bis(trifluoromethyl)tetrazine using the distortion/interaction-activation strain model (D/I-ASM) developed independently by Bickelhaupt and Houk.[4] The s-character of the olefinic carbon C-H bonds increases from $sp^{2.4}$ in cyclohexene to $sp^{1.5}$ in cyclopropene. The differences in the out-of-plane distortion energies of the cycloalkene C-H bonds were verified computationally and are

consistent with the out-of-plane force constants observed in IR studies.[5] Liu *et al.* concluded that the larger degree of s-character lessens the energy required to distort the cycloalkene into the transition state geometry, thereby increasing the reactivity. The same conclusion was drawn earlier by Paton *et al.* to describe the differences in the reactivities of strained cycloalkenones with cyclopentadiene.[6]

We have shown that orbital interactions largely control the reactivity and stereoselectivity in Diels-Alder reactions of cyclopropenes.[7] The experimentally measured highest occupied molecular orbital (HOMO) and lowest unoccupied molecular orbital (LUMO) energies of the strained cycloalkenes are shown in Scheme 2 and range from –9.86 to –8.94 and 1.73 to 2.13 eV, respectively.[8,9] Staley *et al*. computed the ground state geometries of the cycloalkenes at the HF/6-31G(d) level of theory and rationalized the differences in the HOMO and LUMO energies of **1**-**4**.[9] As the ring size of the cycloalkene increases, the alkyl groups reorient, and overlap of the πCH_2 orbitals with the π and π^* orbitals decreases, weakening the hyperconjugative interactions.

Scheme 6.2 Structures of cycloalkenes **1**-**4** and their respective experimental HOMO and LUMO energies (eV).

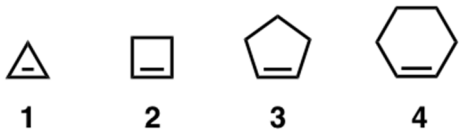

	1	**2**	**3**	**4**
LUMO (eV)	1.73	2.00	2.14	2.13
HOMO (ev)	-9.86	-9.59	-9.18	-8.94

To determine the effect of orbital interactions on the reactivity of the strained cycloalkenes, we have investigated the Diels-Alder reactivity of strained cycloalkenes, **1**-**4**, with the highly reactive cyclopentadiene[10] (**Cp**) and the electron-deficient 3,6-

bis(trifluoromethyl)tetrazine (**Tz**) using the distortion/interaction-activation strain model.[4] Further insight into reactivity is provided from an energy decomposition analysis (EDA).

6.2 Computational Methods

Geometry optimization of all stationary points was performed using *Gaussian 09*, revision D.01,[12] employing the metahybrid M06-2X[13] exchange-correlation functional combined with the double-ζ quality 6-31+G(d) basis set. Single point energies were calculated at the calculated at the M06-2X/6-311++G(d)//M06-2X/6-31+G(d) level of theory. Free energies calculated with the M06-2X functional are known to be more accurate than with other functionals.[14] Energy minima and transition states were verified through vibrational analysis.[15] All minima were found to have zero imaginary frequencies, while all transition states had a single imaginary frequency. The associated eigenvectors were confirmed to correspond to the motion along the reaction coordinate using the intrinsic reaction coordinate (IRC) method.[16] The distortion/interaction-activation strain model and energy decomposition analyses were carried out using the ADF.2016.102 program[17] at the M06-2X level of theory in conjunction with the all electron, triple-ζ quality TZ2P basis set[18] on the geometries optimized at M06-2X/6-31+G(d) in *Gaussian 09*. The accuracy parameter of both the Becke grid integration and ZLMfit were set to VERYGOOD.[19] Additionally, to increase the accuracy of the total energy and, thus, improve convergence, the ADDDIFFUSEFIT keyword was used. This is recommended for all calculations in ADF using the M06-2X exchange-correlation functional. Optimized structures were illustrated using CYLview.[20]

Quantitative insight into how activation barriers arise for Diels-Alder reactions between **Cp** and **Tz** with **1-4** is afforded by the distortion/interaction-activation strain model (D/I-ASM).[4] The potential energy surface $\Delta E(\zeta)$ is decomposed, along the reaction coordinate ζ into the strain $\Delta E_{strain}(\zeta)$ associated with deforming the individual reactants plus the actual interaction $\Delta E_{int}(\zeta)$ between the deformed reactants.

$$\Delta E^{\ddagger}(\zeta) = \Delta E_{strain}(\zeta) + \Delta E_{int}(\zeta) \quad (1)$$

The strain $\Delta E_{strain}(\zeta)$ is primarily determined by the rigidity of the reactants and by the extent to which groups must reorganize or distort to achieve the transition state geometry. The interaction $\Delta E_{int}(\zeta)$ between the reactants depends on their electronic structure and on how they are mutually oriented as they approach each other.

In graphical representations, the IRC is projected onto the average distance of the newly forming C···C bonds. The resulting reaction coordinate ζ undergoes a well-defined change in the course of the reaction from the reactant complex to the C···C distance in the transition state and cycloadducts.

The interaction $\Delta E_{int}(\zeta)$ between the strained reactants is further analyzed in the conceptual framework provided by the Kohn–Sham molecular orbital (KS-MO) model,[21] and is decomposed into three physically meaningful terms:

$$\Delta E_{int}(\zeta) = \Delta V_{elstat}(\zeta) + \Delta E_{Pauli}(\zeta) + \Delta E_{oi}(\zeta) \quad (2)$$

The $\Delta V_{elstat}(\zeta)$ term corresponds to the classical electrostatic interaction between unperturbed charge distributions $\rho_A(r) + \rho_B(r)$ of the deformed fragments A and B and is

usually attractive. The Pauli repulsion $\Delta E_{\text{Pauli}}(\zeta)$ comprises the destabilizing interactions between occupied orbitals and is responsible for any steric repulsion. The orbital interaction ΔE_{oi} accounts for charge transfer (interaction between occupied orbitals on one fragment with unoccupied orbitals of the other fragment, including HOMO–LUMO interactions) and polarization (empty–occupied orbital mixing on one fragment due to the presence of another fragment).

The distortion/interaction-activation strain analysis (D/I-ASA) was performed with the aid of the PyFrag program[22] along the reaction coordinate calculated with *Gaussian 09*.

6.3 Computed Reactivity Trends

The transition structures and the corresponding Gibbs activation free energies ($\Delta G^{\ddagger}$), Gibbs free energies (ΔG), and predicted rates (k_{rel}) relative to the cyclohexene cycloaddition for the Diels-Alder reactions of the cyclic alkenes with cyclopentadiene (**Cp**) and 3,6-bis(trifluoromethyl)tetrazine (**Tz**) are shown in Figure 1. In the normal electron-demand Diels-Alder reaction of cyclopentadiene, the *endo* transition states are favored by 1.7 to 4.2 kcal mol^{-1} over the *exo* transition states, and the relative reaction rates of the cycloalkene series span 11 orders of magnitude. Cyclopropene reacts ~700,000 times faster than cyclobutene with **Cp** in the *endo* transition state. With **Tz** in the inverse electron-demand Diels-Alder reaction, cyclopropene is only ~10 times more reactive than cyclobutene, and the overall reactivity of the strained cycloalkene series spans 6 orders of magnitude. The experimental rates for the Diels-Alder reactions of the strained cycloalkenes with **Tz** (Scheme 1) span 6 orders of magnitude in agreement with these predicted rate constants.[2]

The length of the forming bonds in the transition state are shown in Å. The cycloaddition of cyclopropene has the earliest transition state and is the most exergonic reaction in the series. The transition structures become later in structure and the Gibbs free reaction energies become less exergonic as the ring size of the cycloalkene increases. The change to a later transition structure as the cycloalkene cycloaddition becomes less exergonic is in accordance with the Hammond postulate.

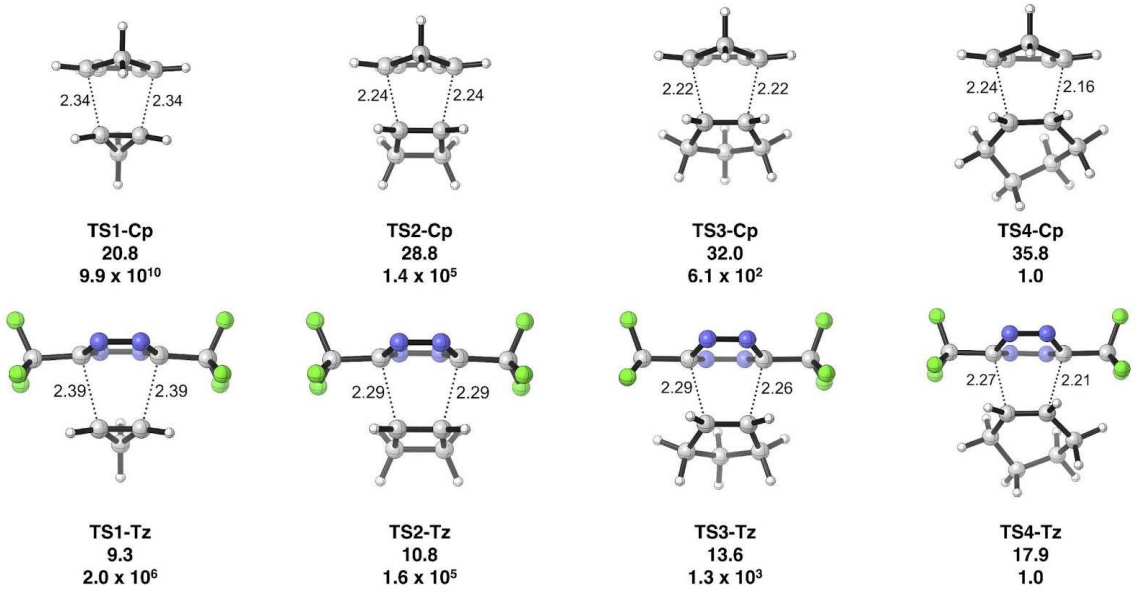

Figure 6.1 Transition structures with forming bond lengths in Å, computed Gibbs activation free energies ($\Delta G^{\ddagger}$, blue, kcal mol^{-1}), relative rate constants (k_{rel}, M^{-1} s^{-1}, black), and Gibbs reaction free energies (ΔG_{rxn}, red, kcal mol^{-1}), for the Diels-Alder reactions of cycloalkenes **1** to **4** with cyclopentadiene and 3,6-bis(trifluoromethyl)tetrazine in the *endo* approach, computed at the M06-2X/6-311++G(d)//M06-2X/6-31+G(d) level of theory.

6.4 Distortion/Interaction-Activation Strain Analysis

The distortion/interaction-activation strain analysis has previously been applied to analyze the transition state geometries of the strained cycloalkene series with **Cp** and **Tz**.[3] Figure 2a and 2b show how the $\Delta E^{\ddagger}$ values correlate with the $\Delta E^{\ddagger}_{d}$ (= ΔE_{strain}) calculated

at the transition state of each reaction for the reactions of **1-4** with **Cp** and **Tz**, respectively.

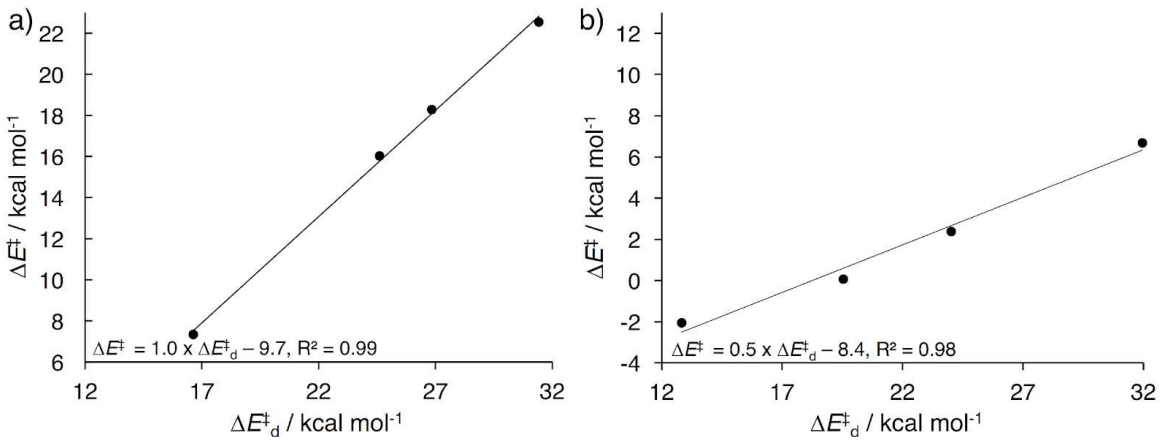

Figure 6.2 Plots of the activation energies ($\Delta E^{\ddagger}$) versus the distortion energy ($\Delta E^{\ddagger}_{d}$) for the reaction of 1-4 with (a) **Cp** and (b) **Tz**. Analysis was performed on transition state structures.

In the current study, we have analyzed the geometries of the Diels-Alder reactions at constant C···C bond-forming lengths because the position of the transition states shifts from early to late as the ring size of the cycloalkene is increased from **1-4**. Figures 3 and 4 show plots of the electronic activation energies ($\Delta E^{\ddagger}$) versus the interaction (ΔE_{int}) and strain (ΔE_{strain}) energies for the Diels-Alder reactions of cycloalkenes, **1-4**, with **Cp** and **Tz**. The comparisons are made on geometries with an average C···C bond forming distance for each series of reactions, that is, at a C 2.34 Å for **Cp** and 2.39 Å for **Tz**.

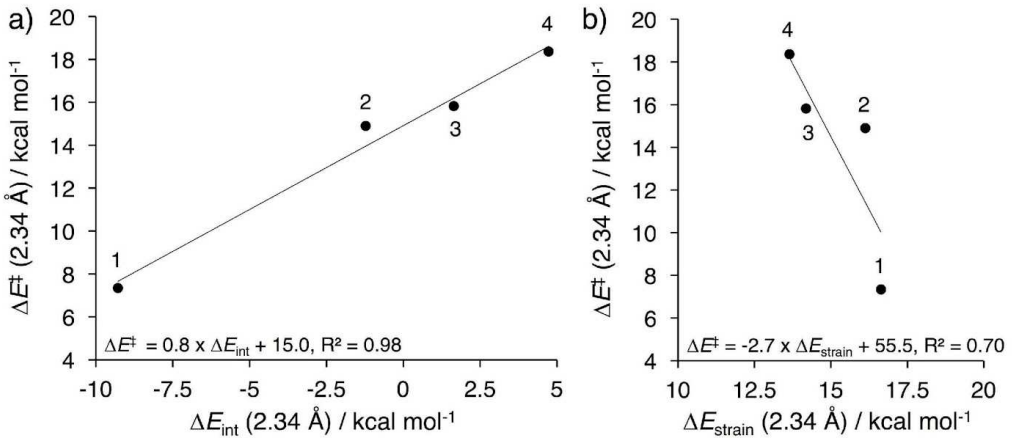

Figure 6.3 Plots of the activation energies ($\Delta E^{\ddagger}$) versus both the (a) interaction energy (ΔE_{int}) and (b) strain energy (ΔE_{strain}) for the reactions of **1**-**4** with **Cp**. Analysis was performed on complexes with C···C bond forming distances of 2.34 Å.

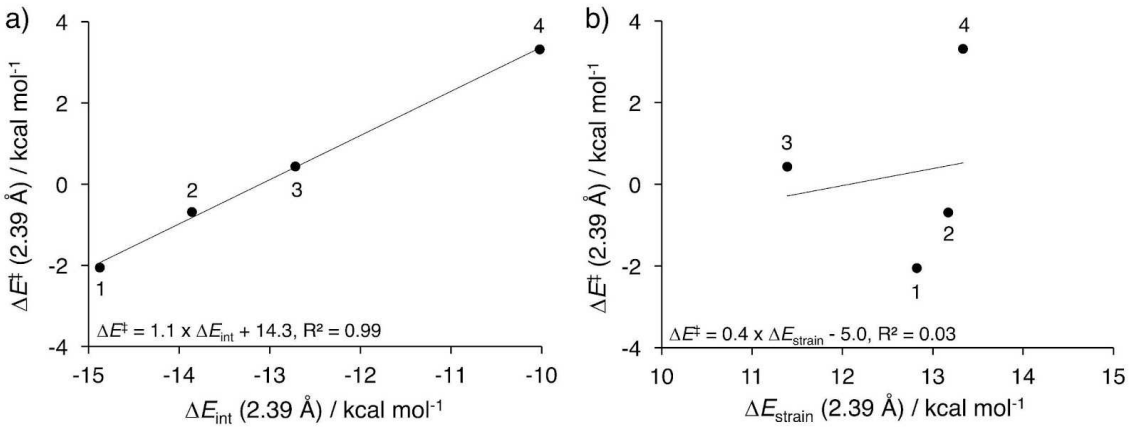

Figure 6.4 Plots of the activation energies ($\Delta E^{\ddagger}$) versus both the (a) interaction energy (ΔE_{int}) and (b) strain energy (ΔE_{strain}) for the reactions of **1**-**4** with **Tz**. Analysis was performed on complexes with C···C bond forming distances of 2.39 Å.

There is a strong correlation ($R^2 \geq 0.98$) between the electronic activation energies and the interaction energy (Figure 2a and 3a). When the reactions of **1**-**4** with **Cp** and **Tz** are compared at analogous geometries, the interaction energies control reactivity. The correlation between the activation energies and distortion is modest in Figure 3b ($R^2 = 0.70$) and non-existent in Figure 4b ($R^2 = 0.03$). When the distortion/interaction activation strain analysis was performed at the transition state geometries (Figure 2),[3,6] the activation energies correlated with the distortion energies

and the interaction energies remain nearly constant. However, it is the differences in the position of the transition state that cause the difference in activation energies to correlate with the differences in distortion energy when the distortion/interaction activation strain analysis is performed on the transition state geometries.

The distortion/interaction-activation strain model (D/I-ASM) has been applied along the intrinsic reaction coordinates defined by the average C···C bond forming distance for the series cycloadditions. Figures 5 and 6 graphically represent how the computed distortion/interaction-activation strain and interaction energy components evolve along the reaction coordinate, respectively. Figure 5 shows that the reactivity differences of the cycloalkene series with **Cp** originate from the differences in the strengths of the interactions between deformed reactants along the reaction coordinate. At a consistent geometry with an average C···C bond forming distance of 2.34 Å, a value of ΔE_{int} = −9.3, −1.2, 1.6, and 4.7 kcal mol^{-1} was computed for the reaction of **Cp** with **1-4**, respectively. The strain energy ΔE_{strain} remains nearly constant at this point for all four reactions. The interaction between the reactants along the reaction coordinate controls the Diels-Alder reactivity of the cycloalkenes.

The different contributors to the total interaction energy, ΔE_{int}, were analyzed by the EDA method as represented in equation 2. In Figure 5b, the EDA terms are plotted along the same reaction coordinate. The orbital interaction ΔE_{oi} term dominates the differences in the interaction energies. At the same average C···C bond forming distance of 2.34 Å, a value of ΔE_{oi} = −38.0, −32.6, −30.6, and −26.9 kcal mol^{-1} for **1-4**, respectively (see Figure 4b). The differences in the stabilizing electrostatic interactions

show the opposite trend as the Pauli repulsion, so the ΔE_{Pauli} and ΔE_{elstat} more or less cancel along the reaction coordinate for all the cycloalkene systems.

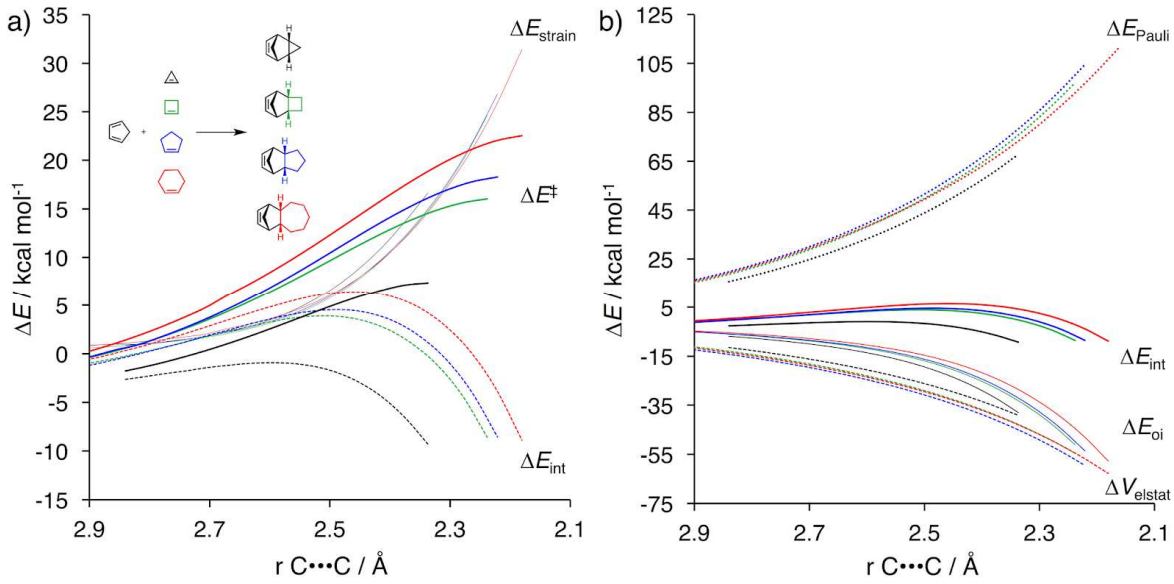

Figure 6.5 (a) Distortion/interaction-activation strain analyses and (b) energy decomposition analyses of the cycloaddition reactions of **Cp** with dienophiles **1-4**. All data were computed at the M06-2X/TZ2P//M06-2X/6-31+G(d) level.

We also analyzed the Diels-Alder reaction of **Tz** with cycloalkenes **1-4** by the D/I-ASM and EDA. The strain curves ΔE_{strain} are nearly identical for the inverse electron-demand cycloadditions of cycloalkenes **1-4** with **Tz** in Figure 5a. The reactivity differences result from the differences in the interaction energies. The ΔE_{int} between the deformed reactants with average C···C bond forming distances of 2.39 Å are ΔE_{int} = −14.8, −13.8, −12.8, and −10.0 kcal mol^{-1} for **1-4**, respectively. The interaction energies of the cycloalkenes with **Tz** are much more favorable than with **Cp**, and differ less in the cycloalkene series than for the **Cp** cycloadditions. This is consistent with the computed relative rates of the of the strained cycloalkenes with **Cp** spanning 11 orders of magnitude, while the relative rates of the cycloalkene series with **Tz** differ by only 6

orders of magnitude. The smaller variation in the interaction energies leads to more similar activation barriers when **Tz** is the diene.

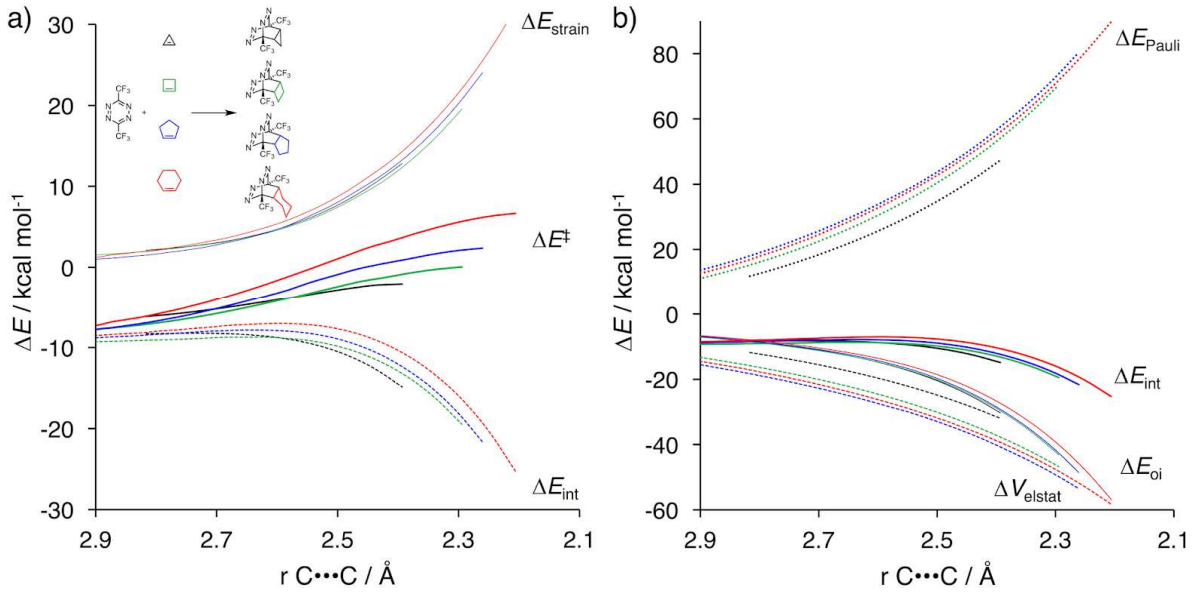

Figure 6.6 (a) Distortion/interaction-activation strain analyses and (b) energy decomposition analyses of the cycloaddition reactions of **Tz** with dienophiles **1-4**, computed at M06-2X/TZ2P//M06-2X/6-31+G(d).

The EDA analysis of the ΔE_{int} values reveals that the Pauli repulsion and electrostatic energy terms offset one another, as shown before with **Cp**. The differences in interaction energies are related to the differences in the orbital interaction energies (Figure 6b). At the same average C···C bond forming distance of 2.39 Å, the values of ΔE_{oi} are −33.3, −30.9, −30.0, and −29.2 kcal mol^{-1} for **1-4**, respectively (see Figure 6b).

6.5 Influence of Primary and Secondary Orbital Interactions on Reactivity

The shapes of the frontier molecular orbitals (FMOs) result in differing degrees of orbital interactions across cycloalkenes series from **1** to **4** with **Cp** and **Tz**. Here we discuss the spatial shape of the FMOs and the influence of the allylic πCH_2 orbitals on the secondary orbital interactions (SOI). Figure 7 shows the Kohn–Sham FMOs of **Cp, Tz,**

and **1-4**. The LUMOs of both dienes interact with the HOMOs of the cycloalkenes in all cases, both in the primary fashion, and with stabilizing secondary interaction between the p orbitals at C_2 and C_3 of the dienes and the Hs on the allylic CH_2 groups of the cycloalkene. This has been shown to be especially strong in the cyclopropene *endo* transition state.[7] There is a decrease in this secondary orbital overlap from **1** to **4** because the πCH_2 orbitals begin to orient towards the outside of the ring across the series. This results in decreasing secondary overlap with the LUMO of **Cp** and **Tz** as the size of the ring increases.

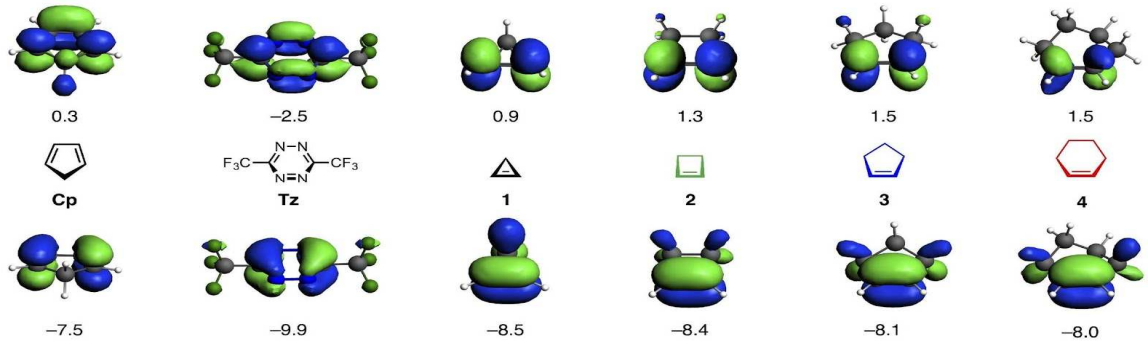

Figure 6.7 FMO diagram (ε, eV, isovalue = 0.05) for ground-state reactants **Cp**, **Tz**, and **1-4** (top row − interacting virtual orbitals, bottom row − interacting occupied orbitals). All data were computed at the M06-2X/TZ2P//M06-2X/6-31+G(d) level.

To provide quantitative evaluation of these orbital interactions, the molecular orbital (MO) diagrams and overlaps were calculated at the MO6-2X/TZ2P level of theory by using Kohn–Sham[11] MO analyses on the geometries at C···C bond forming distances of 2.34 Å and 2.39 Å with **Cp** and **Tz**, respectively. The MO energies and orbital overlap coefficients for the reaction of **Cp** with **1-4** are presented in Figure 8. Both the $HOMO_{diene}$–$LUMO_{dienophile}$ and $HOMO_{dienophile}$–$LUMO_{diene}$ interactions are significant in the reaction of **Cp** with **1-4**. The $HOMO_{diene}$–$LUMO_{dienophile}$ and

$HOMO_{dienophile}$–$LUMO_{diene}$ energy gaps range from 7.5 to 8.3 eV and from 7.8 to 8.1 eV, respectively. The FMO gap with cyclopropene (**1**) is smallest at 7.5 eV compared to 7.8-8.0 eV for cycloalkenes **2-4**. The secondary orbital interactions involve the allylic πCH_2 of the cycloalkene HOMO and the **Cp** LUMO cause the net overlap, 0.21, to be especially large. The overlap decreases as the size of the cycloalkene ring increases. The trend of a diminishing orbital overlap between $HOMO_{dienophile}$–$LUMO_{diene}$ occurs because the cycloalkenes' πCH_2 orbitals bend increasingly outward as the ring size increases, reducing overlap with the LUMO of the diene as discussed earlier for Figure 7. In addition, in both the HOMO and LUMO of the cycloalkenes, the size of the coefficients of the π bond decrease along the series, **1** to **4**, as the π and π* orbitals become more delocalized on more atoms.

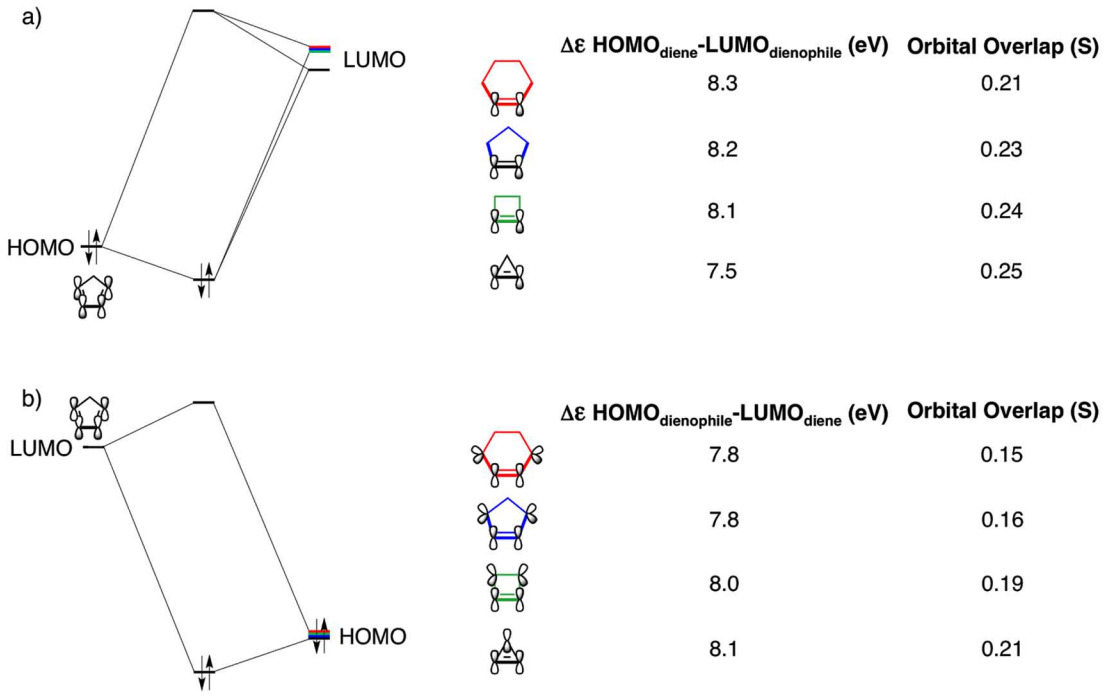

Figure 6.8 (a) MO diagram with orbital energy gap and overlap of the $HOMO_{diene}$–$LUMO_{dienophile}$ interaction, and (b) of the $HOMO_{dienophile}$–$LUMO_{diene}$ interaction for the cycloaddition between **Cp** and **1-4**, computed at M06-2X/TZ2P//M06-2X/6-31+G(d), in all cases at a C···C bond forming distances of 2.34 Å.

The important FMOs in the inverse electron demand Diels-Alder reaction between **Tz** and **1-4** are the $HOMO_{dienophile}$ and $LUMO_{diene}$ (Figure 9). The energy gaps for these MOs are similar and decrease with increasing ring size from 5.1 eV (**1**) to 4.7 eV (**4**). Despite this slight, yet favorable reduction of the $HOMO_{dienophile}$ and $LUMO_{diene}$ FMO interaction with increasing ring size, the overall orbital interaction becomes weaker. This is because the change in the spatial arrangement of the allylic πCH_2 groups in the cycloalkene HOMOs results in less favorable orbital overlap with the LUMO of **Tz** as the ring size of the cycloalkene increases and because the p-orbital coefficient decrease along the series. The orbital overlap between the cycloalkene LUMO and **Tz** HOMO decreases significantly from S = 0.19 to 0.15 across the cycloalkene series from **1** to **4**, respectively.

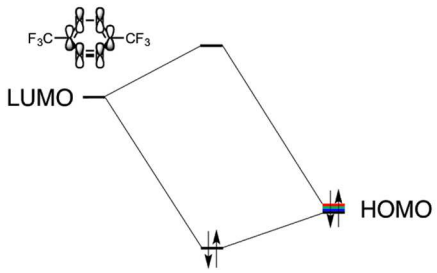

	Δε $HOMO_{dienophile}$-$LUMO_{diene}$ (eV)	Orbital Overlap (S)
	4.7	0.15
	4.8	0.16
	5.0	0.18
	5.1	0.19

Figure 6.9 MO diagram with orbital energy gap and overlap of the $HOMO_{dienophile}$–$LUMO_{diene}$ interaction for the cycloaddition between **Tz** and **1-4**, computed at M06-2X/TZ2P//M06-2X/6-31+G(d) with C···C bond forming distances of 2.39 Å.

The range of reactivities across the cycloalkene series is smaller for the inverse electron-demand Diels-Alder reactions of **Tz** compared to the normal electron-demand Diels-Alder reactions of **Cp**. In the former, the decrease in orbital overlap is countered, although not overruled, by the decreasing $HOMO_{dienophile}$ and $LUMO_{diene}$ energy gap as the size of the cycloalkene ring increases. For **Cp**, both the orbital overlap and the

$HOMO_{diene}$ and $LUMO_{dienophile}$ gap become more favorable across the cycloalkene series from cyclohexene to cyclopropene resulting in a large increase in the reactivity as the size of the cycloalkene ring decreases.

6.6 Conclusions

The factors controlling the reactivities of cycloalkenes with cyclopentadiene and 3,6-bis(trifluoromethyl)tetrazine have been analyzed with the distortion/interaction-activation strain model. The reactivity differences span 11 orders of magnitude in the normal electron-demand Diels-Alder reaction when cyclopentadiene is the diene and 6 orders of magnitude in the inverse electron-demand Diels-Alder reaction with 3,6-bis(trifluoromethyl)tetrazine.

The distortion/interaction-activation strain analysis reveals that the reactivity differences of strained cycloalkenes in these Diels Alder reactions arise from differences in the frontier molecular orbital (FMO) interactions. Orbital interactions involving the cycloalkene HOMO are strongest with cyclopropene and diminish with increasing ring size of the cycloalkene. For the cycloadditions involving **Cp**, both the primary and secondary orbital interactions become less favorable across the series from **1** to **4**. In the **Tz** cycloaddition, the primary orbital interactions become more favorable across the cycloalkene series from **1-4**, because the HOMO-LUMO gap decreases. This counteracts the stabilizing effect of the secondary orbital interactions and lessens the extent of the reactivity differences across the cycloalkene series.

The position of the transition state shifts from early to late across the series of cycloalkenes. The correlation between computed activation energies and distortion energies at the transition states of the cycloalkenes results from the shift of the transition

state from early (low distortion) to late (high distortion) along the series. Performing the distortion/interaction-activation strain analysis along the reaction coordinate, defined by the forming C···C bond distances, reveals that differences in the interaction energies associated with the primary and secondary orbital interactions of the strained cycloalkenes with the dienes control reactivity.

6.7 References

1. Patterson, D. M.; Nazarova, L. A.; Xie, B.; Kamber, D. N.; Prescher, J. A. *J. Am. Chem. Soc.* **2012**, *134*, 18638.

2. Thalhammer, F.; Wallfahrer, U.; Sauer, J. *Tetrahedron Lett.* **1990**, *31*, 6851.

3. Liu, F.; Paton, R. S.; Kim, S.; Liang, Y.; Houk, K. N. *J. Am. Chem. Soc.* **2013**, *135*, 15642

4. (a) Bickelhaupt, F. M.; Houk, K. N. *Angew. Chem. Int. Ed.* 10.1002/anie.201701486. (b) Wolters, L. P.; Bickelhaupt, F. M. *WIRES Comput. Mol. Sci*. **2015**, *5*, 324. (c) Fernández, I.; Bickelhaupt, F. M. *Chem. Soc. Rev.* **2014**, *43*, 4953. (d) van Zeist, W. -J.; Bickelhaupt, F. M. *Org. Biomol. Chem.* **2010**, *8*, 3118; (e) Ess, D. H.; Houk, K. N. *J. Am. Chem. Soc.* **2008**, *130*, 10187. (f) Ess, D. H.; Houk, K. N. *J. Am. Chem. Soc*. **2007**, *129*, 10646. (g) Bickelhaupt, F. M. *J. Comput. Chem.* **1999**, *20*, 114.

5. (a) Mitchell, R. W.; Dorko, E. A.; Merritt, J. A. *J. Mol. Spectrosc.* **1968**, *26*, 197. (b) Craig, N. C.; Borick, S. S.; Tucker, T. R.; Xiao, Y.-Z. *J. Phys. Chem.* **1991**, *95*, 3549. (c) Villarreal, J. R.; Laane, J. *Spectrochim. Acta* **1979**, *35*, 331. (d) Neto, N.; Di Lauro, C. *Spectrochim. Acta* **1967**, *23*, 1763.

6. Paton, R. S.; Kim, S. K.; Ross, A. G.; Danishefsky, S. J.; Houk, K. N. *Angew. Chem., Int. Ed*. **2011**, *50*, 10366.

7. Levandowski, B. J.; Houk, K. N. *J. Am. Chem. Soc.* **2016**, *138*, 16731

8. Staley, S. W.; Howard, A. E.; Strnad, J. T. *J. Org. Chem*. **1992**, *57*, 895.

9. Rademacher, P. *Chem. Rev*. **2003**, *103*, 933.

10. (a) Levandowski, B. J.; Houk, K. N. *J. Org. Chem.* **2015**, *80*, 3530. (b) Levandowski, B. J.; Zou, L.; Houk, K. N. *J. Comput. Chem.* **2016**, *37*, 117.

11 (a) Bickelhaupt, F. M.; Baerends, E. J. In: *Reviews in Computational Chemistry*; Lipkowitz, K. B.; Boyd, D. B. Eds.; Wiley-VCH: New York, **2000**, Vol. 15, pp. 1-86. (b) van Meer, R.; Gritsenko, O. V.; Baerends, E. J. *J. Chem. Theory Comput.* **2014**, *10*, 4432.

12. Frisch, M. J.; Trucks, G. W.; Schlegel, H. B.; Scuseria, G. E.; Robb, M. A.; Cheeseman, J. R.; Scalmani, G.; Barone, V.; Mennucci, B.; Petersson, G. A.; Nakatsuji, H.; Caricato, M.; Li, X.; Hratchian, H. P.; Izmaylov, A. F.; Bloino, J.; Zheng, G.; Sonnenberg, J. L.; Hada, M.; Ehara, M.; Toyota, K.; Fukuda, R.; Hasegawa, J.; Ishida, M.; Nakajima, T.; Honda, Y.; Kitao, O.; Nakai, H.; Vreven, T.; Montgomery, J. A., Jr.; Peralta, J. E.; Ogliaro, F.; Bearpark, M.; Heyd, J. J.; Brothers, E.; Kudin, K. N.; Staroverov, V. N.; Kobayashi, R.; Normand, J.; Raghavachari, K.; Rendell, A.; Burant, J. C.; Iyengar, S. S.; Tomasi, J.; Cossi, M.; Rega, N.; Millam, M. J.; Klene, M.; Knox, J. E.; Cross, J. B.; Bakken, V.; Adamo, C.; Jaramillo, J.; Gomperts, R.; Stratmann, R. E.; Yazyev, O.; Austin, A. J.; Cammi, R.; Pomelli, C.; Ochterski, J. W.; Martin, R. L.; Morokuma, K.; Zakrzewski, V. G.; Voth, G. A.; Salvador, P.; Dannenberg, J. J.;

Dapprich, S.; Daniels, A. D.; Farkas, Ö.; Foresman, J. B.; Ortiz, J. V.; Cioslowski, J.; Fox, D. J. Gaussian 09, Revision D.01; Gaussian, Inc.: Wallingford CT, 2009.

13. Zhao, Y.; Truhlar, D. G. *Theor. Chem. Acc.* **2008**, *120*, 215.

14. (a) Lan, Y.; Zou, L.; Cao, Y.; Houk, K. N. *J. Phys. Chem. A*. **2011**, *115*, 13906; (b) Pieniazek, S. N.; Clemente, F. R.; Houk, K. N. *Angew. Chem. Int. Ed.* **2008**, *47*, 7756.

15. Fan, L. Y.; Versluis, L.; Ziegler, T.; Baerends, E. J.; Ravenek, W. *Int. J. Quantum Chem.* **1988**, *34*, 173.

16. Gonzalez, C.; Schlegel, H. B. *J. Phys. Chem.* **1990**, *94*, 5523.

17. (a) te Velde, G.; Bickelhaupt, F. M.; Baerends, E. J.; Fonseca Guerra, C.; van Gisbergen, S. J. A.; Snijders, J. G.; Ziegler, T. Chemistry with ADF. J. Comput. Chem. 2001, 22, 931−967. (b) Fonseca Guerra, C.; Snijder, J. G.; te Velde, G.; Baerends, E. J. *Theor. Chem. Acc.* **1998**, *99*, 291. (c) ADF2016, SCM, Theoretical Chemistry, Vrije Universiteit, Amsterdam, The Netherlands, http://www.scm.com.

18. (a) van Lenthe, E.; Baerends, E. J. *J. Comput. Chem.*, **2003**, *24*, 1142. (b) Franchini, M.; Philipsen, P. H. T.; van Lenthe, E.; Visscher, L. **2014**, *10*, 1994.

19. (a) Becke, A. D. J. Chem. Phys. **1988**, *88*, 2547. (b) Franchini, M.; Philipsen, P. H. T.; Visscher, L. *J. Comp. Chem.* **2013**, *34*, 1819.

20. Legault, C. Y. CYLview, 1.0b; Université de Sherbrooke: Sherbrooke, QC, Canada, 2009; http://www.cylview.org.

21. (a) Ziegler, T.; Rauk, A. *Inorg. Chem.* **1979**, *18*, 1755. (b) Ziegler, T.; Rauk, A. *Inorg. Chem*. **1979**, *18*, 1558. (c) Bickelhaupt, F. M.; Nibbering, N. M. M.; Van Wezenbeek, E. M.; Baerends, E. J. *J. Phys. Chem.* **1992**, *96*, 4864. (d) Bickelhaupt, F. M.; Diefenbach, A.; de Visser, S. P.; de Koning, L. J.; Nibbering, N. M. M. *J. Phys. Chem. A* **1998**, *102*, 9543. (e) Baerends, E. J.; Gritsenko, O. V. *J. Phys. Chem. A* **1997**, *101*, 5383.

22. van Zeist, W.-J.; Fonseca Guerra, C.; Bickelhaupt, F. M. *J. Comput. Chem.* **2008**, *29*, 312.

Chapter 7. Reactivities and *Endo* and *Exo* Stereoselectivities in Diels-Alder Reactions of 3-substituted cyclopropenes

7.1 Introduction to Cyclopropene Cycloadditions

The Diels–Alder reactions of substituted cyclopropenes are of interest in synthetic[1] and bioorthogonal[2] chemistry. While it is widely accepted that the *endo* stereoselectivity in cyclopropene Diels–Alder cycloadditions results from secondary orbital interactions in the *endo*transition state,[3,4] this conclusion has been questioned. Fujimoto studied the Diels–Alder stereoselectivity for a series substituted butadienes with cyclopropene and concluded that both secondary orbital and electrostatic interactions contribute to the stereoselectivity.[4] Garcia and Burnell have questioned the role of secondary orbital interactions and instead favor steric interactions as control elements in the stereoselectivities of Diels–Alder cycloadditions of cyclopropene and substituted cyclopropenes.[6,7] The influence of secondary orbital, electrostatic, and steric interactions on the stereoselectivity of cyclopropene Diels–Alder reactions is currently an open question.

Scheme 7.1 *Endo* and *Exo* Stereoselectivities for the Diels–Alder reactions of cyclopentadiene with cyclopropene and substituted cyclopropenes

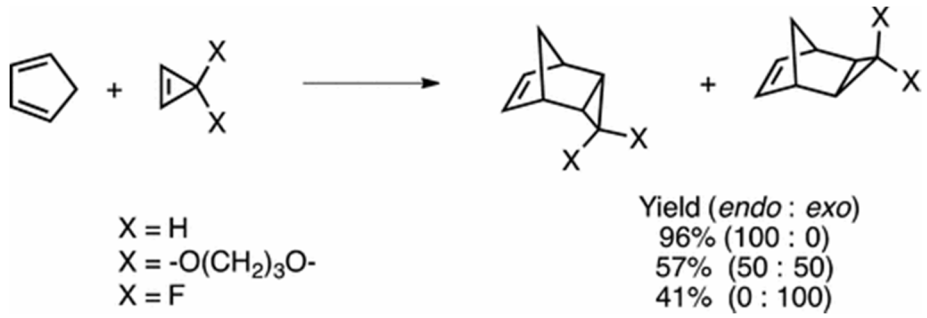

Scheme 1 shows experimental *endo* and *exo* stereoselectivities for the Diels–Alder reactions of cyclopentadiene with cyclopropene, a cyclopropenone ketal, and 3,3-difluorocyclopropene.[8-10] The Diels–Alder cycloaddition of cyclopentadiene with

cyclopropene forms the *endo* adduct exclusively. The cyclopropenone ketal gives the *endo* and *exo* adducts in equal amounts. The reaction of cyclopentadiene with 3,3-difluorocyclopropene gives only the *exo* adduct

The differences between the reactivities of 3-substituted cyclopropenes have previously been described in terms of anomeric effects,[11] frontier molecular orbitals,[2c] and the electronegativity[7] of the substituent. Our lab has shown that the reactivities of 3-substituted cyclopropenes with tetrazine in the inverse electron-demand Diels–Alder reaction correlate with the cyclopropene HOMO energy.[2c] Burnell reported the computed HOMO and LUMO energies for a series of substituted cyclopropenes.[7] The HOMO and LUMO energies range from −9.3 to −11.1 and from 1.0 to 1.2 eV, respectively. The range of LUMO energies is smaller than the HOMO energies, and the frontier molecular orbital interactions cannot explain the reactivity differences of 3-substituted cyclopropenes in the normal electron-demand Diels–Alder reaction. Burnell, and later Poirier, related the reactivities to the electronegativities of the substituents.[7-11] They found that electropositive substituents destabilize the cyclopropene and increase the Diels–Alder reactivity, whereas electronegative substituents have the opposite effect.

Recently, we have shown that the Diels–Alder reactivities of 5-substituted cyclopentadienes are related to the hyperconjugative aromaticity and antiaromaticity of the cyclopentadiene.[12] Schleyer demonstrated that the substituents on the saturated linkage in cyclopropene involve cyclic delocalization of the π electrons via hyperconjugation.[13] To determine if hyperconjugative aromaticity and antiaromaticity determine the Diels–Alder reactivities and stereoselectivities of cyclopropenes, we have studied the origins of reactivity differences and of the *endo* and *exo*s tereoselectivities of

Diels–Alder cycloadditions of substituted cyclopropenes with butadiene. The structures of theoretically investigated cyclopropenes **1**–**16** are shown in Chart 1.

Chart 7.1 Cyclopropene **1**-**16**.

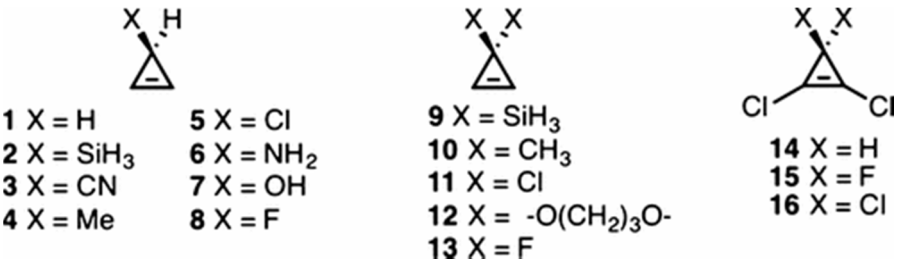

7.2 Computational Methods

Computations were performed using *Gaussian 09*, revision D.0.1.(14) Using the M06-2X(15)functional, geometry optimizations were carried out with the 6-31+G(d) basis set. Single-point calculations were performed with the 6-311++G(d,p) basis set. Solvation effects of dichloromethane (DCM) using the conductor polarized continuum model (CPCM)(16) with a standard state of 1 M were included in geometry and single-point calculations. Truhlar's quasiharmonic correction was applied by setting all positive frequencies below 100 cm^{-1} to 100 cm^{-1}.(17) Orbital coefficients and atomic charges were calculated at the HF/6-31G level of theory. The orbital coefficients are obtained from the outer function of the split-valence 6-31G basis set.

7.3 Interplay of Hyperconjugative, Secondary Orbital, Electrostatic and Steric Effects on Reactivity and Stereoselectivity

Figure 1 shows the *endo* and *exo* transition structures and Gibbs free energies of activation for the Diels–Alder cycloadditions of cyclopropenes **1**, **2**, and **8** with butadiene. The Gibbs free energies of activation for the Diels–Alder reactions of cyclopropenes **1**–**8** with butadiene range from 21 to 27 kcal/mol and from 25 to 28 kcal/mol in the *endo* and *exo* transition states, respectively. When cyclopropene is

substituted, the substituent is preferentially *anti* to butadiene in both the *endo* and *exo* transition states. With cyclopropene the *endo* cycloaddition is favored by 2.8 kcal/mol. The 3-silyl substitution increases the preference for the *endo* cycloaddition to 4.3 kcal/mol, whereas 3-fluoro substitution decreases the preference to only 1.1 kcal/mol.

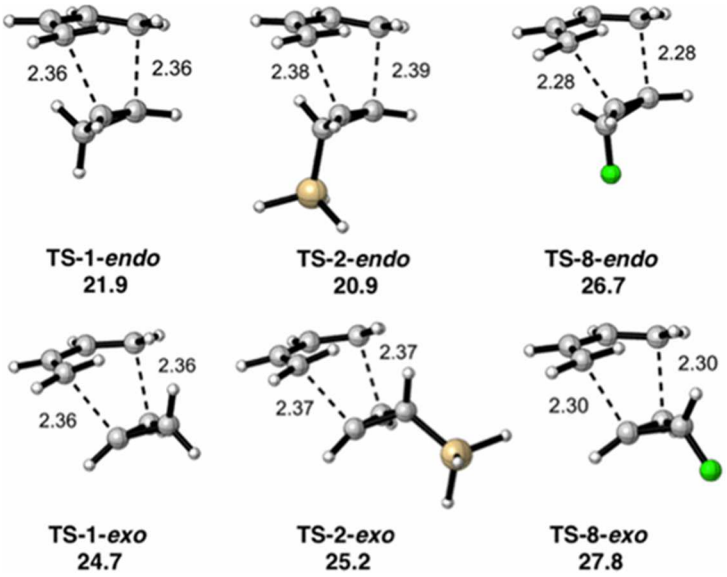

Figure 7.1 Transition structures and Gibbs free energies of activation ($\Delta G^{\ddagger}$) for the endo and exo Diels–Alder reactions of cyclopropenes 1, 2, and 8 with butadiene. Gibbs free energies of activation are reported in kcal/mol and bond lengths are reported in angstroms.

Hyperconjugative interactions involving the σ-bond of the C_3 substituent with the cyclopropene π-system influence the π-delocalization.(13) The hyperconjugative aromatic and antiaromatic stabilization enthalpies (ΔH_{ASE}) of the cyclopropene ground states were calculated using the isodesmic equation shown in Figure 2. The isodesmic equation relates the stability of a substituted cyclopropene to the same substituted cyclopropane that does not include the hyperconjugative interactions of the C_3–X σ-bond with the cyclopropene π-system. A positive reaction enthalpy in the isodesmic equation means that the hyperconjugative interaction of the substituent with the π system is

stabilizing. The calculated reaction enthalpy of 3-fluorocyclopropene is 9.4 kcal/mol. This stabilization is mainly the result of hyperconjugative aromaticity.(13) Hyperconjugation of the C_3–F bond gives the cyclopropene ring two-electron aromatic character. For 3-silylcyclopropene the computed reaction enthalpy is −2.8 kcal/mol. The silyl group is a hyperconjugative donor that destabilizes the cyclopropene ring by giving it four-electron antiaromatic character.

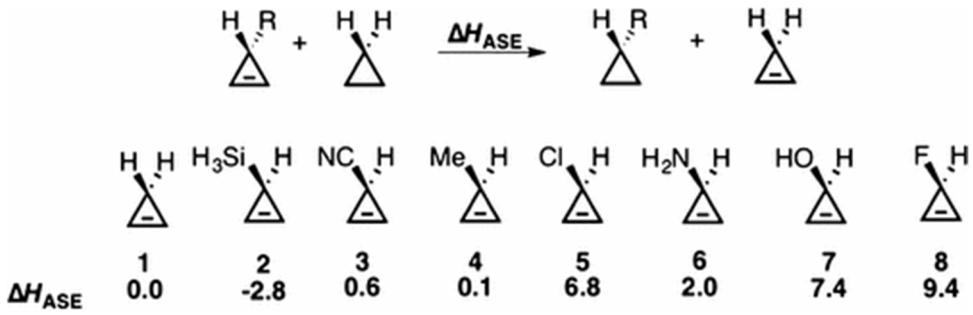

Figure 7.2 Isodesmic equation and aromatic stabilization enthalpies (ΔH_{ASE}) of cyclopropenes **1**–**8**. Positive values reflect stabilization of the cyclopropene.

The ground state geometries of cyclopropenes **1**–**8** are shown in Figure 3. The hydrogen atoms in cyclopropene are positioned 123° from the plane of the cyclopropene. When the C_3–X substituent is a σ-acceptor, the p character of the carbon atom increases and the C_3–X bond distorts toward the plane of the cyclopropene, although the changes are sometimes small or actually opposite with 3-hydroxycyclopropene **7**. This distortion improves the orbital overlap of the σ* C_3–X orbital with the cyclopropene π-system to maximize the stabilizing effect of the hyperconjugative aromaticity.(12) When C_3–X is a σ-donor the distortion is in the opposite direction away from the cyclopropene and minimizes the destabilizing effects of the hyperconjugative antiaromaticity. In the 3-substituted cyclopropenes **2**–**8**, the C_3–H bond distorts in the opposite sense from the C_3–

X bond. The C_3–X bond distorts toward the cyclopropene ring when X is a σ-acceptor and away from the cyclopropene ring when X is a σ-donor.

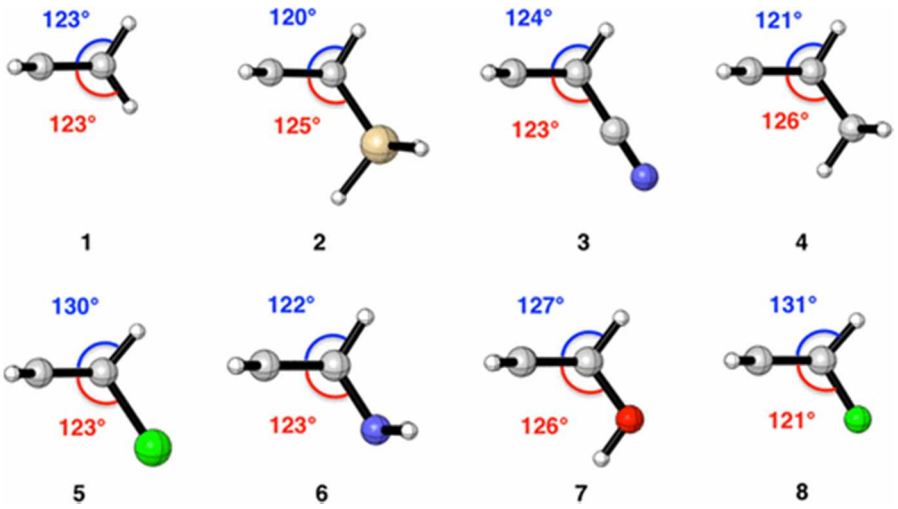

Figure 7.3 Ground state structures for cyclopropenes **1–8** showing the C_{3-X} (red) and C_{3-H} (blue) angles.

Figure 4 shows a plot of the activation enthalpy against the hyperconjugative aromatic stabilization enthalpy for the *endo* and *exo* Diels–Alder reactions of cyclopropenes **1**–**8** with butadiene. The LUMO energies of the cyclopropenes are similar, ranging from 2.5 to 2.9 eV. The modest linear correlations suggest that differences in the Diels–Alder reactivities of the cyclopropenes result from the differences in the hyperconjugative aromaticities of the cyclopropenes. The *endo* selectivity diminishes as the C_3–X substituent becomes a stronger σ-acceptor.

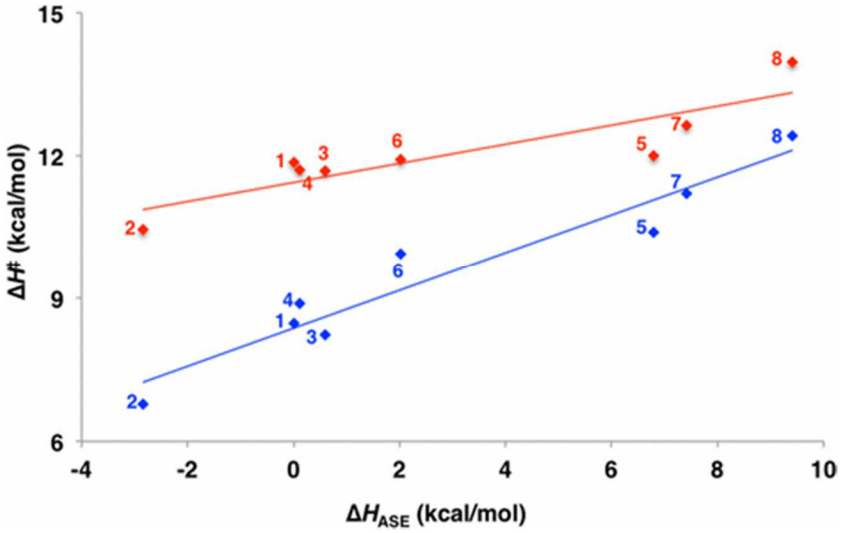

Figure 7.4 Plot of the activation enthalpy ($\Delta H^{\ddagger}$) against the hyperconjugative aromatic stabilization enthalpy (ΔH_{ASE}) for the *endo* (blue) and *exo* (red) Diels–Alder reactions of butadiene with cyclopropenes **1**–**8**. $\Delta H^{\ddagger}_{endo} = 0.40\ \Delta H_{ASE} + 8.4$, $r_2 = 0.93$. $\Delta H^{\ddagger}_{exo} = 0.20\ \Delta H_{ASE} + 11.4$, $r^2 = 0.77$.

To understand the origins of the *endo* and *exo* stereoselectivity in the Diels–Alder reactions of cyclopropenes, we have analyzed the transition states of cyclopropenes **1**–**8** with the distortion/interaction(18) (or Activation Strain)(19) model.(20) Activation energies ($\Delta E^{\ddagger}$), not the Gibbs free energies of activation ($\Delta G^{\ddagger}$), are used in this analysis. The distortion energy ($\Delta E^{\ddagger}_{d}$) is the energy required to deform the ground states of the reactants into their transition state geometries. The interaction energy ($\Delta E^{\ddagger}_{i}$) results from the stabilizing interactions between these distorted transition structures. The results from the distortion/interaction analysis are summarized in Table 1. The distortion energies of the *endo* and *exo* transition states of cyclopropenes **1**–**8** with butadiene are nearly identical, differing by 0.9 kcal/mol at most. The interaction energies always favor the *endo* transition state by 2–3 kcal/mol.

Table 7.1 Distortion/Interaction analysis for the Diels–Alder Reactions of Cyclopropenes **1**–**8** with Butadiene.[a]

TS	$\Delta\Delta E^{\ddagger}$	$\Delta\Delta E^{\ddagger}_{d}$	$\Delta\Delta E^{\ddagger}_{i}$
1	−3.2	−0.5	−2.7
2	−3.9	−0.9	−3.0
3	−3.5	−0.5	−3.0
4	−2.8	−0.2	−2.6
5	−1.7	0.6	−2.3
6	−2.0	0.3	−2.3
7	−1.4	0.6	−2.0
8	−1.5	0.8	−2.2

[a] Energy differences ($E_{endo} - E_{exo}$) are given in kcal/mol.

Figure 5 shows a plot of the *endo* and *exo* stereoselectivity (measured by $\Delta\Delta E^{\ddagger}$) versus the difference between the interaction energies in the *endo* and *exo* transition states. There is a linear correlation: the stereoselectivities result from the differences between the interaction energies of the *endo* and *exo* transition states. The interaction energies may include charge transfer interactions, related to filled-vacant orbital interactions, closed-shell repulsion between occupied orbitals (steric effects), electrostatic effects, and dispersive interactions.

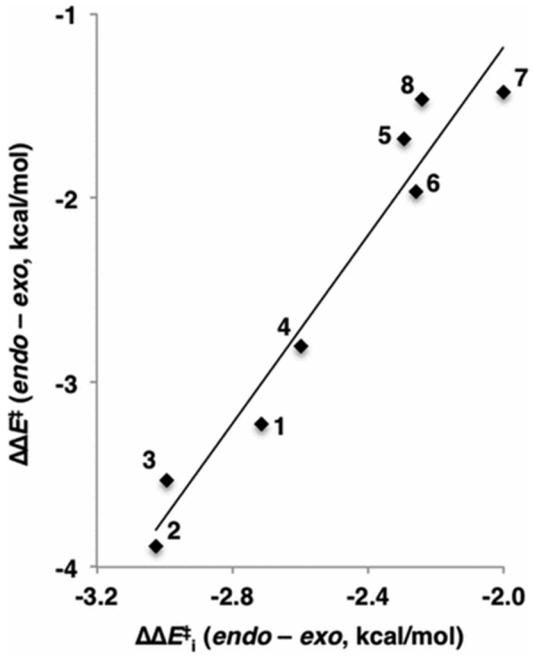

Figure 7.5 Plot of the differences in the electronic activation energies ($\Delta\Delta E^{\ddagger} = \Delta E^{\ddagger}_{endo} - \Delta E^{\ddagger}_{exo}$) versus the differences in the interaction energies ($\Delta\Delta E^{\ddagger}_{i} = \Delta E^{\ddagger}_{i\ endo} - \Delta E^{\ddagger}_{i\ exo}$) between the *endo* and *exo* transition states for the Diels–Alder reactions of cyclopropenes **1**–**8** with butadiene. $\Delta\Delta E^{\ddagger} = 2.6\ \Delta\Delta E^{\ddagger}_{i} + 3.9$, $r^2 = 0.95$.

To determine the contribution of the secondary orbital and electrostatic interactions in the *endo*transition states to the stereoselectivity, we have evaluated quantities that we assume are the major stabilizing interactions. These quantities are reported in Table 2 and include the s-orbital coefficients in the HOMO of the cyclopropene ground state, the natural bond order (NBO) charges for the *syn* hydrogen of cyclopropenes **1**–**8**, the sum of charges at C_2 and C_3 of butadiene, and the distance between the *syn* hydrogen and the forming π-bond in the *endo* transition state. The s-orbital HOMO coefficients of the *syn* hydrogen atoms are similar, ranging from 0.16 to 0.21 in the ground states. The forming π-bond in the *endo* transition state of butadiene is electron-rich with the sum of charges across C_2 and C_3 of butadiene ranging from −0.56 to −0.57. The *syn* hydrogen atoms are positively charged and range from 0.21 to 0.27 in

the *endo* transition states. Although the orbital coefficients and charges are similar in magnitude across the cyclopropene series, the strength of the secondary orbital and electrostatic interactions is also distance dependent. The distance between the *syn* hydrogen atom and the forming π-bond, measured as the distance between the *syn* hydrogen and the center of the C_2C_3 bond in butadiene, as shown in Figure 6, ranges from 2.32 to 2.51 Å in the *endo* transition states of cyclopropenes **1**–**8**. A closer distance increases the favorable secondary orbital overlap and attractive electrostatic interaction, further stabilizing the *endo* transition state.

Table 7.2 S-orbital coefficients in the HOMO for the *syn* hydrogen computed from the ground state, NBO Charges at the *syn* hydrogen of the cyclopropene, the sum of charges at C_2 and C_3 of Butadiene, and the CH/π distances in the *endo* transition states of cyclopropenes **1**−**8**

TS	H s-orbital coefficient (HOMO)	Charge *syn* H (Cyclopropene)	C_2C_3 charge (Butadiene)	CH/π distance (Å)
1	0.19	0.21	−0.57	2.37
2	0.19	0.24	−0.57	2.32
3	0.17	0.27	−0.56	2.34
4	0.19	0.22	−0.57	2.36
5	0.16	0.26	−0.56	2.46
6	0.21	0.22	−0.57	2.43
7	0.16	0.22	−0.56	2.47
8	0.17	0.21	−0.56	2.51

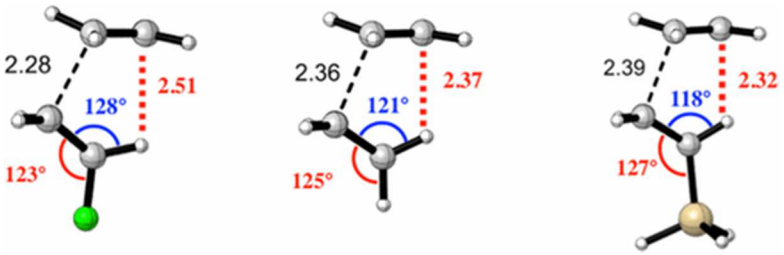

Figure 7.6 CH/π interactions in the *endo* transition states of cyclopropenes **1**, **2**, and **8**. The angle that the *syn* hydrogen atom is distorted from the plane of the cyclopropene ring is shown in blue. Bond lengths are reported in angstroms.

The CH/π distance is related to the position of the transition state and the angle by which the *syn*hydrogen atom is distorted from the plane of the cyclopropene. The angle ranges from 118° to 128° in the *endo* transition states of cyclopropenes **1**–**8** and is linked to the hyperconjugative aromaticity of the cyclopropene. When the C_3 substituent is a σ-acceptor, the C_3–H bond is distorted away from the cyclopropene ring resulting in a further CH/π distance in the *endo*transition state. In addition, a later transition state results in greater pyramidilization of the carbons involved in bonding. Figure 7 shows a plot of the differences in the interaction energies between the *endo* and *exo* transition states versus the CH/π distance. The interaction energies favor *endo*as the CH/π distance decreases because of the increase in the secondary orbital overlap of the *syn* hydrogen s-orbital in the HOMO of the cyclopropene with the C_2C_3 π-orbitals of the butadiene LUMO and the increase in the strength of the stabilizing electrostatic interactions of the partial positively charged *syn* hydrogen with the electron-rich forming π bond in butadiene as the CH/π distance decreases.

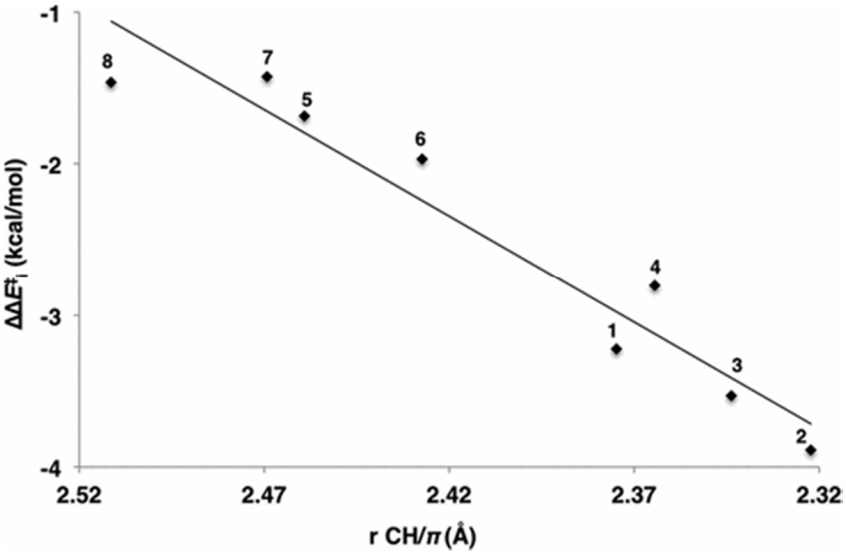

Figure 7.7 Plot of the difference in the interaction energies of *endo* and *exo* transition states ($\Delta\Delta E^{\ddagger}_{i} = \Delta E^{\ddagger}_{i\ endo} - \Delta E^{\ddagger}_{i\ exo}$) versus the CH/π distance in the *endo* transition states of cyclopropenes **1**–**8**. $\Delta\Delta E^{\ddagger}_{i} = 14.0\,r - 36.3$, $r^2 = 0.93$.

Figure 8 shows the *endo* and *exo* transition states for the Diels–Alder reaction of 3,3-difluorocyclopropene with butadiene. The *exo* cycloaddition is favored by 2.0 kcal/mol, consistent with experiments.[10] In the *endo* transition state, the fluorine atom bears a partial negative charge of −0.43 and is 2.78 Å away from the forming π-bond. The CF/π electrostatic interaction in the *endo* transition state is destabilizing, and *exo* stereoselectivity is favored.[21]

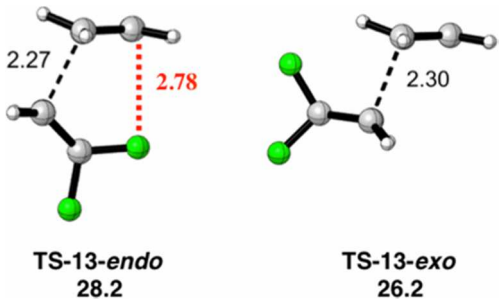

Figure 7.8 *Endo* and *exo* transition structures for the Diels–Alder reactions of 3,3-difluorocyclopropene with butadiene. Gibbs free energies of activation ($\Delta G^{\ddagger}$) are reported in kcal/mol and bond lengths are reported in angstroms.

To calculate the total contribution of the secondary orbital interactions and electrostatic interactions to the stereoselectivity we have compared the strength of the orbital and electrostatic interactions along the intrinsic reaction coordinate (IRC) for the *endo* and *exo* transition states of butadiene with cyclopropene and 3,3-difluorocyclopropene. The analysis was performed with the Amsterdam Density Functional (ADF) program developed by Baerends et al.[22,23] Figure 9shows a plot of the orbital and electrostatic interactions along the IRC for the *endo* and *exo*reactions of cyclopropene, 3-fluorocyclopropene, and 3,3-difluorocyclopropene, from forming C–C bond distances of 2.7 Å to the transition state. For the Diels–Alder reaction of cyclopropene with butadiene, both the secondary orbital and the CH/π electrostatic interactions favor the *endo*transition state, resulting in *endo* stereoselectivity. For the 3-fluorocyclopropene, the smaller preference for *endo* results from the diminished strength of the secondary orbital and electrostatic interactions along the reaction coordinate in the *endo* transition state. In the reaction of 3,3-difluorocyclopropene with butadiene, the orbital interactions are nearly identical along the reaction coordinate, and the electrostatic CF/π interaction, which is destabilizing in the *endo* transition state, and all along the reaction coordinate, results in *exo* stereoselectivity.

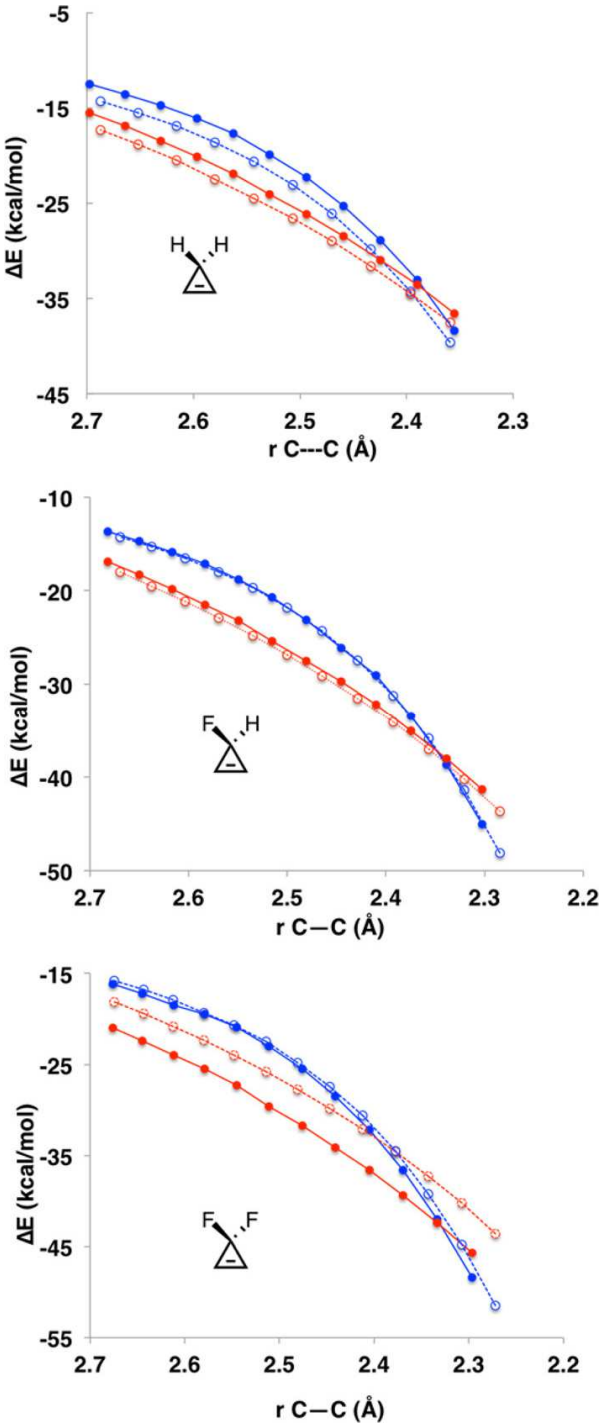

Figure 7.9 Plot of the electrostatic (red) and orbital (blue) interactions along the intrinsic reaction coordinates for the *endo* (dashed) and *exo* (solid) Diels–Alder reactions of butadiene with cyclopropene (top), 3-fluorocyclopropene (middle), and 3,3-difluorocyclopropene (bottom). The plots end at the transition state geometries.

The hyperconjugative interactions are related to the electronic nature of the cyclopropene substituents, which can be represented by the charge at C_3. Figure 10 shows a plot of the *end*o and *exo* stereoselectivity versus the charge at C_3 in the *endo* transition state for the Diels–Alder reactions of cyclopropenes **1**–**16** with butadiene. There is a linear correlation between the *endo*and *exo* stereoselectivity and the charge at C_3. The stereoselectivity for the Diels–Alder reactions of 3,3-disubstituted cyclopropenes **9**–**11** and **16** deviate further toward *exo* selectivity from the established correlation with the NBO charge at C_3 as the size of the substituent increases (SiH_3 > Cl > Me ≫ OR, F, H). The deviation is a consequence of a steric interaction between butadiene and the C_3–X substituent *syn* to butadiene that results in an unfavorable distortion of the C_3–X bond from the plane of the cyclopropene in the *endo* transition state. For 3,3-difluorocyclopropene **13** and the cyclopropeneketal **12**, this steric interaction is weak, and the predicted stereoselectivities correlate well with the NBO charge at C_3. In the *endo* transition states of butadiene with cyclopropenes **9**, **10**, and **11** the steric interaction results in a 3.7, 3.1, and 3.5 kcal/mol deviation toward the *exo* transition state, respectively. The stereoselectivity of the 1,2-dichloro substituted analogs **14**–**16** is similar to that of cyclopropenes **1**, **11**, and **13**. Chlorine substitution across the double bond of a cyclopropene does not significantly influence the stereoselectivity.

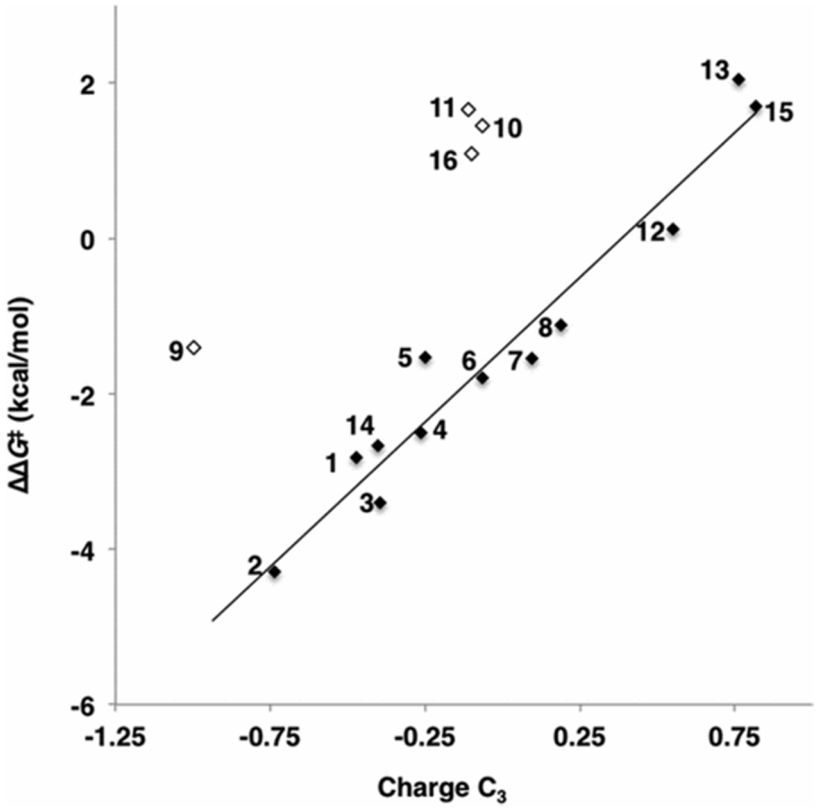

Figure 7. 10 Plot of the differences in the activation free energies ($\Delta\Delta G^{\ddagger} = \Delta G^{\ddagger}_{endo} - \Delta G^{\ddagger}_{exo}$) versus the charge at the C_3 carbon for the Diels–Alder reactions of cyclopropenes **1**–**16** with butadiene. $\Delta\Delta G^{\ddagger} = 3.73\ C_3 - 1.43$, $r^2 = 0.95$.

7.4 Conclusions

The Diels–Alder reactivity and *endo* selectivity increases when the C_3 substituent is a σ-donor. σ-Donors destabilize the cyclopropene ring by giving it four-electron antiaromatic character. In the ground state the C_3–X bond distorts away from the plane of the cyclopropene ring minimizing the antiaromatic character. This distortion results in a more favorable geometry for the secondary orbital and the CH/π electrostatic interactions in the *endo* transition state. An acceptor substituent stabilizes and bends toward the three-membered ring. The charge at C_3 is an indicator of the substituent electronic effects and is useful as a simple predictive property in determining the reactivity

and *endo* and *exo* stereoselectivity of cyclopropene Diels–Alder cycloadditions in the absence of steric interactions, which decrease the reactivity and *endo* stereoselectivity.

7.5 References

1. (a) Rubin, M.; Rubina, M.; Gevorgyan, V. *Synthesis* **2006**, 1221. (b) Marek, I.; Simaan, S.; Masarwa, A. Angew. *Chem., Int. Ed*. **2007**, *46*, 7364. (c) Zhu, Z.-B.; Wei, Y.; Shi, M. *Chem. Soc. Rev*. **2011**, *40*, 5534. (d) Shi, Y.; Wilmot, J. T.; Nordstrøm, L. U.; Tan, D. S.; Gin, D. Y. *J. Am. Chem. Soc*. **2013**, *135*, 14313. (e) Oblak, E. Z.; VanHeyst, M. D.; Li, J.; Wiemer, A. J.; Wright, D. L. *J. Am. Chem. Soc*. **2014**, *136*, 4309.

2. (a) Liang, Y.; Mackey, J. L.; Lopez, S. A.; Liu, F.; Houk, K. N. *J. Am. Chem. Soc.* **2012**, *134*, 17904. (b) Kamber, D. N.; Nazarova, L. A.; Liang, Y.; Lopez, S. A.; Patterson, D. M.; Shih, H.-W.; Houk, K. N.; Prescher, J. A. *J. Am. Chem. Soc*. **2013**, *135*, 13680. (c) Yang, J.; Liang, Y.; Š eckute, J.; Houk, K. N.; Devaraj, N. K. *Chem. - Eur. J.* **2014**, *20*, 3365.

3. Hoffmann, R.; Woodward, R. B. *J. Am. Chem. Soc*. **1965**, *87*, 4388.

4. (a) Matzner, E.; Apeloig, Y. *J. Am. Chem. Soc.* **1995**, *117*, 5375. (b) Jursic, B. S. *J. Org. Chem*. **1997**, *62*, 3046. (c) Wannere, C. S.; Paul, A.; Herges, R.; Houk, K. N.; Schaefer, H. F., III; Schleyer, P. v. R. *J. Comput. Chem.* **2007**, *28*, 344.

5. Imade, M.; Hirao, H.; Omoto, K.; Fujimoto, H. *J. Org. Chem*. **1999**, *64*, 6697.

6. García, J. I.; Mayoral, J. A.; Salvatella, L. *Acc. Chem. Res*. **2000**, *33*, 658.

7. Xidos, J. D.; Gosse, T. L.; Burke, E. D.; Poirier, R. A.; Burnell, D. J. *J. Am. Chem. Soc*. **2001**, *123*, 5482.

8. Wiberg, K. B.; Bartley, W. J. *J. Am. Chem. Soc*. **1960**, *82*, 6375.

9. Boger, D. L.; Brotherton, C. E. *Tetrahedron* **1986**, *42*, 2777.

10. Battiste, M. A.; Posey, R. G. J. *J. Fluorine Chem*. **2000**, *102*, 285.

11. Gosse, T. L.; Poirier, R. A. *Can. J. Chem*. **2004**, *82*, 1589.

12. This distortion is also observed in the C_5−X bonds of cyclopentadiene, but in the opposite direction for donors and acceptors. Levandowski, B. J.; Zou, L.; Houk, K. N. *J. Comput. Chem*. **2016**, *37*, 117.

13. Fernandez, I.; Wu, J. I.; Schleyer, P. v. R. *Org. Lett*. **2013**, *15*, 2990.

14. Frisch, M. J.; Trucks, G. W.; Schlegel, H. B.; Scuseria, G. E.; Robb, M. A.; Cheeseman, J. R.; Scalmani, G.; Barone, V.; Mennucci, B.; Petersson, G. A.; Nakatsuji, H.; Caricato, M.; Li, X.; Hratchian, H. P.; Izmaylov, A. F.; Bloino, J.; Zheng, G.; Sonnenberg, J. L.; Hada, M.; Ehara, M.; Toyota, K.; Fukuda, R.;

Hasegawa, J.; Ishida, M.; Nakajima, T.; Honda, Y.; Kitao, O.; Nakai, H.; Vreven, T.; Montgomery, J. A., Jr.; Peralta, J. E.; Ogliaro, F.; Bearpark, M.; Heyd, J. J.; Brothers, E.; Kudin, K. N.; Staroverov, V. N.; Kobayashi, R.; Normand, J.; Raghavachari, K.; Rendell, A.; Burant, J. C.; Iyengar, S. S.; Tomasi, J.; Cossi, M.; Rega, N.; Millam, M. J.; Klene, M.; Knox, J. E.; Cross, J. B.; Bakken, V.; Adamo, C.; Jaramillo, J.; Gomperts, R.; Stratmann, R. E.; Yazyev, O.; Austin, A. J.; Cammi, R.; Pomelli, C.; Ochterski, J. W.; Martin, R. L.; Morokuma, K.; Zakrzewski, V. G.; Voth, G. A.; Salvador, P.; Dannenberg, J. J.; Dapprich, S.; Daniels, A. D.; Farkas, Ö.; Foresman, J. B.; Ortiz, J. V.; Cioslowski, J.; Fox, D. J. Gaussian 09, Revision D.01; Gaussian, Inc.: Wallingford, CT, 2009.

15. Zhao, Y.; Truhlar, D. G. *Theor. Chem. Acc*. **2008**, *120*, 215.

16. (a) Barone, V.; Cossi, M. *J. Phys. Chem. A* **1998**, *102*, 1995. (b) Cossi, M.; Rega, N.; Scalmani, G.; Barone, V. *J. Comput. Chem*. **2003**, *24*, 669.

17. Zhao, Y.; Truhlar, D. G. *Phys. Chem. Chem. Phys*. **2008**, *10*, 2813.

18. (a) Ess, D. H.; Houk, K. N. *J. Am. Chem. Soc*. **2007**, *129*, 10646. (b) Ess, D. H.; Houk, K. N. *J. Am. Chem. Soc.* **2008**, *130*, 10187. (19) (a) van Zeist, W.-J.; Bickelhaupt, F. M. *Org. Biomol. Chem.* **2010**, *8*, 3118. (b) Fernandez, I.; Bickelhaupt, F. M. *Chem. Soc. Rev*. **2014**, *4*3, 4953.

20. Levandowski, B. J.; Houk, K. N. *J. Org. Chem*. **2015**, *80*, 3530.

21. Kawahara, S.; Tsuzuki, S.; Uchimaru, T. J. J. *Phys. Chem. A* **2004**, *108*, 6744.

22. (a) ADF2013, SCM, Theoretical Chemistry, Vrije Universiteit, Amsterdam, The Netherlands, http://www.scm.com. (b) Guerra, C. F.; Snijders, J. G.; te Velde, G.; Baerends, E. J. *Theor. Chem. Acc*. **1998**, *99*, 391. (c) te Velde, G.; Bickelhaupt, F. M.; Baerends, E. J.; Guerra, C. F.; van Gisbergen, S. J. A.; Snijders, J. G.; Ziegler, T. *J. Comput. Chem*. **2001**, *22*, 931.

23. Baerends, E. J.; Ellis, D. E.; Ros, P. *Chem. Phys.* **1973**, 2, 41.

Chapter 8. *Endo* and *Exo* Stereoselectivity of Triafulvene Diels-Alder Reactions

8.1 The Unusual *Exo* Selectivity in Cyclopropenone Cycloadditions

In 1969, Breslow reported that the Diels-Alder reaction of cyclopropenone with 1,3-diphenylisobenzofuran proceeds with unusual *exo* stereoselectivity (Scheme 1).[1] Berson reinvestigated this reaction in 1994 and confirmed the *exo*-selectivity of cyclopropenone with 1,3-diphenylisobenzofuran by obtaining the crystal structures of the *endo* and *exo* Diels-Alder adducts.[2] Analysis of the reaction kinetics at –30° C revealed an estimated preference of 50:1 *exo*:*endo*.

Scheme 8.1 Diels-Alder reaction of cyclopropenone and 1,3-diphenylisobenzofuran.

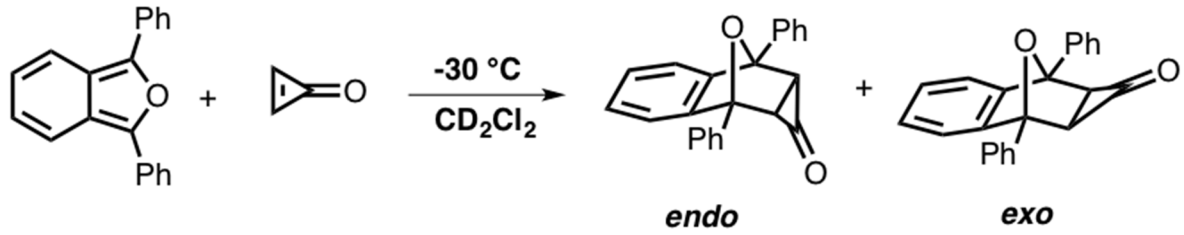

Bachrach computationally analyzed the Diels-Alder reaction between cyclopropenone and furan at the MP2 level.[3] He computed a 1.8 kcal/mol kinetic and a 6.4 kcal/mol thermodynamic preference for the *exo* adduct. The *exo* preference was attributed to a stabilizing electrostatic interaction between the oxygen atom of furan and the carbonyl carbon of the cyclopropenone in the *exo* transition state (Scheme 2).[3] Recently, we computed that cyclopropenone also reacts with *exo* stereoselectivity when cyclopentadiene is the diene,[4] in contrast to the highly *endo* selective cyclopropene.[5] This discovery, and the fact that cyclopropenones have emerged as stable, minimally invasive probes for bioorthogonal labelling studies,[6] prompted us to systematically study the origins of the *endo* and *exo* Diels-Alder stereoselectivity of

cyclopropenone, (**1**), cyclopropenethione, (**2**), iminocyclopropene, (**4**), and the iminium derivative, (**3**), and triafulvenes, (**5-7**), with butadiene (**Bd**). (Scheme 3).

Scheme 8.2 Stabilizing electrostatic interaction proposed by Bachrach in the *exo* transition state for the Diels-Alder reaction of furan with cyclopropenone.[3]

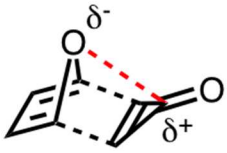

Scheme 8.3 Cyclopropenone and analogs.

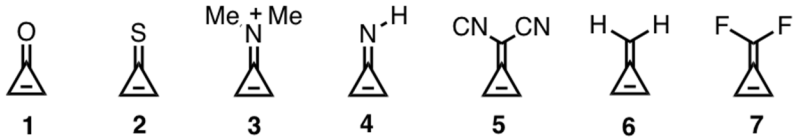

2. Computational Methods

Computations were carried out with *Gaussian 09*, revision D.01.[7] Geometry optimizations and vibrational frequency calculations were performed using the M06-2X[8] density functional with the 6-31+G(d) basis set. Single-point energies were calculated at the M06-2X/6-311++G(d,p) level of theory. The M06-2X functional has been shown to provide relatively accurate energies for cycloadditions.[9] Solvation effects of dichloromethane (DCM) were included in the optimizations and single-point energies using the self-consistent reaction field (SCRF) using the CPCM model.[10] Normal mode analysis was used to verify each stationary point as either a first-order saddle point or a minimum. The thermal corrections were computed from unscaled M06-2X/6-31+G(d) frequencies for a 1 M standard state and 298.15 K. Truhlar's quasiharmonic correction was applied by setting all positive frequencies below 100cm^{-1} to 100 cm^{-1}.[11] The molecular orbital coefficients from the outer Gaussian function charges were calculated

from natural bond orbital (NBO) analysis at the HF/6-31G(d)//CPCM-(DCM)-M06-2X/6-31+G(d) level of theory.[12]

Insight into the origins of the *endo* and *exo* stereoselectivity was provided by the distortion/interaction-activation strain model (D/I-ASM).[13] This analysis was performed using the ADF.2016.102 program[14] at the M06-2X/TZ2P[8,15] level of theory on the geometries optimized at CPCM-(DCM)-M06-2X/6-31+G(d) in *Gaussian 09*. In this framework, the potential energy surface in solution $\Delta E_{solution}(\zeta)$ is decomposed along the reaction coordinate ζ into the energy of the solute $\Delta E_{solute}(\zeta)$, specifically the reaction system in vacuum with the solution phase geometry, plus the solvation energy $\Delta E_{solvation}(\zeta)$.[16]

$$\Delta E_{solution}(\zeta) = \Delta E_{solute}(\zeta) + \Delta E_{solvation}(\zeta) \quad (1)$$

Next, the intrinsic energy of the solute $\Delta E_{solute}(\zeta)$ is separated into the strain $\Delta E_{strain}(\zeta)$ associated with deforming the individual solute reactants, plus the interaction $\Delta E_{int}(\zeta)$ between the deformed solute reactants.

$$\Delta E_{solute}(\zeta) = \Delta E_{strain}(\zeta) + \Delta E_{int}(\zeta) \quad (2)$$

The $\Delta E_{int}(\zeta)$ between the reactants is further analyzed by an energy decomposition analysis (EDA) in the conceptual framework provided by the Kohn–Sham molecular orbital (KS-MO) model[17] and is decomposed into three physically meaningful terms:

$$\Delta E_{int}(\zeta) = \Delta V_{elstat}(\zeta) + \Delta E_{Pauli}(\zeta) + \Delta E_{oi}(\zeta) \quad (3)$$

The $\Delta V_{elstat}(\zeta)$ term corresponds to the classical electrostatic interaction between unperturbed charge distributions, $\Delta E_{Pauli}(\zeta)$ is responsible for any steric repulsion, and the $\Delta E_{oi}(\zeta)$ accounts for charge transfer (HOMO–LUMO interactions) and polarization.

8.3 Influence Secondary Orbital Interactions on Stereoselectivity

Figure 1 shows the *endo* and *exo* transition states for the Diels-Alder reactions of butadiene (**Bd**) with triafulvenes (**1-7**). The computed activation free energies ($\Delta G^{\ddagger}$) are shown below each structure, in kcal/mol. For the *endo* and *exo* Diels-Alder reactions with **Bd**, the activation free energies range from 21–29 and 20–27 kcal/mol, respectively.

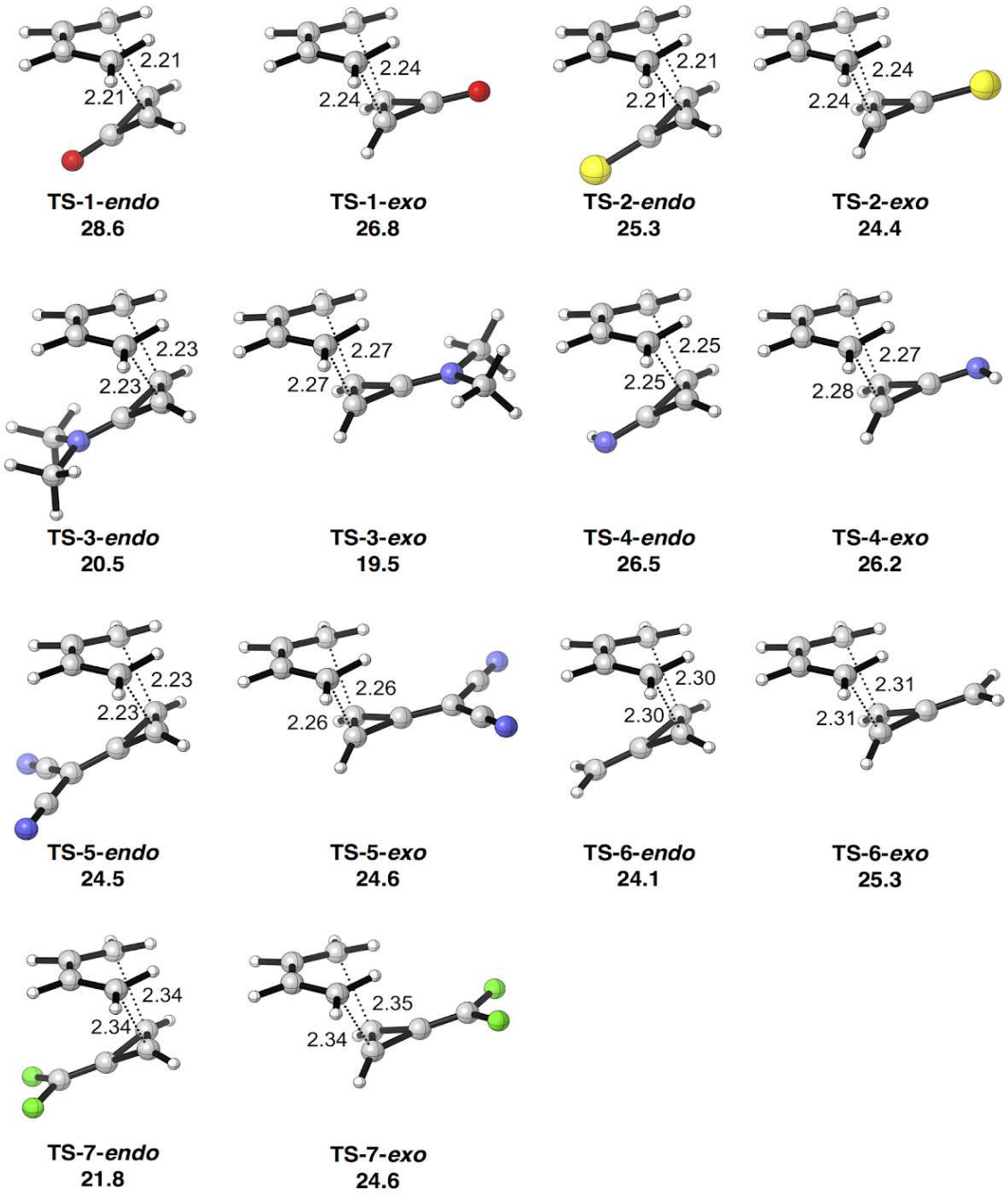

Figure 8.1 Computed Diels-Alder transition structures for the reactions of butadiene (**Bd)** with triafulvenes **1**-**7**. The two forming bond lengths are reported in Ångstroms and activation free energies $\Delta G^{\ddagger}$ are reported in kcal/mol.

The stereoselectivities of the triafulvene cycloadditions range from a 1.8 kcal/mol *exo* preference to a 2.8 kcal/mol *endo* preference. The cycloaddition of **Bd** with

cyclopropenone (**1**) favors the *exo* approach by 1.8 kcal/mol, whereas the 3-difluoromethylene triafulvene (**7**) cycloaddition favors the *endo* reaction by 2.8 kcal/mol. The activation free energies for neutral triafulvene analogs range from 21.8 to 28.6 and from 24.4 to 26.8 in the *endo* and *exo* reactions, respectively. The activation free energies for the positively charged iminium cyclopropene (**3**) with a low lying lowest unoccupied molecular orbital (LUMO) energy are 20.5 and 19.5 for the *endo* and *exo* transition states, respectively.

The effect of each exocyclic cyclopropene group on the stability of **1**-**7** was assessed using the isodesmic reaction shown in Figure 2, which relates the stability of the triafulvene to a similarly substituted cyclopropane.

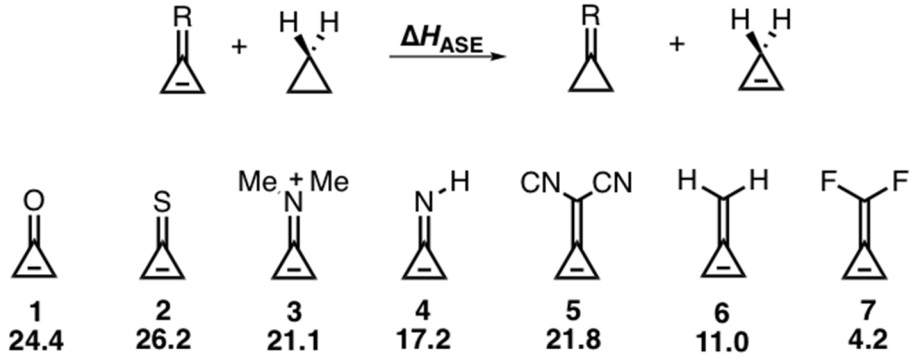

Figure 8.2 The isodesmic equation relating the stability of substituted cyclopropenes (triafulvenes) to substituted cyclopropanes with the computed reaction enthalpies (ΔH_{ASE}) of triafulvenes **1**-**7** in the above isodesmic equation.

All of the groups stabilize the cyclopropene to a greater extent than they stabilize the cyclopropane. We call this aromatic stabilization energy (ASE) since the substituted cyclopropenes have cyclic, potentially aromatic conjugation in the 3-membered ring. A more positive number represents a greater stability of the substituted cyclopropene compared to the substituted cyclopropane. Schleyer has shown that effects of resonance and hyperconjugation are also included in this isodesmic equation.[18] The substituents

have a strong influence on the stability of the cyclopropene. For triafulvenes **1-7**, the calculated aromatic stabilization enthalpies (ASE) are all stabilizing and range from 4.2 to 26.2 kcal/mol. The variation in stabilization arises primarily from differences in the aromaticity of the unsaturated three-membered ring. Electronegative substituents polarize the exocyclic double bond away from the cyclopropene ring, which causes the cyclopropene rings of these compounds to more closely resemble the 2π electron aromatic cyclopropenylium cation. The π-donor F destabilizes the triafulvene motif by increasing the four electron character**,** thus decreasing the aromatic character of the cyclopropene ring.

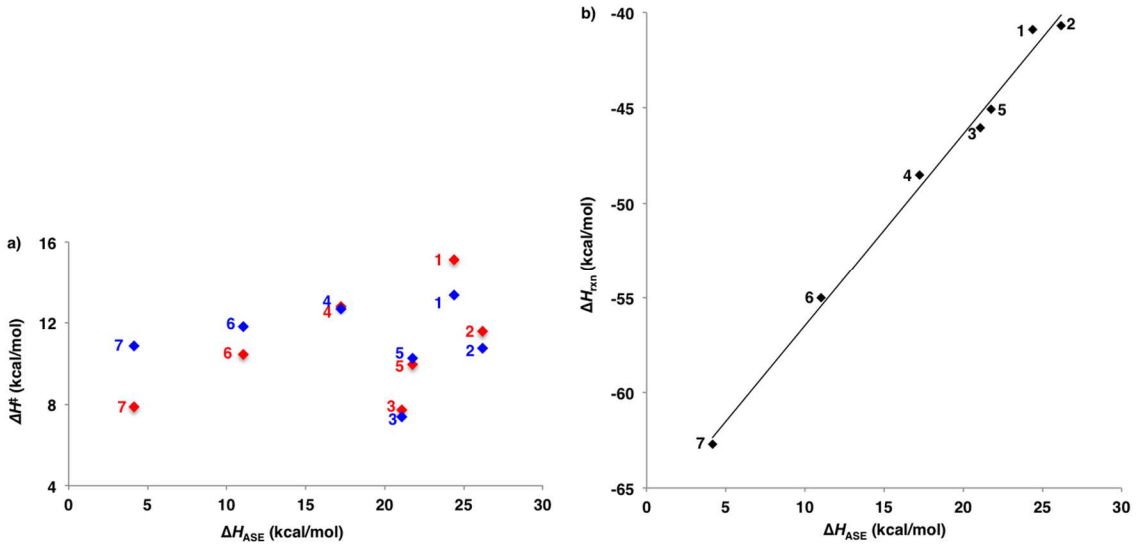

Figure 8.3 (a) Plot of the activation enthalpies ($\Delta H^{\ddagger}$) of the Diels-Alder reactions of **1-7** with butadiene (**Bd**) versus the aromatic stabilization enthalpies (ΔH_{ASE}) (blue *endo*, red *exo*) (b) Plot of the reaction enthalpies (ΔH_{rxn}) versus the aromatic stabilization enthalpies (ΔH_{ASE}) for the Diels-Alder reactions of **1-7** with butadiene (**Bd**) ($\Delta H_{rxn} = 1.00\ \Delta H_{ASE} - 66.5$, $r^2 = 0.99$).

The Diels-Alder reactions of **Bd** with cyclopropenes **(1-7)** are exergonic by –41 to –63 kcal/mol. Consistent with the Hammond postulate, the timing of the transition structures generally becomes earlier as the reaction is more exergonic. As shown in Figure 3a, there is no correlation between the activation enthalpies and the aromatic

stabilization enthalpies (**2**, **3**, and **5** are outliers). Figure 3b shows that there is a linear correlation between the exothermicity of reaction (ΔH_{rxn}) and the aromatic stabilization energy of the triafulvene. The substituents have a significant effect on the reaction free energy, by stabilizing the reactants, but have little effect on the product or on the activation energies.

Application of the distortion/interaction-activation strain model (D/I-ASM) provided quantitative insight into the origins of the reactivity differences and *endo* and *exo* stereoselectivity.[13] Figure 4a shows the results of our analysis for the *endo* (black) and *exo* (red) Diels-Alder reactions of **Bd** with 3-difluoromethylene triafulvene (**7**). The strain, or distortion, curves are nearly identical along the respective reaction coordinates and the *endo* selectivity is a result of the differences in the interaction energies. Figure 4b shows the decomposition of the interaction energy for the *endo* (black) and *exo* (red) Diels-Alder reactions of **Bd** with **7** along the reaction coordinate. The Pauli repulsion and electrostatic terms are nearly identical along the reaction coordinate. The differences in the strength of the orbital interactions in the *endo* and *exo* reactions are responsible for the *endo* Diels-Alder stereoselectivity of **7**.

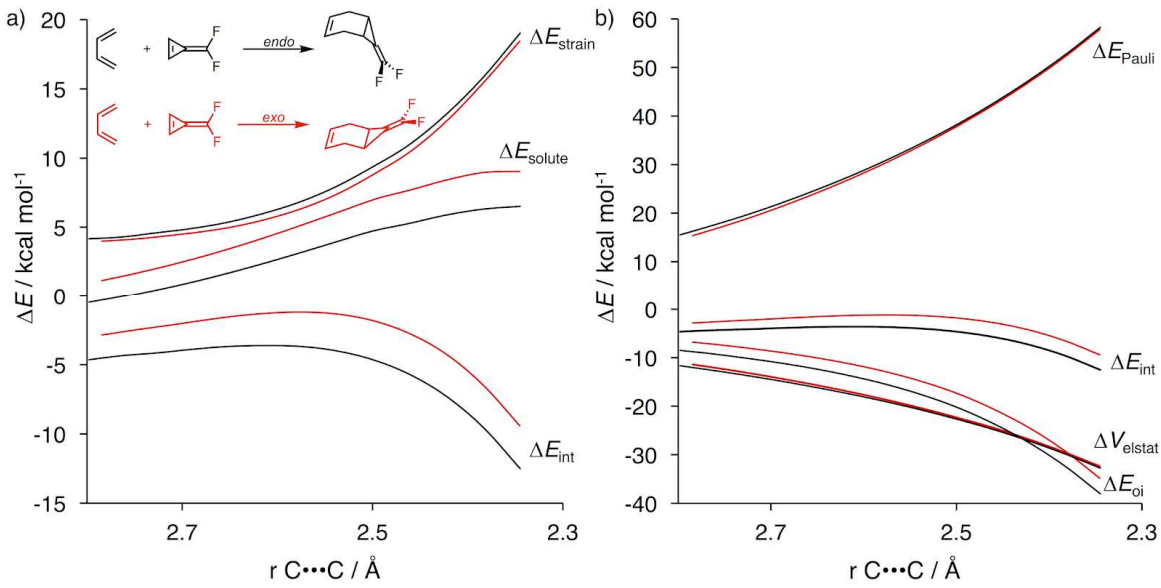

Figure 8.4 (a) Distortion/interaction-activation strain and (b) energy decomposition analyses of the *endo* (black) and *exo* (red) cycloaddition reactions of butadiene (**Bd**) with 3-difluoromethylene triafulvene (**7**).

The results from the distortion/interaction-activation strain model along the reaction coordinate for the *endo* (black) and *exo* (red) Diels-Alder reactions of **Bd** with cyclopropenone (**1**) are shown in Figure 5a. The strain curves are nearly identical for the *endo* and *exo* reactions, and the *exo* stereoselectivity results from differences in interaction energies. Figure 5b shows the decomposition of the interaction energies into the electrostatic, Pauli repulsion and orbital components along the IRC. The *exo* selectivity of cyclopropenone (**1**) results from the combination of the electrostatic and orbital interactions, which overrule the *endo* preference of the Pauli repulsion and favor the *exo* transition state.

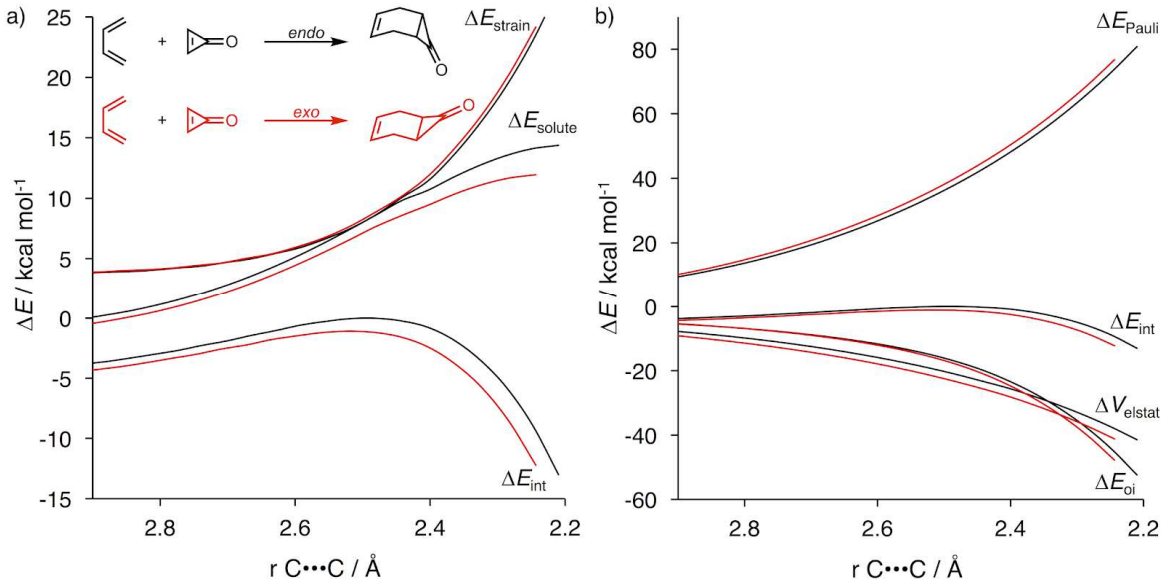

Figure 8.5 (a) Distortion/interaction-activation strain and (b) energy decomposition analyses of the *endo* (black) and *exo* (red) cycloaddition reactions of butadiene (**Bd**) with cyclopropenone **1**.

Figure 6 summarizes the NBO charges at the C_3 position of the triafulvene and heteroatom analogs **1-7**, along with the sum of charges across all atoms of **Bd**, and the C_3 p-orbital coefficient of the triafulvene HOMO in the *endo* transition states. Secondary orbital interactions (SOI) involve overlap of the C_2 and C_3 p-orbitals of the **Bd** LUMO with the C_3 p-orbital of the cyclopropene HOMO in the *endo* transition state. The C_3 p-orbital coefficients in the HOMO of **1-7** range from 0.0 to 0.26. The charges at the C_3 position of **1-7** range from –0.18 to 0.61. Polarization of the exocyclic π-bond diminishes the π-electron density at the C_3 position and weakens the strength of the SOI. 3-Difluoromethylene has the largest p-orbital coefficient and the most negative charge at C_3 and is the most *endo* selective. Cyclopropenone (**1**) with the smallest p-orbital HOMO coefficient and the strongest positive charge at the C_3 is the most *exo* selective.

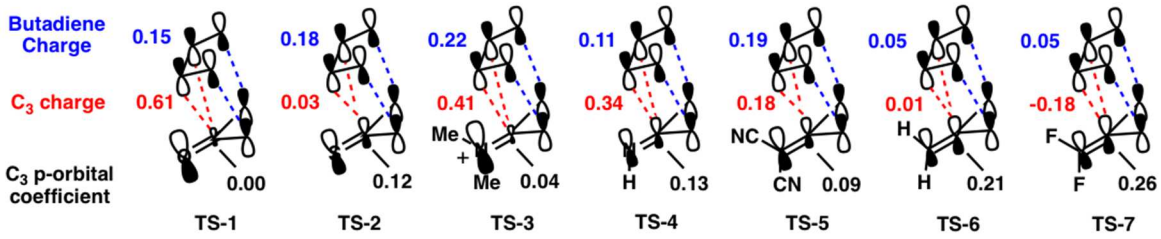

Figure 8.6 Sum of charges across the butadiene (**Bd**) atoms, charge at the C_3 position of the triafulvene, and the C_3 p-orbital coefficient of the triafulvenes and heteroanalogs HOMO obtained from the *endo* transition state structures for triafulvenes **1**-**7**. Primary orbital interactions and secondary orbital interactions are represented by blue and red lines, respectively.

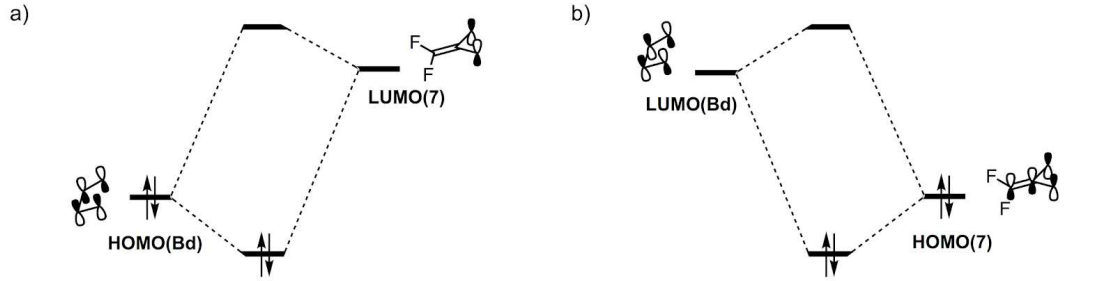

	Δε HOMO(Bd)–LUMO(7) (eV)	Orbital Overlap (S)
endo	6.3	0.25
exo	6.3	0.25

	Δε HOMO(7)–LUMO(Bd) (eV)	Orbital Overlap (S)
endo	6.4	0.17
exo	6.4	0.11

Figure 8.7 (a) MO diagram with orbital energy gap and overlap of the HOMO(**Bd**)–LUMO(**7**) interaction, and (b) of the HOMO(**7**)–LUMO(**Bd**) for the cycloaddition between butadiene (**Bd**) and 3,3-difluoromethylene triafulvene (**7**), computed on structures with C···C bond forming distances of 2.24 Å.

We next performed molecular orbital analyses to quantify the contribution of the SOI in the *endo* reactions of **1** and **7** with **Bd**. The molecular orbital (MO) diagrams and overlaps were calculated at the M06-2X/TZ2P//CPCM-(DCM)-M06-2X/6-31+g(d) level of theory by using Kohn–Sham[19] MO analyses on the geometries at C···C bond forming distances of 2.24 Å. In the Diels-Alder reaction of **7** with **Bd**, the FMO energy gap (Δε = 6.3 eV) and the orbital overlap (S = 0.25) of HOMO(**Bd**)–LUMO(**7**) interaction are the same for the *endo* and *exo* transition states.

The HOMO(**7**)–LUMO(**Bd**) interaction includes the effects of the SOIs in the *endo* transition state. The HOMO(**7**)–LUMO(**Bd**) of *endo* and *exo* transition states are both gaps are both $\Delta\varepsilon$ = 6.4 eV. The orbital overlap of the HOMO(**7**)–LUMO(**Bd**) in the *endo* transition state (S = 0.17) is significantly greater than in the *exo* transition state (S = 0.11). A result of the SOI that arises from the overlap of the p-orbital at the C_3 position in the HOMO of **7** with the C_2 and C_3 p-orbitals in the LUMO of Bd in the *endo* transition state.

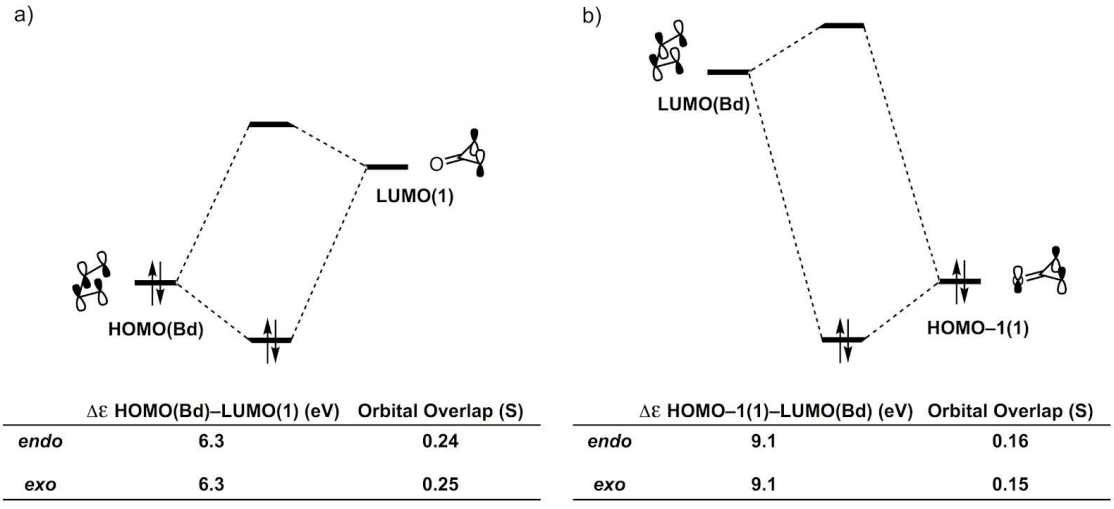

	Δε HOMO(Bd)–LUMO(1) (eV)	Orbital Overlap (S)
endo	6.3	0.24
exo	6.3	0.25

	Δε HOMO–1(1)–LUMO(Bd) (eV)	Orbital Overlap (S)
endo	9.1	0.16
exo	9.1	0.15

Figure 8.8 MO diagram with orbital energy gap and overlap of the HOMO(**Bd**)–LUMO(**1**) interaction for the cycloaddition between butadiene (**Bd**) and cyclopropenone (**1**), computed on structures with C···C bond forming distances of 2.24 Å.

The reaction between **Bd** and **1** proceeds primarily through a normal electron demand Diels-Alder cycloaddition, where the key FMO interaction is between the HOMO(**Bd**)–LUMO(**1**) with an FMO energy gap of 6.3 eV for both the *endo* and *exo* approach. The orbital overlaps are similar for the *endo* and *exo* approach with overlaps of 0.24 and 0.25, respectively. The lower lying HOMO–1(**1**) interacts with the LUMO(**Bd**), however this interaction has a relatively large energy gap of 9.1 eV for both the *endo* and *exo* cycloadditions. The orbital overlaps for the *endo* and *exo* approach are

similar at 0.16 and 0.15, respectively. Similar orbital overlap of the HOMO–1 of **1** with the LUMO of **Bd** in the *endo* and *exo* transition state is evidence of weak secondary orbital interactions in the *endo* transition state. The weak SOIs with **1** are a result of the poor overlap between the small p-orbital coefficient at the C_3 position in the HOMO of **1** with the p-orbitals of the newly forming π-bond in the LUMO of **Bd**. Weak SOI explains why the *endo* selectivity disappears from **7** to **1**, but does not explain why cyclopropenone is *exo* selective.

The charge transfer between the triafulvene and **Bd** also appears in the orbital interaction term. The charge at the C_3 position of the triafulvene and heteroatom analogs **1**-**7** ranges from −0.18 to 0.61 in the *endo* transition states (Figure 6). The reactions are normal electron-demand Diels-Alder reactions and **Bd** becomes partially positively charged as a result of charge transfer to the dienophile. The magnitude of the charge transfer generally increases as the dienophile becomes more electron-deficient. The sum of charge across all the atoms of **Bd** ranges from 0.05 to 0.22 in the *endo* transition states of **1**-**7**. Figure 9 shows a qualitative representation of a charge transfer interaction between the C_3 position of the triafulvene and **Bd** in the *endo* transition states. The charge transfer in the *endo* transition state can be understood as being more stabilizing when the C_3 carbon is negatively charged and destabilizing when the C_3 carbon is positively charged. Due to the increased distance between the C_3 position and the diene, this interaction is much weaker in the *exo* transition state. The lack of secondary orbital interactions and the unfavorable charge transfer between the electropositive **Bd** fragment and the electropositive C_3 position of cyclopropenone (**1**) in the *endo* transition state

explains why there is a preference for the *exo* transition state in the Diels-Alder reaction of **Bd** with cyclopropene (**1**).

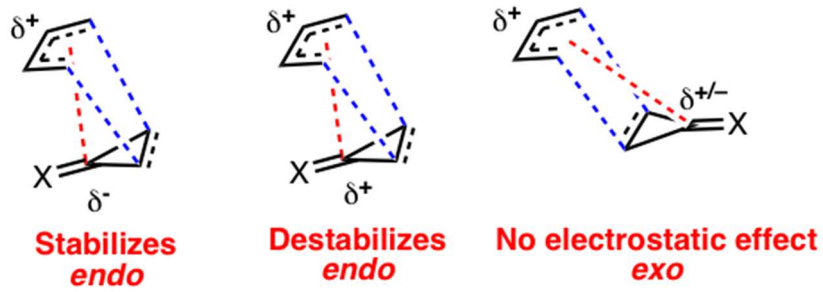

Figure 8.9 Charge transfer in the *endo* and *exo* transition structures for the Diels-Alder reactions of butadiene (**Bd**) with a generic triafulvene. The primary orbital interactions and charge transfer are represented by blue and red lines, respectively.

We have previously shown that both secondary orbital and electrostatic interactions play a role in determining the *endo* and *exo* Diels-Alder stereoselectivity in reactions of 3-substituted cyclopropenes.[5b] The charge at the C_3 position of the cyclopropene correlates with the cyclopropene stereoselectivity in the absence of steric effects and serves as a useful way to predict the stereoselectivity of cyclopropene Diels-Alder reactions. Figure 10 shows a linear correlation between the stereoselectivity ($\Delta G^{\ddagger}_{endo} - \Delta G^{\ddagger}_{exo}$) and the NBO charge at the C_3 position of the triafulvene for the Diels-Alder reactions of triafulvenes **1-7** with **Bd**. The stereoselectivity increases linearly with increasing positive charge at the C_3 position of **1-7** with cyclopropenethione **2**, an obvious outlier, represented by the unfilled diamond.

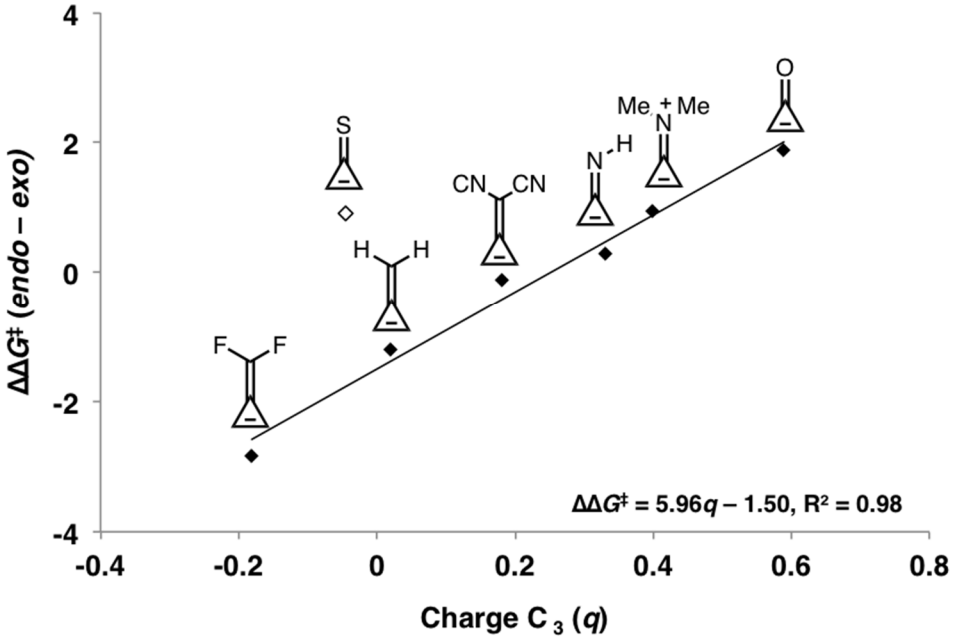

Figure 8.10 Plot of the stereoselectivities measured as the difference in the activation free energies ($\Delta\Delta G^{\ddagger}$) between the *endo* and *exo* Diels-Alder reactions of triafulvenes **1**-**7** with butadiene (**Bd**) versus the computed NBO charge at C_3 in the triafulvene ground state.

The π-densities and charges at the C_3 positions are determined by the polarization of the exocyclic double bond. Compared to the C=O double bond of cyclopropenone (**1**), the C=S double bond of the cyclopropenethione (**2**) is less polarized because of the smaller difference in the electronegativities of carbon and sulfur compared to that of carbon and oxygen. However, sulfur is a strong π acceptor and because of its size, it can accommodate additional π-electron density compared to oxygen. Theoretical studies by Wiberg *et. al.* found that the π-densities of the C=O bond in cyclopropenone and the C=S bond in cyclopropenethione are similar, despite the differences in the polarization of the C=S of C=O bonds.[20] This is consistent with **1** and **2** having similarly small HOMO orbital coefficients at the C_3 carbon, but different charges at the C_3 carbon (See Figure 6).

Figure 11 shows the distortion/interaction-activation strain and energy decomposition analyses for the *endo* and *exo* Diels-Alder reaction of **Bd** with cyclopropenethione (**2**). The slightly *exo* stereoselectivity in the Diels-Alder reaction of **Bd** with **2** results from poor stabilization of the *endo* transition state through secondary orbital and electrostatic interactions.

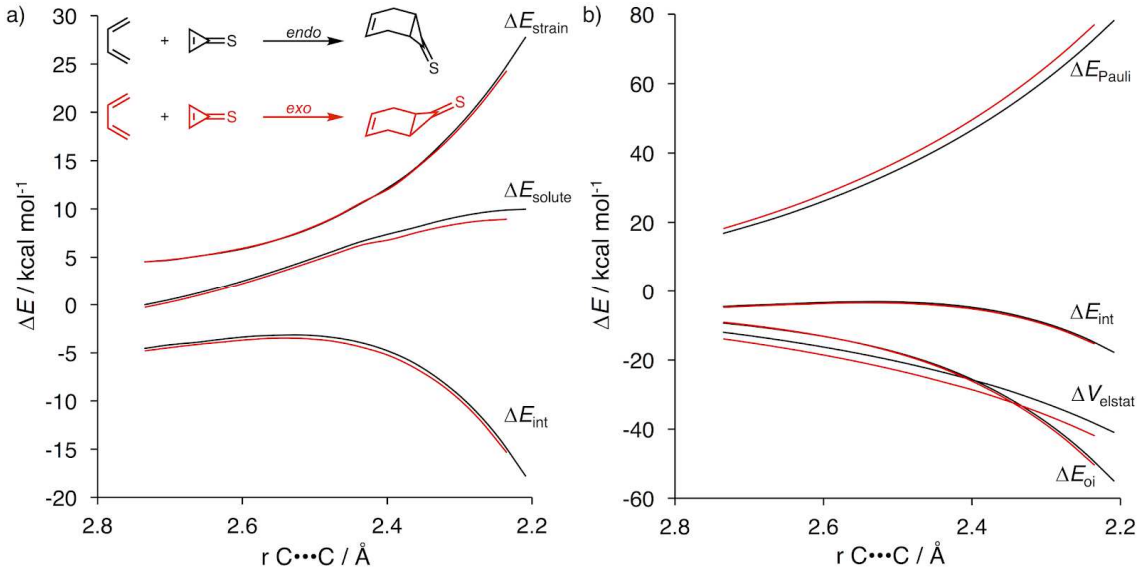

Figure 8.11 (a) Distortion/interaction-activation strain analyses and (b) energy decomposition analyses for the *endo* (black) and *exo* (red) Diels-Alder reactions of butadiene (**Bd**) with cyclopropenethione (**2**).

8.4 Conclusions

The reactivities and stereoselectivities of Diels-Alder reactions of cyclopropenone and triafulvene analogs are controlled by both the charge and HOMO coefficient at the C_3 carbon. In the *endo* transition state, polarization of the exocyclic bond by electron withdrawing groups weakens the strength of the stabilizing secondary orbital interactions and creates unfavorable charge transfer between the electropositive C_3 position of the triafulvene and butadiene that favors *exo* stereoselectivity. The Diels-Alder reactivities of

the triafulvene and heteroanalogs decrease as the size of the HOMO coefficient at the C_3 carbon decreases as a result of weaker secondary orbital and charge transfer interactions. We predict that *exo* stereoselectivity is favored when the exocyclic triafulvene group is O, S, or NR_2^+, *endo* stereoselectivity when CR_2 is the exocyclic group, and poor stereoselectivity when NR is exocyclic substituent.

8.5 References

1. Breslow, R.; Ryan, G.; Groves, J. T. *J. Am. Chem. Soc*. **1970**, *92*, 988.

2. Cordes, M. H. J.; Gala, de S.; Berson, J. A. *J. Am. Chem. Soc.* **1994**, *116*, 11161.

3. Bachrach, S. M. *J. Org. Chem.* **1995**, *60*, 4395.

4. Paton, R. S.; Kim. S.; Ross, A. G.; Danishefsky, S. J.; Houk, K. N. *Angew. Chem. Int. Ed.* **2011**, *50*, 10366.

5. (a) Wiberg, K. B.; Bartley, W. J. *J. Am. Chem. Soc.* **1960**, *82*, 6375. (b) Levandowski, B. J.; Houk, K. N. *J. Am. Chem. Soc.* **2016**, *138*, 16731. (c) Levandowski, B. J.; Hamlin, T. A.; Bickelhaupt F. M.; Houk, K. N. *J. Org. Chem.* **2017**, *82*, 8668.

6. (a) Shih, H.-W.; Prescher, J. A. *J. Am. Chem. Soc.* **2015**, *137,* 10036. (b) Shih, H.-W.; Alexander, A. T.; Mehl, R. A.; Prescher, J. A. *J. Am. Chem. Soc*. **2017**, *139*, 7370.

7. Frisch, M. J.; Trucks, G. W.; Schlegel, H. B.; Scuseria, G. E.; Robb, M. A.; Cheeseman, J. R.; Scalmani, G.; Barone, V.; Mennucci, B.; Petersson, G. A.; Nakatsuji, H.; Caricato, M.; Li, X.; Hratchian, H. P.; Izmaylov, A. F.; Bloino, J.; Zheng, G.; Sonnenberg, J. L.; Hada, M.; Ehara, M.; Toyota, K.; Fukuda, R.; Hasegawa, J.; Ishida, M.; Nakajima, T.; Honda, Y.; Kitao, O.; Nakai, H.; Vreven, T.; Montgomery, J. A., Jr.; Peralta, J. E.; Ogliaro, F.; Bearpark, M.; Heyd, J. J.; Brothers, E.; Kudin, K. N.; Staroverov, V. N.; Kobayashi, R.; Normand, J.; Raghavachari, K.; Rendell, A.; Burant, J. C.; Iyengar, S. S.; Tomasi, J.; Cossi, M.; Rega, N.; Millam, M. J.; Klene, M.; Knox, J. E.; Cross, J. B.; Bakken, V.; Adamo, C.; Jaramillo, J.; Gomperts, R.; Stratmann, R. E.; Yazyev, O.; Austin, A. J.; Cammi, R.; Pomelli, C.; Ochterski, J. W.; Martin, R. L.; Morokuma, K.; Zakrzewski, V. G.; Voth, G. A.; Salvador, P.; Dannenberg, J. J.; Dapprich, S.; Daniels, A. D.; Farkas, Ö.; Foresman, J. B.; Ortiz, J. V.; Cioslowski, J.; Fox, D. J. Gaussian 09, Revision D.01; Gaussian, Inc.: Wallingford CT, 2009

8. Zhao, Y.; Truhlar, D. G. *Theor. Chem. Acc.* **2008**, *120*, 215.

9. (a) Pieniazek, S.; Houk, K. N. *Angew. Chem. Int. Ed.* **2006**, *45*, 1442. (b) Pieniazek, S.; Clemente, F. R.; Houk, K. N. *Angew. Chem. Int. Ed*. **2008**, *47*, 7746.

10. (a) Barone, V.; Cossi, M. *J. Phys. Chem. A* **1998**, *102*, 1995. (b) Cossi, M.; Rega, N.; Scalmani, G.; Barone, V. *J. Comput. Chem.* **2003**, *24*, 669.

11. Zhao, Y.; Truhlar, D. G. *Phys. Chem. Chem. Phys.* **2008**, *10*, 2813.

12. (a) Foster, J. P.; Weinhold, F. *J. Am. Chem. Soc.* **1980**, *102*, 7211. (b) Reed, A. E.; Weinhold, F. *J. Chem. Phys.* **1985**, *83*, 1736. (c) Reed, A. E.; Weinstock, R. B.; Weinhold, F. *J. Chem. Phys.* **1985**, *83*, 735. (d) Reed, A. E.; Curtiss, L. A.; Weinhold, F. *Chem. Rev.* **1988**, *88*, 899.

13. (a) Bickelhaupt, F. M.; Houk, K. N. *Angew. Chem. Int. Ed.* **2017**, *56*, 10070. (b) Wolters, L. P.; Bickelhaupt, F. M. *WIRES Comput. Mol. Sci.* **2015**, *5*, 324. (c) Fernańdez, I.; Bickelhaupt, F. M. *Chem. Soc. Rev.* **2014**, *43*, 4953. (d) van Zeist, W.-J.; Bickelhaupt, F. M. *Org. Biomol. Chem.* **2010**, *8*, 3118. (e) Ess, D. H.; Houk, K. N. *J. Am. Chem. Soc.* **2008**, *130*, 10187. (f) Ess, D. H.; Houk, K. N. *J. Am. Chem. Soc.* **2007**, *129*, 10646. (g) Bickelhaupt, F. M. *J. Comput. Chem.* **1999**, *20*, 114.

14. (a) te Velde, G.; Bickelhaupt, F. M.; Baerends, E. J.; Fonseca Guerra, C.; van Gisbergen, S. J. A.; Snijders, J. G.; Ziegler, T. Chemistry with ADF. *J. Comput. Chem.* **2001**, *22*, 931. (b) Fonseca Guerra, C.; Snijder, J. G.; te Velde, G.; Baerends, E. J. *Theor. Chem. Acc.* **1998**, *99*, 291. (c) ADF2016, SCM, Theoretical Chemistry, Vrije Universiteit, Amsterdam, The Netherlands, http://www.scm.com.

15. (a) van Lenthe, E.; Baerends, E. J. *J. Comput. Chem.* **2003**, *24*, 1142. (b) Franchini, M.; Philipsen, P. H. T.; van Lenthe, E.; Visscher, L. **2014**, *10*, 1994.

16. (a) Laloo, J. Z. A.; Rhyman, L.; Ramasami, P.; Bickelhaupt, F. M.; de Cózar, A. *Chem. Eur. J.* **2016**, *22*, 4431. (b) Hamlin, T. A.; van Beek, B.; Wolters, L.; Bickelhaupt, F. M. *Chem. Eur. J.* **2018**, *24*, DOI: 10.1002/chem.201706075.

17. (a) Ziegler, T.; Rauk, A. *Inorg. Chem*. **1979**, *18*, 1755. (b) Ziegler, T.; Rauk, A. *Inorg. Chem.* **1979**, *18*, 1558. (c) Bickelhaupt, F. M.; Nibbering, N. M. M.; Van Wezenbeek, E. M.; Baerends, E. J. *J. Phys. Chem.* **1992**, *96*, 4864. (d) Baerends, E. J.; Gritsenko, O. V. *J. Phys. Chem. A* **1997**, *101*, 5383.

18. (a) Schleyer, P. v. R.; Pühlhofer, F. *Org. Lett.* **2002**, *4*, 2873. (b)Wang, Y.; Fernandez, I.; Duvall, M.; Wu, J. I.-C.; Li, Q.; Frenking, G.; Schleyer, P. v. R. *J. Org. Chem.* **2010**, *75*, 8252.

19. (a) Bickelhaupt, F. M.; Baerends, E. J. In: *Reviews in Computational Chemistry*; Lipkowitz, K. B., Boyd, D. B., Eds.; Wiley- VCH: New York, 2000; Vol. 15, pp 1−86. (b) van Meer, R.; Gritsenko, O. V.; Baerends, E. J. *J. Chem. Theory Comput.* **2014**, *10*, 443.

20. (a) Wiberg, K. B.; Rablen, P. R. *J. Am. Chem. Soc.* **1995**, *117*, 2201. (b) Wiberg, K. B.; Marquez, M. *J. Am. Chem. Soc.* **1998**, *120*, 2932.